



The
University
Of
Sheffield.

Iron-based Rechargeable Batteries for Large-scale Battery Energy Storage

By

Abdallah H Abdalla

A thesis submitted in partial fulfillment of the requirements for the degree of
Doctor of Philosophy

The University of Sheffield
Faculty of Engineering
Department of Chemical and Biological Engineering

March 2017

ABSTRACT

It is a global challenge to develop green, sustainable power source for modern portable devices, and stationary power generation. Energy storage systems (ESS) can improve the stability and quality of the power grid. Moreover, ESS can be used for peak shaving, integration viable renewable sources to the electricity network. Several ESSs technologies are existing, electrical, thermal, mechanical, and electrochemical storage technologies. This thesis proposes the potential of iron-based electrode batteries such as Nickel-Iron (NiFe) batteries to be implemented for large-scale grid power. This proposal applies to other types of iron-based electrode rechargeable batteries. Iron-based electrode batteries such as Ni-Fe batteries are particularly attractive and compelling to utilise the energy generated from renewable resources. NiFe battery clearly stood out in view of their cost-effective, robust, and eco-friendly materials. Numerous problems have hindered their developments. Those limitations are poor discharge capability and charge efficiency. In fact, the performance of these batteries is drastically reduced by the parasitic evolution of hydrogen. The key is to develop electrode/electrolyte electroactive materials as additives to improve the performance of the battery. This approach has been successful in many rechargeable batteries. In this thesis, investigation of several electrode/electrolyte additives for advanced NiFe batteries is conducted. In this, an effort is made to improve the performance of the NiFe battery by including different electrode and electrolyte additives to suppress the hydrogen evolution (HER) despite the fact that the addition of various percentages of Bi_2S_3 , FeS , K_2S , CuSO_4 or other sulfide elements to the electrode and electrolyte, utilization of electroactive materials is a very effective method of suppressing the HER.

In this study, paste-type and hot-pressed types electrode samples were used to produce the electrode samples. Galvanostatic charge/discharge cycling, and cyclic voltammetry were used to investigate the electrochemical properties of the electrode samples. The prepared and cycled electrode samples were characterised a variety of physical techniques including X-ray diffraction (XRD), atomic force microscopy (AFM), scanning electron microscopy (SEM) and transmission electron microscopy (TEM).

It has been found in this study that, the presence of iron sulfide in the electrode has a real incidence on increasing the reversibility and performance of the electrode samples than using copper alone. Addition of 4.5% wt. bismuth sulfide additives to the iron electrodes significantly improves the reversibility of the electrodes reaction with coulombic efficiency on average of $\eta_Q \approx 30\%$. The Coulombic efficiencies in the order of $\eta_Q \approx 40\%$ and enormous capacities exceeding 300 mA g^{-1} were ware observed in the iron electrode of Fe-loaded 5% FeS and certain amount of 3 – 5% wt. CuSO_4 .

Therefore, this improves the overall performance of NiFe batteries; however, due to the fact that we have used commercial grade reactants and materials, this technology definitely has the potential to be further developed in the long run and could provide a cost-effective solution to large-scale energy storage.

Acknowledgements

I would like to express sincere gratitude to my supervisors, Prof. Pete Hall, for the continuous support, academic guidance, encouragement and advice during my PhD studies. Without his advice and guidance this thesis would not have been possible.

This thesis is dedicated to my mother, my father, brothers, sisters and all my family.

I would like to acknowledge the Libyan High education for the scholarship provided and the financial support during my PhD study.

I would especially like to thank Dr J O Posada and Dr A Rennie for their continual advice, encouraging me to deepen my knowledge, and for the support, they provided in the first months of my PhD.

I would also like to express my special thanks to my entire group member, and colleagues for their thought provoking conversations on a wide range of interesting topics. Also, I would like to express my appreciation to the academic and secretary staff at the Department of Chemical and Biological Engineering.

Finally, I extend my thanks to my amazing family for the support that they have all given me over the years.

Table of Contents

Abstract	I
Acknowledgements	III
Table of Contents	IV
List of Figures	X
List of Tables	XIV
Nomenclature	XV
List of Acronyms and Abbreviations	XV
<i>Chapter 1 Introduction</i>	<i>1</i>
1.1 Introduction	1
1.2 Global energy demand and usage	2
1.3 Thesis Objective	6
1.4 Structure of Thesis	7
<i>Chapter 2 Renewable Energy</i>	<i>9</i>
2.1 The role of Renewable Energy (RE) and sustainable development	9
2.2 Renewable Resources	11
2.3 Challenges in integration variable renewable energy (RES)	15
<i>Chapter 3 Energy Storage Technologies (ESS)</i>	<i>17</i>
3.1 The concept of energy storage	17
3.2 The benefits of energy storage	18

3.3	Classification of Electrical Energy Storage System (ESS)	21
3.3.1	Mechanical Energy Storage (MES)	23
3.3.2	Thermal Energy Storage Systems (TES)	27
3.3.3	Electrical Storage Systems (EES)	28
3.4	Chemical Energy Storage Systems (CES)	31
3.4.1	Battery Storage Systems (BESS)	32
3.4.2	Hydrogen based fuel cell energy storage (HES)	37
3.5	Technical Comparison of Energy Storages Technologies	38
3.6	General Remarks	45
<i>Chapter 4 Literature Review and Research purpose</i>		47
4.1	Introduction to Batteries	47
4.1.1	Principle of operation	48
4.1.2	Battery characteristics	49
4.2	Batteries Charging Techniques	56
4.3	Iron-based batteries	57
4.3.1	Introduction	57
4.4	Rechargeable nickel-Iron battery (NiFe)	62
4.4.1	Introduction	62
4.4.2	Operating Principle of Nickel-Iron (NiFe) Batteries	65
4.4.3	Negative Electrode	65
4.5	Positive Electrode	66
4.6	Electrolyte	68
4.7	Conventional Cell Construction	68

4.7.1	The Negative Electrode _____	69
4.8	Performance _____	70
4.9	NiFe Battery Application and Developments _____	74
4.10	Motivation for the Research on NiFe Batteries _____	76
4.10.1	Problems and Challenges Facing NiFe Batteries _____	77
4.11	Approaches for improving the performance of iron electrodes for NiFe batteries. _____	81
4.11.1	Hydrogen evolution inhibitors _____	85
<i>Chapter 5 Experimental section _____</i>		<i>87</i>
5.1	Introduction _____	87
5.2	Materials and Electrolyte _____	87
5.3	Preparation of Active Material _____	89
5.3.1	Electrode samples preparation _____	89
5.3.2	Paste-type electrode _____	89
5.3.3	Hot-pressed type electrode _____	91
5.4	Experimental Procedures _____	91
5.4.1	Data analysis _____	92
5.5	Electrochemical Techniques Principles of Equipment _____	94
5.5.1	Electrochemical testing _____	94
5.5.2	Galvanostatic charge- Discharge cycling _____	95
	The testing protocol performed was _____	96
5.5.3	Voltammetric technique: Cyclic voltammetry _____	96

5.5.4	Equipment/Instrumentation for cyclic voltammetry measurements	101
5.6	Physical Characterization Techniques	103
5.7	Principles of characterization methods	104
5.7.1	X-ray powder diffraction analysis (XRD)	104
5.7.2	Atomic force microscopy (AFM)	106
5.7.3	Scanning Electron Microscopy (SEM)	107
5.7.4	Transmission electron microscopy (TEM)	108
5.7.5	Energy dispersive X-ray spectroscopy (EDS)	109
<i>Chapter 6 Anode materials for NiFe battery</i>		110
6.1	Bismuth sulfide (Bi_2S_3) as anode additives materials	110
6.1.1	Introduction	110
6.1.2	Materials and electrode samples preparation	112
6.1.3	Electrochemical testing methods	115
6.1.4	Results and Discussion	116
6.1.5	Cyclic voltammetry study of iron electrode samples	120
6.1.6	Characterisation of the electrodes	128
6.1.7	X-ray powder diffraction results	128
6.1.8	HRTEM analysis	131
6.2	Summary	132
6.3	Iron-Copper as anode materials	134
6.3.1	Introduction	134
6.3.2	Materials and Solutions	136
6.3.3	Characterization techniques	137

6.4	Electrochemical measurements	137
6.4.1	Charge-discharge cycling	137
6.5	Results and discussion	138
6.5.1	Cycling performance	138
6.5.2	X-ray powder diffraction results	141
6.6	Summary	143
6.7	Iron sulfide and copper sulfide as anode materials	145
6.7.1	Introduction	145
6.7.2	Experimental Methods	149
6.7.3	Charge-discharge cycling	151
6.7.4	Cycling voltammetry measurements	152
6.7.5	Characterization techniques	152
6.7.6	Results and discussion	153
6.7.7	Summary	168
6.8	Effect of K ₂ S additives to the electrolyte	169
6.8.1	Introduction	169
6.8.2	Cyclic Voltammogram Study	169
6.8.3	Results and discussion	170
6.8.4	Summary	175
<i>Chapter 7 Overall summary and conclusions</i>		176
7.1	Conclusions	176
7.2	Recommendation and future work	178
7.3	References	179

7.4 Appendix A _____195

7.5 Appendix B _____197

7.6 Appendix C _____198

List of Figures

<i>Figure 1.1 Share of World Total Energy Consumption by Source for the last 50 Years, based on BP Statistical Review of World Energy 2015 (BP, 2015c).</i>	3
<i>Figure 2.1 The global Renewables-based on Energy production relative to 2009 by Technology in the New Policies Scenario (IEA, 2011).</i>	11
<i>Figure 2.2 Estimated Renewable Energy Share of Global Electricity Production at the end of 2014 (REN21, 2015).</i>	13
<i>Figure 2.3 Onshore wind annual addition by region (IEA, 2015b).</i>	14
<i>Figure 3.1 Energy storage concept, Adapted with permission from ref (Aneke and Wang, 2016)</i>	18
<i>Figure 3.2 The global installed, grid connected, electrical storage capacity (MW). Adapted with permission from ref (Mahlia et al., 2014).</i>	20
<i>Figure 3-3 Schematic of the Battery connected Renewables power systems.</i>	21
<i>Figure 3.4 Classification of Energy Storage Technologies by the form of stored energy. Adapted with permission from ref (Evans et al., 2012).</i>	23
<i>Figure 3-5 Schematic diagram of Pumped hydroelectric storage. Adapted with permission from ref (Chen et al., 2009).</i>	27
<i>Figure 3.6 Schematic diagram of CAES. Adapted with permission from ref (Mahlia et al., 2014).</i>	27
<i>Figure 3.7 The capacitor storage system. Adapted with permission from ref (Kousksou et al., 2014).</i>	30
<i>Figure 3.8 Superconducting magnetic energy storage.</i>	31
<i>Figure 3.9 Schematic representation of a lead-acid cell (Posada et al., 2017).</i>	34
<i>Figure 4.2 The polarisation curve for a typical battery, Adapted with permission from ref (Cho et al., 2015).</i>	51
<i>Figure 4.3 The improvement in the battery performance over the last 10 years (Tan et al., 2013).</i>	59
<i>Figure.4.5 Conventional pocket plate type NiFe cell, available from :(Changhongbatteris, 2013).</i>	69

Figure 4-6 Typical Charge - discharge curves for a Ni-Fe cell (Shukla et al, 2001).....	71
Figure 4.7 Discharge curves at various rates for a NiFe cell (Shukla et al, 2001).....	72
Figure 4.8 Expected cycle life against depth of discharge (DOD) for NiFe cells, available from: (Changhongbatteris, 2014).	73
Figure 4.9 Illustrate the principle of alkaline water electrolysis and hydrogen evolution reaction.	80
Figure 4.10 Typical charge-discharge curves of the iron electrode (McKerracher et al, 2015).	80
Figure 4.11 Approaches for improving the performance of the iron electrodes.	86
Figure 5.1 Electrode samples preparation.	90
Figure 5.2 Schematic diagram for experimental procedure.	92
Figure 5.3 Schematic of the Cell configuration.....	94
Figure 5.4 Photo of 60-channel Arbin electrochemical battery tester (SCTS169395).....	95
Figure 5.5 A typical cyclic voltammogram curve showing the important peak parameters.	98
Figure 5.6 Schematic diagram of working electrode preparation and the cell assembly for voltammetric measurements.....	103
Figure 5-7 X-ray diffraction and Bragg's law	105
Figure 5-8 Atomic force microscope block diagram.....	107
Figure 6.1 Charge/discharge constant current curves of the iron electrodes vs. Hg/HgO reference electrode of 17 th and the last (30 th) cycles.....	117
Figure 6.2a-b Constant current charge-discharge capacity curves for the 5- 60 cycles with different quantities of bismuth sulfide (0-20wt.%).....	119
Figure 6.3 Cyclic Voltammetric of Fe in 5.1M KOH with a scan rate of 2, 5, 10, 20, 50, 100 mV s ⁻¹	122
Figure 6.4 Peak current dependence with square root of scan rate of Fe in 5.1M KOH solution.	122
Figure 6.5 Cyclic voltammetry of Fe in 0.1M, 0.5M, 1M, 5.1M KOH with scan rate of 10mV s ⁻¹	123
Figure 6.6 Anodic peak current vs. square root of scan rate of Fe, in 0.1, 0.5, 1, and 5.1M KOH and anodic regressions equation.....	124

<i>Figure 6.7 Cyclic voltammetry for the pasted iron powder electrode with Bi₂S₃, and without Bi₂S₃ additives.</i>	125
<i>Figure 6.8 Cyclic Voltammogram of iron electrode in 28.5% KOH at scan rate of 10mV s⁻¹, with 4.5% Bi₂S₃ additive, for -0.8 V to 1.6 V potential window.</i>	127
<i>Figure 6-9 XRD powder pattern (sample S1) for iron electrode with bismuth-sulfide.</i>	129
<i>Figure 6-10 Powder XRD pattern (sample S2) for iron electrode with bismuth-sulfide.</i>	130
<i>Figure 6-11 Powder XRD pattern (sample S3) for iron electrode with bismuth-sulfide.</i>	130
<i>Figure 6.12 a-d, HRTEM images of Fe-Bi₂ S₃ electrodes, EDS results of Fe-Bi₂ S₃ electrodes.</i>	132
<i>Figure 6.13 Voltage-time discharge curves of paste-type iron electrodes with and without additives at a C/5 rate.</i>	139
<i>Figure 6.14 Discharge capacity for the iron electrode versus cycle number.</i>	140
<i>Figure 6.15 Cyclic voltammograms of the (a) Fe/ Bi₂S₃-Cu mixed electrode (b) Fe/Bi₂S₃ mixed electrode additives, at scan rate of 5 mV s⁻¹.</i>	141
<i>Figure 6.16 XRD powder pattern for the: (a) as prepared iron electrodes, (b) the iron electrode after extended cycling.</i>	143
<i>Figure 6.17 Schematic of the Cell configuration.</i>	151
<i>Figure 6.18. a) Charge-discharge curves of the first cycle of an iron electrode vs. Hg/HgO reference electrode at a C/5 rate, b) charge-discharge curves of the cycles from 17th-35th among 60 cycles.</i>	154
<i>Figure 6-19 The cell performance as a function of composition. Squares and circles denote capacity and coulombic efficiency respectively. Likewise, cyan and yellow colours denote to compositions of 0% (curves on a lower part of the diagram) and 5% (curves on an upper part of the diagram) respectively of Fe</i>	155
<i>Figure 6.20 Coulombic efficiency versus cycle number for selected electrode formulations. The lower curves on the diagram (cyan colour) correspond to 0% FeS; likewise, the upper curves (gold) correspond to 5% FeS.</i>	157
<i>Figure 6.21 Cyclic voltammetry for the prepared iron electrode, (a) without additives (b) with additives, for the 10th, 15th, 20th, 30th, and 40th cycles, at a scan rate of 10 mV s⁻¹ in the voltage range of -0.8 -1.6 V.</i>	160

<i>Figure 6.22 X-ray powder diffraction pattern for the iron electrode (a) before charging (b-c) after charging. Powder diffraction cards: Fe (00-006-0696), Fe₃O₄ (00-065-0731), FeS (04-003-01443), CuSO₄ (01-077-1900), Cu₂O (01-078-2076).</i>	162
<i>Figure 6.23. Soft tapping-mode AFM images: (a) Height sensor image of the iron powder electrode with additive before discharge/charge cycling;(b-e) cross section along the line in phase image;(c-f) the corresponding phase image, z-range; (d) Height sensor of the image iron powder electrode with additives after 60 cycles of charge and discharge.</i>	164
<i>Figure 6.24 SEM images of (a) Ni foam free additives (b-d) Fe electrode as prepared.</i>	166
<i>Figure 6.25 SEM images of (e-h) after formation cycling (i and j) EDX measurements of the cycled iron electrodes.</i>	167
<i>Figure 6.26 Cyclic voltammograms response of 0.1M K₂S in KOH solution with a scan rate of 2, 5, 10, 20, and 50 mVs⁻¹ at GCE.</i>	171
<i>Figure 6.27 Anodic and cathodic peak current versus square root of scan rate of K₂S in KOH solution.</i>	171
<i>Figure 7-1 Charge/discharge constant current cycling (up to 60 cycles) of the selected mixed iron electrodes vs. Hg/HgO reference electrode of (a) Fe/Bi₂S₃ (b) Fe/FeS-CuSO₄.</i>	195
<i>Figure 7-2i EDX measurement of the mixed iron electrode after been subjected to charge-discharge cycling</i>	196
<i>Figure 7-3j EDX measurement of the mixed iron electrode after been subjected to charge-discharge cycling.</i>	196

List of Tables

<i>Table 2-1 The main types of renewable sources and their usage options.....</i>	<i>12</i>
<i>Table 3-1 Comparison of different energy storages types.....</i>	<i>41</i>
<i>Table 3-2 Comparison of selected battery technologies.....</i>	<i>43</i>
<i>Table 3-3 A summary of batteries storage technologies.....</i>	<i>44</i>
<i>Table 4-1 Iron Electrode Battery Systems (Linden and Reddy, 2002).....</i>	<i>61</i>
<i>Table 4-2 Iron Electrode Characteristics</i>	<i>61</i>
<i>Table 4-3 Comparative specific energies of NiFe and Pd-acid batteries at two discharge rate.....</i>	<i>63</i>
<i>Table 4-4 Variation in capacity with discharge rate (Linden and Reddy, 2002).</i>	<i>72</i>
<i>Table 4-5 The NiFe characteristics (Chakkaravarthy et al., 1991).</i>	<i>75</i>
<i>Table 4-6 Nickel-iron battery performance {Crompton, 2000 #112}.....</i>	<i>75</i>
<i>Table 4-7 Different types of selected anode materials for NiFe cells</i>	<i>84</i>
<i>Table 5-1 Descriptions of materials and chemicals used in this study.</i>	<i>88</i>
<i>Table 6-1 Experimental determinations of factors and levels.....</i>	<i>113</i>
<i>Table 6-2 Experimental determinations of factors and levels.....</i>	<i>114</i>
<i>Table 6-3 Example of proposed composition.....</i>	<i>120</i>
<i>Table 6-4 The peak current and peak potentials for the iron electrode with and without additives.</i>	<i>126</i>
<i>Table 6-5 Conditions for the diffraction acquisitions.....</i>	<i>129</i>
<i>Table 6-6 The experimental design determinations of factors and levels.....</i>	<i>136</i>
<i>Table 6-7 Main factors and levels used in experiments.....</i>	<i>150</i>
<i>Table 6-8 Example of proposed composition for the Fe/FeS-CuSO4.....</i>	<i>156</i>
<i>Table 6-9 The peak current and peak potentials for the 0.1 M K₂S in KOH solution at.....</i>	<i>170</i>
<i>Table 6-10 Main factors and levels used in experiments</i>	<i>172</i>
<i>Table 6-11 Corrosion kinetics, corrosion current in inhabitation efficiencies, associated with Tafel polarization measurements recorded for iron electrodes in 5.1M KOH solution with and without different concentration of electrolyte additives.</i>	<i>174</i>
<i>Table 7-1 Summary of some additives used and the results achieved.....</i>	<i>178</i>

Nomenclature

List of Acronyms and Abbreviations

A

AFM Atomic Force Microscopy

Ah Ampere-Hours

B

BESS Batteries Energy Storages Systems

C

CAES Compressed Air Energy Storage

CC Constant Current

CCCV Constant Current Constant Voltage

CE Coulomb Efficiency

CE Counter Electrodes

CES Chemical Energy Storage Systems

CV Cyclic Voltammetry

D

DOE Design of experiments

DoD Depth of Discharge

E

EDLCs Electrochemical Double Layer Capacitors

EDS Energy Dispersive Spectroscopy

EE	Energy Efficiency
EIS	Electrical Impedance spectroscopy
EMF	Electromotive Force
ECs	Electrochemical capacitors
ESS	Energy Storage System
EES	Electrical Storage systems

F

FLA	Flooded lead-acid
FC	Fuel Cell
FCC	Fast Constant Current
FES	Flywheels Energy Storage
FTIR	Fourier Transform Infrared Spectroscopy

G

GCE	Glassy-carbon Electrodes
GHG	Greenhouse Gasses

H

HER	Hydrogen Evolution Reaction
HRTEM	High Resolution TEM
HES	Hydrogen Energy Storage
HTTES	High-Temperature Thermal Energy Storage

I

IEA The International Energy Agency

IISD The International Institute for Sustainable Development

L

LA Lead-acid Battery

Li-ion Lithium-ion

LPT Low-Pressure Turbine

LTTES Low-Temperature Thermal Energy Storage

M

MENA Middle East and North Africa

MES Mechanical Storage Systems

MMO Mercury/Mercury Oxide

N

NHE Normal Hydrogen Electrode

NiCd Nickel Cadmium

NiFe Nickel-iron battery

NiMH Nickel metal hydride

O

OCV Open-circuit Voltage

OECD Organization for Economic Cooperation and Development

P

PC Pulse Charging

PHS Pumped hydroelectric storage

PV	Photovoltaic
PTFE	Polytetrafluoroethylene

R

RE	Reference Electrode
RES	Renewable Energy Sources
RSM	Response Surface Methodology
RHE	Reversible Hydrogen Electrode

S

SEM	Scanning electron microscopy
SHE	Standard Hydrogen Electrode
SMES	Superconducting magnetic energy storage

T

TEM	Transmission electron microscopy
TES	Thermal Energy Storages

V

VRLA	Valve-regulated lead-acid (battery)
VE	Voltage Efficiency

W

WE	Working electrode
WEO	World Energy Outlook

X

XRD	X-ray diffraction
-----	-------------------

Constants

Symbol	Description	Unit
F	The Faraday constant	C mol ⁻¹
e	Elementary charge	C
R	Gas constant	J/K.mol

Roman symbols

Symbol	Description	Unit
E	Cell voltage	V
E	Energy	Wh
E°	Standard Electrode Potential	V
E	Electromotive Force of cell	V
ΔG	Gibbs Free Energy	J/mol
ΔG°	Free Energy Change	J/mol
I	Current	A
P	Power	W
Q	Charge	C
SoC	State of Charge	--
D	Diffusion Coefficient	cm ² S ⁻¹
i	Current Density	A/cm ²
i_{corr}	Corrosion current densities	A/cm ²
\tilde{i}_{corr}	Corrosion current densities with additives	A/cm ²
IE	Corrosion inhibition efficiency	%
n	Electrons/Redox Species	Moles e ⁻ /moles Fe ²⁺
A	The Electrode Area	cm ²
$C\text{-rate}$	Charge or discharge rate	mA
m	Active Material Weight	g

ED	Energy Density	Wh L^{-1}
PD	Power Density	W L^{-1}
Q_{ch}	Specific Charge Capacity	mAh g^{-1}
Q_{dis}	Specific Discharge Capacity	mAh g^{-1}
t	Time	h or s
T	Temperature	K or °C

Greek Symbols

Symbol	Description	Unit
η	Overpotential	V
θ	Bragg Scattering Angle	degree
η	Efficiency	%
λ	Wavelength of X-Ray	Å^0
β	The full width of half-maximum in radians	nm

Chapter 1 INTRODUCTION

This work aims to explore the potential of the implementation of the iron-based battery (such as Nickel-Iron batteries) for large-scale energy. This chapter aims to give a review of the world energy demand and outline the rising global energy demand and the concern over the used fuel on the environment, and the need for alternative sustainable energy sources.

1.1 Introduction

Energy is fundamental to human society and poverty reduction and a critical enabler of development (Leopold *et al.*, 2014). Access to modern energy services is vital for social development, public health, enhancing education, and to promote economic growth. Nevertheless, in developing countries particularly, sustainable development cannot be achieved without access to affordable (inexpensive), reliable, and clean energy services (Bhattacharyya, 2012). Increased access to energy sources is fundamental for economic development.

The International Energy Agency (IEA) adopted a definition of energy access as “*a household having reliable and affordable access to clean cooking facilities, a first connection to electricity and then an increasing level of electricity consumption over time to reach the regional average*”. Therefore, access to modern energy involves three forms of energy: less polluted energy for heating and catering, electricity for powering housing and public facilities such as school, and mechanical energy from either electricity or other sources to improve the labour productivity (Corbyn *et al.*, 2013).

IEA (2010) estimates that about 1.2 billion people across the world lack access to energy (IEA). It stated that approximately 1.6 billion people, who do not have access to modern energy. However, more than 2.8 billion people in rural areas rely on traditional fuels including; coal, wood to meet their daily cooking and heating needs (Leopold *et al.*, 2014). Therefore, meeting the need of 1.2 billion people presently did not have access to energy are well known global challenges.

1.2 Global energy demand and usage

The moving toward global sustainable energy development and reduction of greenhouse gases (GHG) can be assessed by consideration of the trend of the global energy demand and supplies.

According to IEA in 2012 (IEA, 2014), following the industrial revolution, there is a significant increase of the global population and considerably increase in energy demand and consumption. The IEA indicate that the global population is estimated to rise from 6.8 billion in 2010 to 8.6 billion by 2035. Over the last twenty years, the global energy consumption is increased for all fuels (BP, 2015a).

A recent report by World Energy Outlook (WEO) stated that the global energy demand is expected to increase by 1.2 % per year by 35% between 2010 until 2035 (IEA, 2014). Most of Global Energy is provided mainly from carbon-based, and fossil fuels. It is estimated that by 2035; 20% of global primary energy is coming from non-fossil fuels, 66% of this consumption is coming from fossil fuel based on unsustainable energy sources such as coal, oil, and natural gas. Coal remains the dominant world fuel. Roughly one-third of the global Energy is provided by non-fossil fuels, two-third provided from gas, oil, and coal (BP, 2015c, BP, 2015a). Energy production is the primary source of CO₂ emission, and the share of energy generation

in a total of greenhouse gases emission is estimated to increase from 40% to 45% in 2050 (IEA, 2014, BP, 2015b).

Nuclear power could be an alternative to fossil fuels energy, but the crucial issues of safety, health, environmental concerns, and human risk to avoid disasters like the incident that witnessed recently in Japan’s Fukushima nuclear power plant in March 2011 has raised the demand for alternative energy sources.

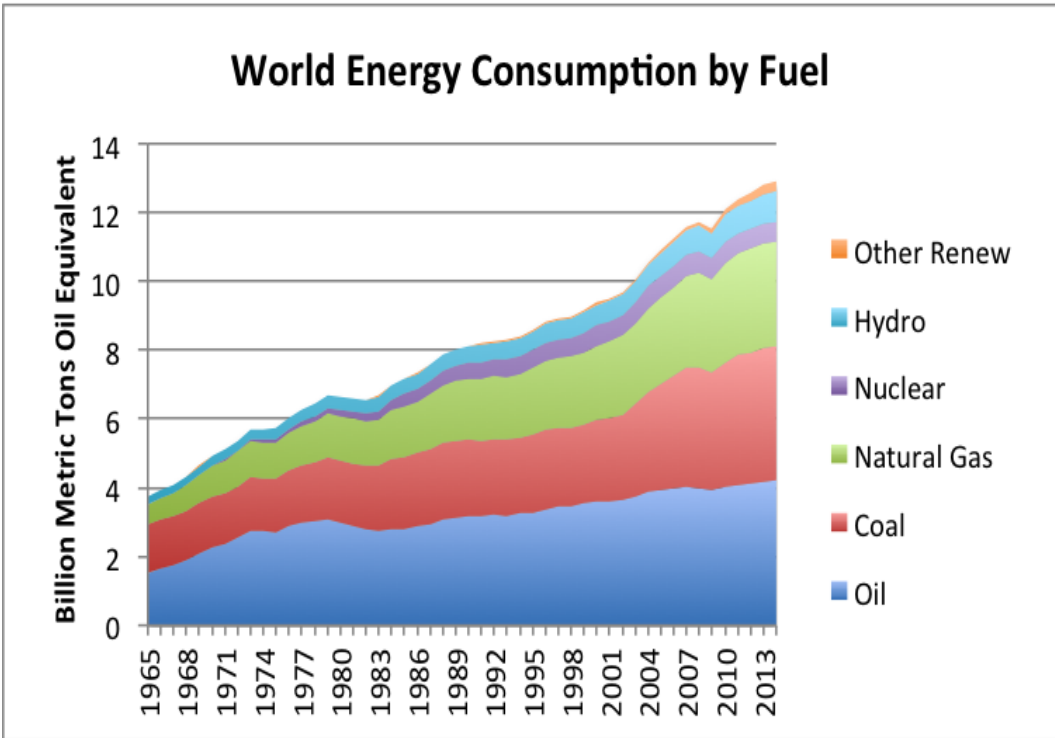


Figure 1.1 Share of World Total Energy Consumption by Source for the last 50 Years, based on BP Statistical Review of World Energy 2015 (BP, 2015c).

The IEA’s forecast of the global demand for primary energy in 1990 - 2040 is shown in Fig. 1.2. The outlook provides detailed demand, the supply of energy, and carbon dioxide for ten world regions. The 10 world regions are OECD North America, OECD Europe, OECD Pacific, Central and Eastern Europe countries, as OECD group;

Non-OECD group, China South Asia, East Asia, Africa, Middle East MENA, Latin America region. According to the World Economic Outlook (WEO) report (IEA, 2012), the energy demand will increase by almost three-quarter, from a current capacity of 5 429 GW in 2011 to 9 340 GW by 2035. Moreover, the prospect of global energy depends on the action of non-OECD countries (Khatib, 2012).

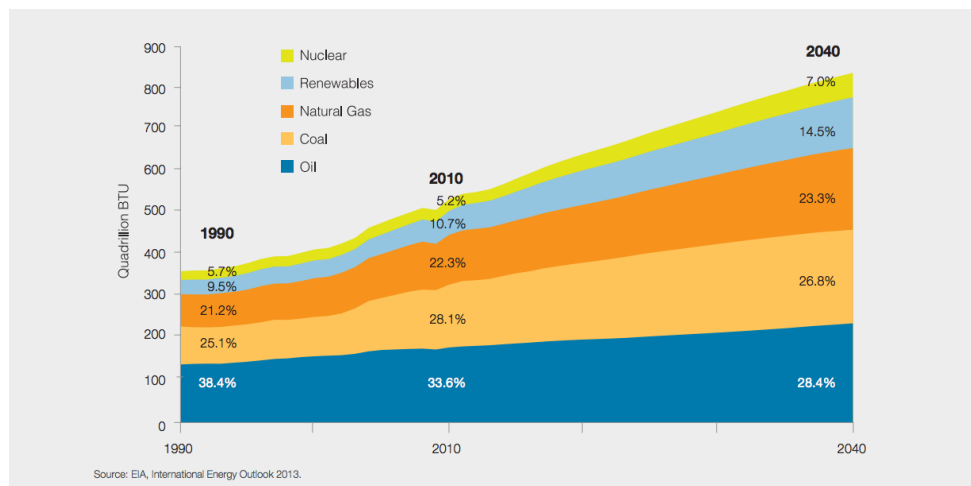


Figure 1.2 Future global energy demand by fuel , (IEA, 2013).

All these concerns led to a vital interest in raising awareness in developing alternative, sustainable energy to mitigate the greenhouse gas, CO₂ emission, limitation of natural resources, population growth, keeping the environment clean, and meeting the increasing demand for Energy. Solutions such as; efficient low-carbon, sustainable sources of energy and storage are a major option. Moreover, achieving secure, reliable, affordable energy services is critical for social development and economic growth.

Today, the interest in the utilisation of renewable resources and its applications has become ever more important and has increased significantly. Utilisation of the renewable resources as a supplement to fossil fuel energy has thus become a major

option. To mitigate the intermittency of the renewable energy generation, reduce the GHG emission, and meet the increasing demand for different energy variables approaches can be adopted, such as demand-side management and network solutions such as using the energy storage system (ESS). It has been suggested that renewable energy sources integration with ESS systems is an approach for a greater commercial penetration and improving the grid quality and stability. Moreover, comprehensive research and rapid development in several technologies are needed to increase the exploitation of renewable sources. The use of ESS has been motivated by the necessity of a device that can, (i) store a significant amount of energy and increase the renewable energy penetration, (ii) improve the power quality, and (iii) mitigate the GHS emissions, which will be the focus of this thesis.

1.3 Thesis Objective

The study commenced with a literature review of current energy, renewable energy sources, energy storage technologies, and possible potential technologies. The research work of this thesis is to explore benefits and the potential of battery energy storage, such as Nickel-Iron (NiFe) rechargeable batteries, to be used for large-scale energy storage.

The aims of this research are:

- I. To identify the current and future energy sources, and indicate the issues of integration of renewables into the grid.
- II. To review the energy storage systems and evaluate their potential application for renewable energy integration.

❖ The overall goal of the research is to review the iron-based battery, and to propose the potential of nickel-iron batteries for use in grid applications.

❖ Specific objectives

The main specific aims of the research are:

- I. Explore the charge/discharge cycling stability of NiFe cells.
- II. Explore the optimum weight of the iron electrode with additives.
- III. Explore the effects of several additives (such as carbon-black, bismuth sulfide, copper) on the electrochemical performance of iron-based battery electrodes.
- IV. To investigate the electrochemical mechanism of the iron-based electrode in the presence of several additives.

1.4 Structure of Thesis

The development and implementation of battery energy storage systems (BESS) are crucial for the future of renewable intermediate and grid application. Hence, there is a need to develop cost-effective, safe, environmental friendly BESS to meet these purposes.

The thesis will focus on the potential energy storages and benefits of a battery energy storage systems such as iron-based electrode battery.

Chapter 1- This section aims to give a review of the world energy demand and outline the rise in global energy demand, and the concern over the impact of used fuel on the environment, and the need for alternative sustainable energy sources.

Chapter 2 - This will detail the overview of renewable energy recourses, the role of energy storage with renewables and its potential in the energy market, highlight the challenges in using and integration of the renewable sources, and give a brief introduction to the energy storage, classification, and technical comparison of energy storage technologies.

Chapter 3 - Introduces the energy storages systems (ESS), the concept of ESS, the benefits of ESS, classification of the electrical energy storages systems, and the research challenges for the implementation of ESS, and technical comparison of the varies ESS types.

Chapter 4 - A literature review was undertaken, covering the following:

Introduction to battery systems, and to a general background for Iron-based electrodes batteries such as nickel-iron batteries, including : the history of NiFe batteries, general principle operation of the battery advantages, major limitations, some approaches for

improving the overall performance of the battery, characterization of battery performance, recent research and development of the battery, motivation and justification of the research, our approaches for improving the electrochemical performance of NiFe battery.

Chapter 5 -The main contributions of this section are: list of materials in this thesis are included, preparation of the electrodes active materials, the experimental procedures, a design of experiment for the electrochemical testing methods and characterizations techniques. It describes the principal instrumentations that is used in this study.

Chapter 6 -The influence of different electrode/electrolyte additives on the electrochemical properties of the iron anode electrodes are investigated, discussed, giving results, and summaries. Galvanostatic charge-discharge and cyclic voltammetry are used to evaluate the cells cycling performance. The physicochemical techniques used were; scanning electron microscopy (SEM), X-ray diffraction (XRD), atomic force microscopy (AFM), transmission electron microscopy (TEM) and High-resolution TEM (HRTEM) with energy dispersive X-ray analysis (EDS).

Chapter 7 - This section draws together the general conclusions derived from this thesis and proposes a future recommendation and target based on this thesis, followed by appendixes and lists of references. It is worth noting that the work in this thesis is supported by journal and conference paper publications.

Chapter 2 RENEWABLE ENERGY

Having discussed the energy review in chapter 1. This chapter will detail the overview of the renewable energy recourses and the role of energy storage with renewables.

2.1 The role of Renewable Energy (RE) and sustainable development

The affording of sufficient, reliable, and affordable energy source, in an environmental secure, conformity with economic development, is an important element of sustainable development. Energy is essential for improving human welfare, raising living standards, and eradicating poverty. Nonetheless, most of the current patterns of energy supply and use come from unsustainable sources of energy standards (UN, 2012).

There are many definitions of sustainable development, including this common one given by the international institute for sustainable development (IISD): *"Development that meets the needs of the present without compromising the ability of future generations to meet their own needs."* A simple concept of sustainability is this: no reduction of global resources with unlimited supply of clean energy.

To achieve sustainable energy development strategies, several major technological approaches must be applied: balancing supply and energy demand, efficiency improvements of the energy production, and more integration of renewable energy.

Nowadays, coal, oil, and gas provide 81% of the global energy needs (IEA, 2014). However, emission of carbon dioxide and other GHGs from fossil fuels in open areas have significant environmental and global warming effects. The high cost of

electricity and lack of access to clean energy, makes the unsustainable sources the frequent-choice energy in rural areas. However, the important issue of global warming and the growing trend of carbon dioxide emissions and GHGs from fossil fuels are restricting any sustainable development (Corbyn *et al.*, 2013). Energy from unsustainable sources, especially from fossil fuels, has its effects on the human health and environment. Balance between environmental preservation, economic growth, and energy productions is required. In short, development is not possible without energy. Hence, any sustainable development cannot be achieved without sustainable energy (UN, 2012).

Renewable, sustainable energy sources are crucial for our future energy and have the potential in replacing current fossil fuel energy sources, and carbon dioxide mitigation. Moreover, renewable energy sources seem to be a promising and attractive alternatives way of producing clean and sustainable energy. Furthermore, clear policy should be made and implemented by the governments and local utilities for such successful energy projects. Nowadays, several developing countries have made enormous strides and set targets and associated strategies in reducing their energy intensity and improve the energy access (Corbyn *et al.*, 2013). However, switching from the usual use of fuels (non-sustainable sources) remains challenging. Combinations of energy efficient technologies could be another option for investigation.

As populations continue to grow, the demand for more energy will increase. Nonetheless, the energy demand and supply are not only related to global warming, but also to several environmental concerns as air pollution, and greenhouse gases emission. One solution to these concerns is to make much more use of the renewable energy resources and technologies.

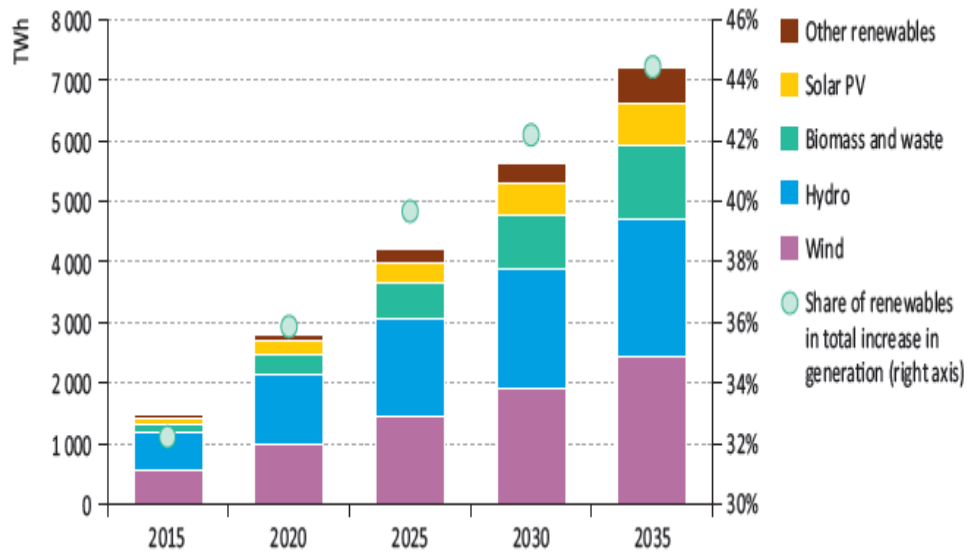


Figure 2.1 The global Renewables-based on Energy production relative to 2009 by Technology in the New Policies Scenario (IEA, 2011).

2.2 Renewable Resources

Renewable resources are considered as most clean, sustainable sources of energy. There are many forms of renewable energy. These sources can be divided into two groups; (a) natural renewable resources (wind, solar, hydro, geothermal, etc.) and (b) renewable resources resulting from human activity (landfill gas, biomass, and industrial heat recovery power system) (REN21, 2015). The main forms of renewable energy sources are given in Table.1.1 (Demirbaş, 2006).

Table 2-1 The main types of renewable sources and their usage options

Energy sources	Energy conversion and usage forms
Biomass	Pyrolysis, gasification, digestion
Geothermal	Urban heating, power generation, hydrothermal, hot dry rock
Solar	Solar home system, solar dryers, solar cookers
Direct solar	Photovoltaic, thermal power generation, water heaters
Wind	Power generation, wind generators, windmills, water pumps
Tidal	Barrage, tidal stream
Hydropower	Power generation
Wave	Numerous designs

Most of these renewable energies depend on the way or another on sunlight (solar), the wind and hydroelectric power. In 2014, the global share of different renewable sources (RES) to the total electricity generation were estimated to be 3.10% wind, 1.8% bio-power, 0.67% geothermal, 0.40% solar (Solar Thermal and PV) and 0.90% (REN21, 2015) as is presented in Figure 2.2.

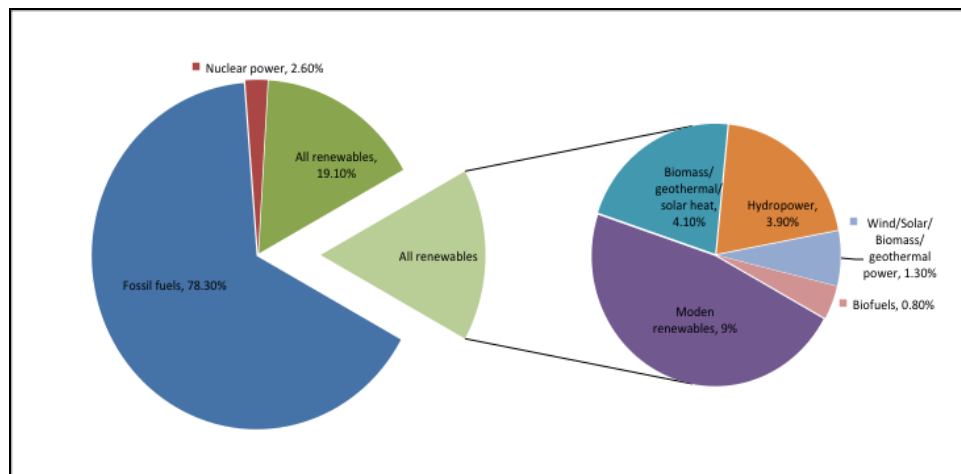


Figure 2.2 Estimated Renewable Energy Share of Global Electricity Production at the end of 2014 (REN21, 2015).

These renewable resources such as wind power and solar energy are widely available, abundant, and have vast energy potential, that can reduce greenhouse gas emissions and dependence on fossil fuels (IEA, 2014, Gutiérrez-Martín *et al.*, 2013). Wind and solar power are one of the most promising sources of alternative energy. Moreover, interest in solar and wind energy application has grown significantly over the last two decades (IEA, 2011). According to IEA, in a proposed renewable scenario, the total renewable contribution will be between one-third and one-half of all energy generated by 2020 (IEA, 2011). Moreover, it is estimated that by 2035 renewables will supply 43% of overall electricity in the European Union.

REN21's Report (Renewable 2015 Global Status Report), shows that , the global contribution of wind power, in particular, has grown rapidly over the past decade at a rate of 30% of adding global installed wind turbine of 51GW in 2014 (REN21 2015). Furthermore, in 2015, it is estimated that about 1.7 GW was added from grid-

connected offshore wind energy, with a global total exceeding 8.5GW. The Global Electricity production from wind raised by 27% and solar PV power by 42% per year during the period from 2000 to 2010 (IEA, 2014).

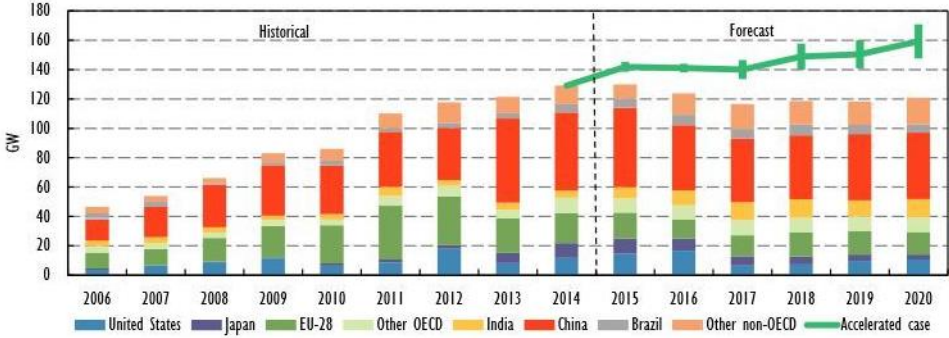


Figure 2.3 Onshore wind annual addition by region (IEA, 2015b).

PV power represents the world’s renewable source with the highest energy potential. Several PV power plants are operating already around the world. Solar photovoltaic installed capacity has grown rapidly from 67 GW 2011 to 600 GW in 2035. Energy generation from wind power increased from about 238 GW in 2011 to 1 100 GW in 2035. The offshore wind power capacity increased rapidly from 4 GW to 175 GW from the period from 2011 to 2035 (IEA, 2015a).

2.3 Challenges in integration variable renewable energy (RES)

With expanding of the power networks and the integration of renewable sources (RES) in small and large-scale power systems, the developing of new technologies for better renewable energy integration and utilisation is becoming a current global concern. However, achieving the RE target significantly can mitigate greenhouse gases (GHG's) and CO₂ emissions. The uncertainty, variability and fluctuations of these sources can pose challenges for a grid network, and require action to balance the system (Zakeri and Syri, 2015) , (Sundararagavan and Baker, 2012, Hasan *et al.*, 2013). However, Utilising all of the renewable energy would require an additional method to store the energy from renewable sources during the low demand, and then it release when needed. Moreover, RE such as the wind and solar PV power are not fully technically viable and are uncertain, because the wind does not continuously blow, and the sun does not always shine at any region, which would restrict generation from these sources. These resources are limited by environmental consideration and can be used only when resources are available. Nevertheless, energy generated from renewable sources cannot be directly stored, and most these renewable sources do not provide a constant energy supply; secondary storage systems are therefore required (Hill *et al.*, 2012). Therefore, to preserve system stability and flexibility, renewables must be used in combining with energy storage systems (ESS) (Loisel, 2012, Miller *et al.*, 2010). ESS is needed in a stand-alone wind and photovoltaic power system for the purpose of ensuring constant power flow, as these resources are usually located in an inaccessible area with limited grid connection (Lund, 2012).

Currently, ESS is considered one of the main strategies to integrate viable renewable energy sources. It can be utilised in different ways to help and optimise the existing grid. For instance, uncontrollable energy generation from renewable can be

stored during off-peak (when the electricity demand is low) and discharged during peak hour supply (high demand) (Benitez *et al.*, 2008, Zakeri and Syri, 2015). Hybrid technology in renewable energy sources has been used over recent years. It is accepted that REs are unavailable during a period, and intermittent renewables can not provide continuous renewable energy without energy storage systems (Chen *et al.*, 2009). Nevertheless, the utilisation and the adoption of the renewable technologies in large-scale is possible only if efficient, cost-effective storage technology is developed and implemented (Kaldellis and Zafirakis, 2007).

Various options are available and can be adopted to address the RES integration challenges, combining the energy generation from renewable sources (wind , solar, water turbine) with the large-scale energy storage power systems. ESS has the potential to provide backup power and play a vital role to balance the fluctuating supply to the current changing demand and enhance smoothing, and so secure the power quality (Ahmed *et al.*, 2008, Howlader *et al.*, 2013, Hasan *et al.*, 2013). However, the main barriers to utilisation of renewables are economy and technology. The technical challenges, system integration and public acceptance are other issues that may limit, and impact on RES development (REN21, 2015). As the share of renewables increases in the energy market, technologies and strategies are needed to solve the issues of intermittency of renewables. ESS is one of the main options proposed to achieve this purpose. ESS can be used in a several ways, and these can be divided into several categories: transmission and distribution, energy generation services, end-user, and renewable integration. In this thesis, the main issue will be the integration of potential renewables with ESS; this will be discussed in the next section, where ESS technologies and their benefits will be introduced.

Chapter 3 ENERGY STORAGE TECHNOLOGIES (ESS)

Having discussed an overview of current global energy consumption and demand, and the renewable resources and the role of energy storage with the renewables, this chapter, will detail the concept and the classification , potential ESS in the energy market, and will highlight the challenges in using and integration of the renewable sources.

3.1 The concept of energy storage

In engineering terms, energy storage (ES) technology refers to the method of converting energy from one form (such as wind/solar) into a storable form and then converted back into a chemical, electrochemical, mechanical or thermal form of energy to reused later whenever needed (Figure.3.1). Most of the stable forms of energy is are primary energy, which usually obtained in storable forms such as crude oil, and natural gas stored in tank farms. Biomass is another form of primary energy that may be retained as wood logs, and wood pellets. Coal also can be stored, either at coal fired power stations or industrial plants. On other hand, some primary forms of energy, such as the renewable resources, are not storable naturally. However, since primary energy can only be found in natural form, that cannot be used as a medium form for storing another form of energy. The increasing share of energy from renewable has eager to find new solutions to the intermittency of the renewable power. The wind, tidal, wave and solar power are the typical examples of renewable energy sources. However, these resources can only be stored by converting them to secondary forms of energy. Converting energy in a primary form such as renewables sources to the form of secondary form is a major challenge. From this point onward, the focus of

this work will be the potential for using energy storage technologies for capturing and storing energy from variable renewable energy resources.



Figure 3.1 Energy storage concept, Adapted with permission from ref (Aneke and Wang, 2016)

3.2 The benefits of energy storage

Nowadays, the wind and solar PV power are the most popular renewable energy sources (RES) that achieved rapid development and growth (IEA, 2012). Naturally, the wind and solar power renewable sources are intermittent. Several solutions supported by theory, experience, and test suggest, which energy storage systems (ESS) can be used. ESS seems to have potential solutions, which are already introduced and established on the market. ESS is the key to increasing the power transmitted to the grid and to dealing with the naturally intermittent renewable sources , and supply the bulk stored energy when needed.

The history of the use of energy storage technologies to integrate energy from renewable sources began in the early 20th century (Baker and Collinson, 1999, Chanson *et al.*, 1989). In the recent years as energy storage continue to grow in usage, several types of ESSs have been extensively developed and examined as storage for shifting viable renewable energy needed, and for grid support (peak shaving) to

achieve its economic dispatch. Moreover, storing the primary forms of energy such as renewables helps to reduce the demand for the fossil fuels consumed and lowers the greenhouse gas emissions that are associated with global warming. The following are some applications of ESS:

- Load levelling: it is defining as the utilisation of the stored energy at peak periods.
- Energy arbitrage: it is referred to the method of storing electricity at off-peaks where is the demand for energy and costs is low, and discharge it at periods of high demand when the cost of energy is high. Energy storage can store the excess of energy generation from renewables such as the wind and solar power energy.
- Spinning reserve: it is the way of using energy storage to reduce the requirement for the idling generation in the power grid.
- Side peak shaving: energy storage can be utilised as a backup to increase the reliability of a power system.
- Renewables integration: energy storage can be used to minimise the effect of intermittency of renewable by increasing their penetration in the power system.

Recently, there is a variety of globally installed electrical energy storage systems available, including; flywheels, compressed, capacitors, and battery energy storage. Batteries energy storages systems (BESS) are the focus of this thesis because BESS can store a significant amount of energy, efficiently. They can be distributed, located anywhere, and installed near residential areas (Figure 3.2). The other ESS systems lack some of these characteristics and therefore are not selected as the main topic of this thesis.

In the past decade, various BESSs such as lead-acid, Li-ion, alkaline batteries (Hori *et al.*, 2014, McDowall, 2006) has emerged, and been used, and have the advantages and potential to be used for grid applications (Figure.3.1). However, on other the hand, integration of variable renewable sources using storage technologies is facing several challenges.

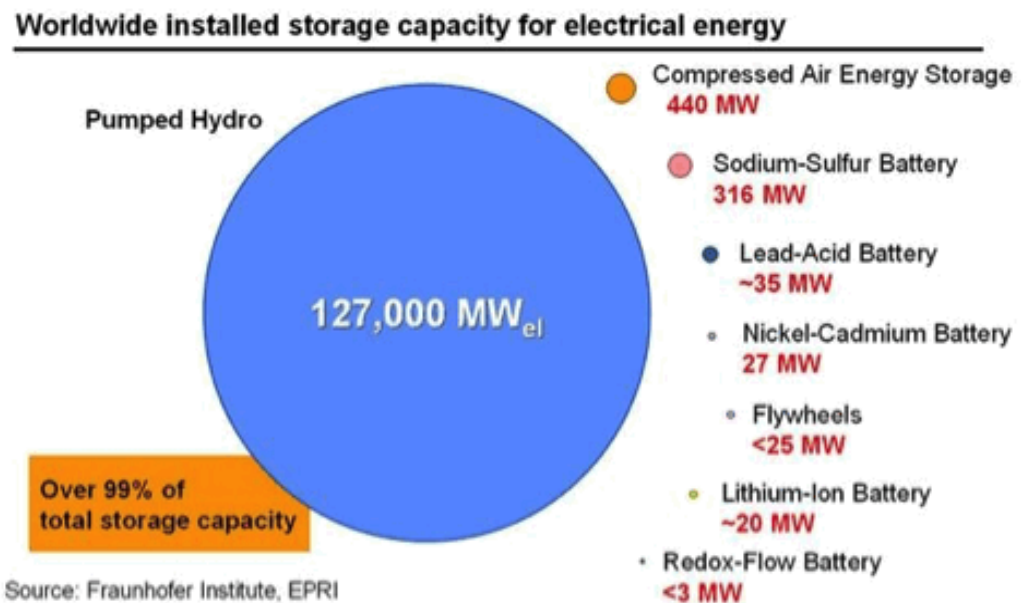


Figure 3.2 The global installed, grid connected, electrical storage capacity (MW). Adapted with permission from ref (Mahlia *et al.*, 2014).

Generally speaking, BESS can be charged with the random renewable wind turbine and PV output energy during low demand and discharged during high demand (Figure.3.2). The critical challenge in very high penetration levels is finding bulk energy storage options that are durable, efficient, and not prohibitively expensive (Qin *et al.*, 2014, Kaldellis *et al.*, 2009). To be able to explore and argue for the deployment and development of energy storage in combination with renewable, it is important to

clarify the classification and benefits of ESS. However, the variety of complex characteristics makes it difficult to adopt a specific technology for a particular purpose. Advantages, limitations, applications and cost, are common features in comparative of ESS.

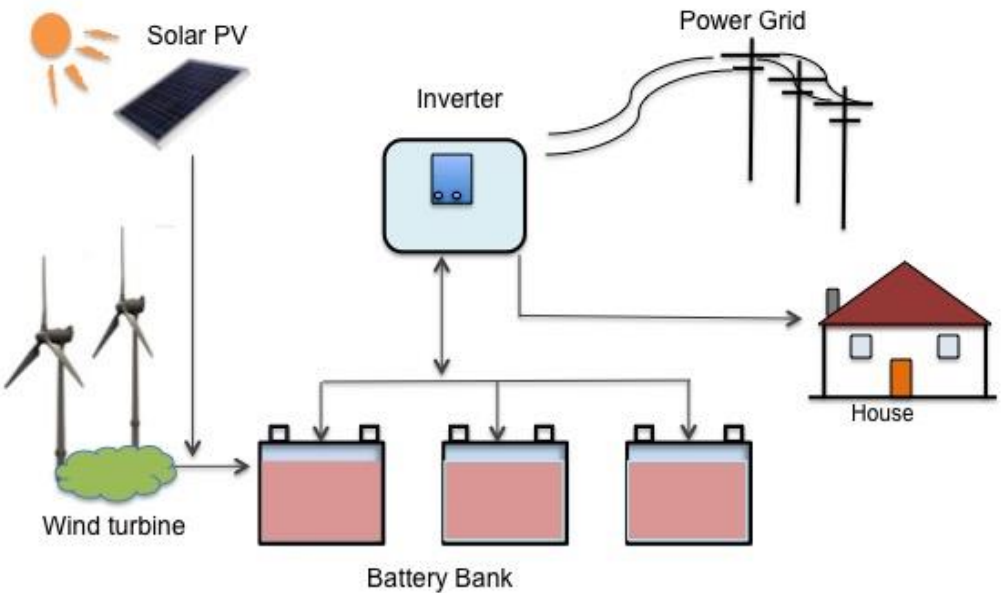


Figure 3-3 Schematic of the Battery connected Renewables power systems.

3.3 Classification of Electrical Energy Storage System (ESS)

There are several suggested ways for categorisation of ESS Technologies, such as their response time, their stored energy, and their storage durations (Chen *et al.*, 2009). In general, each type of ESS has its unique features/characteristics that can help in the determination of suitable energy storage technologies which can be adopted in any given circumstance. Fundamentally, by the form of storage, energy storage devices can be categorised into four main types as is illustrated in (Figure 3.4). Electrical storage includes capacitors, SMES, and supercapacitors, mechanical (e.g. flywheel,

pumped hydroelectricity storage), thermal (e.g. low and high-temperature energy storage) and chemical (e.g. Rechargeable batteries and hydrogen storage devices) (Chen *et al.*, 2009).

Overall, ESS can be classified into two broad categories. The first group is the group of ESS that is suited for power applications (since they have the capacity to store modest amounts of energy per rated MW output power in short period of discharge time), such as a flywheel, SMES, and capacitors. The second group is best suited for energy applications (which require relatively large amount of energy), such as pumped hydro, CAES, thermal, and batteries) (Chen *et al.*, 2009). For different ESS applications, the power and energy rating, capital cost, efficiency, self-discharge and cycle life are taken into consideration when characterising ESSs (Akinyele and Rayudu, 2014). Most of ESS has been classified in terms of power and energy applications. The classification of (EES) in this section categorised in term of their stored energy. A short description of the potential and commonly used ESS is presented in this chapter.

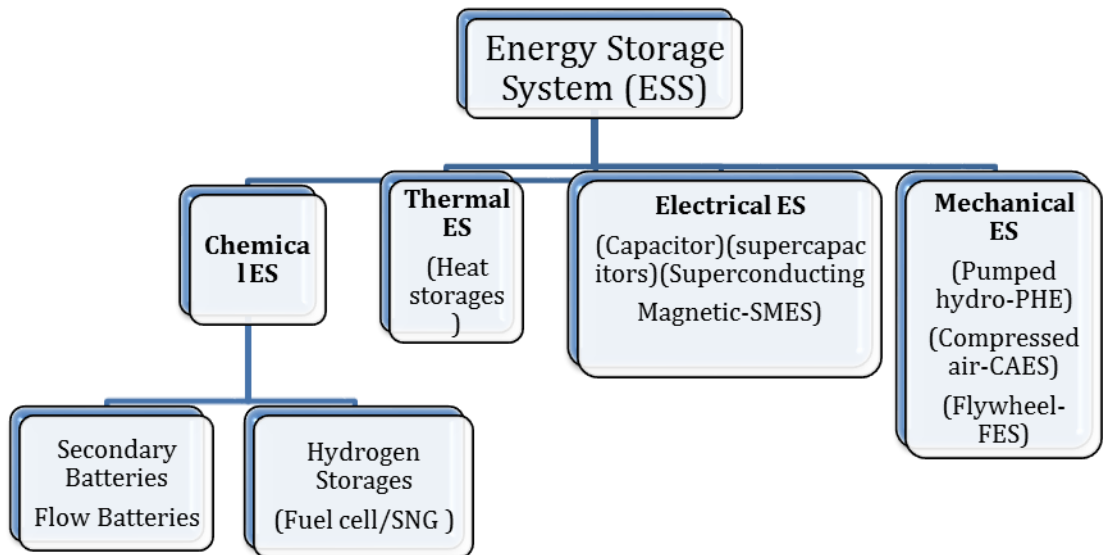


Figure 3.4 Classification of Energy Storage Technologies by the form of stored energy.

Adapted with permission from ref (Evans *et al.*, 2012).

3.3.1 Mechanical Energy Storage (MES)

Mechanical storage systems (MES) are devices that store energy in the form of kinetic energy in rotating mass. Pumped hydroelectric storage (PHS), compressed air energy storage (CAES) and flywheels (FES) are the primary known mechanical storage systems. These devices are not new and have been used for years to store energy and stabilise variable speed operation of the rotating machine. CAES and PHS systems can be adopted for large scale ES, while FES is more suitable for transitional storage.

3.3.1.1 Pumped Hydroelectric Energy Storage (PHS)

Pumped hydro energy storage (PHS) systems work through storing and producing energy by pumping water from low-level reservoir to some high dam or

tank. Then the stored water is released from the upper reservoir to the lower reservoir via a hydro turbine to produce electricity once the demand of the energy is high (Figure 3-5) (Mahlia *et al.*, 2014). Hence, the amount of the stored energy is ideally equal to the height difference between the two tanks and the amount of the accumulated water (Luo *et al.*, 2015). Their characteristics make them an ideal technology for load levelling, smoothing, and peak shaving. The efficiency of PHS storage is in the region of 65-85% (Yekini Suberu *et al.*, 2014), and the lifetime is around 30-50 years. However, the efficiency is limited by the effectiveness of the turbine unit. There are new sites under construction or in planning phase, and around 300 PHS systems operating worldwide (Dursun and Alboyaci, 2010).

PHS has very low energy and power densities. A large area and the proper terrain is required for storing such a large quantities of low density, which make building such a large facility difficult and costly. PHS plants may have negative impacts on the surrounding environment; but they have lower greenhouse emissions than fossil fuel-fired generators, which make them considered for renewable energy utilisation. However, the high cost of construction and the environmental concerns are the major limitations in the commercial deployment of the PHS. Yet, slight improvements in costs can be achieved with advanced new designs of the turbine and generator.

3.3.1.2 Flywheels Energy Storage (FES)

The method of storing energy using flywheel energy storage (FES) dates back to the Potters' Wheel, where has been a key element for industrial processes (Kousksou *et al.*, 2014). The first FES technology was used to smooth steam engine generation for large electric power systems. Commercial FES began to emerge in the 1990s and have been used to maintain the reliability and quality of the energy supply (Mears *et al.*,

2003). FES is a device that can store electrical energy in forms of rotational kinetic energy and its release on demand (Tan *et al.*, 2013). The mass rotates on two magnetic bearings in order to decrease the friction at high speed. Hence, the energy will transfer to or from the flywheel which functions as a generator/motor, that charges the ES device (Luo *et al.*, 2015). FES will be charged when the electric system regenerates through the drive. However, the maximum stored energy is dependent on the tensile strength of the flywheel materials. Thus, the highest specific energy is determined by the ratio of the energy density, rotating speed and density of the materials of the rotating disk (Luo *et al.*, 2015). Typically, there are two forms of flywheel; the standard steel rotor flywheel, and the advanced composite flywheels.

FES has favourable advantages compared with other ESs. FES are able to provide up to an hour of stored energy, and they have very high charge/discharge cycles, long lifetime (> 20 years), and high cycling capability. Furthermore, their disposal does not have environmental concerns, with the potential for integration of FES with the renewable power applications (Hadjipaschalis *et al.*, 2009). FES is used for power stabilisation purposes for underground train and trams. However, the relatively poor energy density, self-discharge (about 20%), major concerns for possible hazardous contingencies, operating noise and the high-cost are the major drawback for using FES for long-term energy (Hadjipaschalis *et al.*, 2009). Further research on the development of FES includes cost-effective materials and manufacturing is required to achieve cost reduction and durable mechanical stability. Development of high-speed and low-cost high mass FES are two major trends of ongoing research.

3.3.1.3 Compressed Air Energy Storage (CAES)

Compressed air energy storage (CAES) systems consist of a motor (to compress the air), high-pressure turbine (HPY), low-pressure turbine (LPT), and generator

Figure 3.6. CAES uses compressed air to store energy in a vessel underground and extracts the stored compressed air through a heat process before letting into turbine during off-peak electrical generation. There are three types of reservoir are considered; natural gas fields, that used for storing natural gas, mechanically formed reservoirs, and solution-mined salt caverns (Kousksou *et al.*, 2014). The interest in CAES began in the early 1970s; in 1978 the first CAES facility in Germany was operated and used to store off-peak load energy from a nuclear power plant (Mears *et al.*, 2003). The use of CAES is not globally widespread. Only two plants have been constructed so far; one is located in Huntorf, Germany with a storage capacity of 290 MW and the second one is located in McIntosh, Alabama, USA with a storage capacity of 110 MW (Mears *et al.*, 2003). The average storage capacity of CAES is in the ranges from 300 to 400 MW, with efficiency estimated at 68-75%, and lifetime at approximately 40 years (Mears *et al.*, 2003). The installation of CAES systems needs certain geological requirements, which has limited their deployments worldwide.

3.3.1.3.1 Research Challenges for prospects:

In order to make PHE, FES and CAES commercially viable for large-scale storage, reducing the cost (per KWh) of storage, time of construction, and the environmental issues are relatively important. Generally, the cost of CAES is similar to PHS and depends on the prices of facility size, containment vessel, and operating technology. However, the capital cost of CAES is much lesser than PHS, since the capital cost of CAES depends on the underground storage conditions (Swider, 2007).

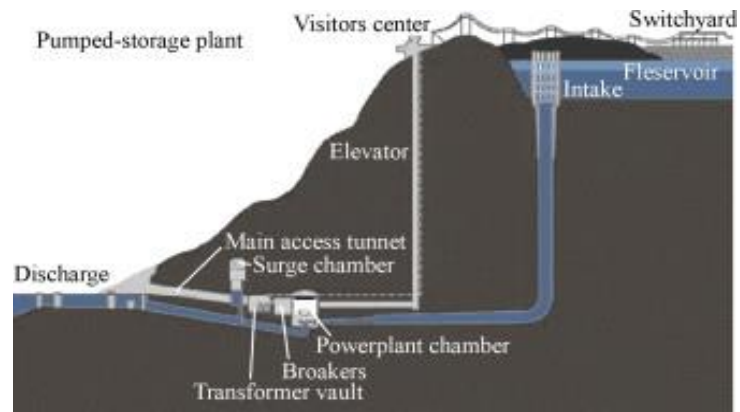


Figure 3-5 Schematic diagram of Pumped hydroelectric storage. Adapted with permission from ref (Chen *et al.*, 2009).

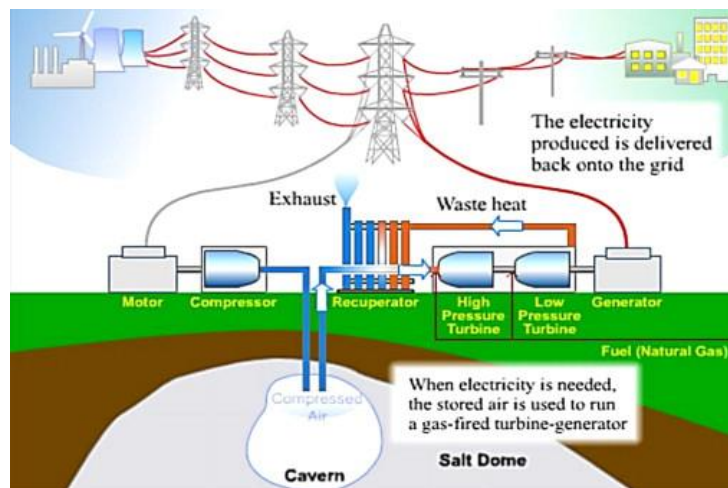


Figure 3.6 Schematic diagram of CAES. Adapted with permission from ref (Mahlia *et al.*, 2014).

3.3.2 Thermal Energy Storage Systems (TES)

Thermal energy storage technology (TES) is used to store a large amount of heat energy obtained by heating or cooling a storage media, to re-use it later in heating and cooling applications (Fernandes *et al.*, 2012). TES systems can store energy by changing the temperature of the storage medium (phase change; rock, soil, water, etc.).

TES in medium term ESSs can operate in similar regions to PHE and CAES systems. Depending on the running temperature, TES systems can be classified into two types: low-temperature thermal energy storage (LTTES) which operates in a temperature range below 200 °C and high-temperature thermal energy storage (HTTES), which operates from 200 °C to a high temperature (Fernandes *et al.*, 2012).

TES systems have the running of increasing the efficient use of thermal energy for large-scale switching. Moreover, recently there is great interest in using TES for solar thermal purposes such as cooling, heating, and air conditioning. TES can provide short and long-term storage for peak-load (Kousksou *et al.*, 2014). Due of their low heat losses, TES are suitable for long-term energy storage. However, the low-efficiency energy density and storage initial costs are the major challenges in the development of TES.

3.3.2.1.1 Research Challenges for prospects:

Research and development of TES systems, and in the field of cost-effective materials, high energy density, high efficiency, chemically and into the mechanically stable HTTES for the thermo-economic optimisation of TES systems is required in order to make TES more attractive for industrial processes (Fernandes *et al.*, 2012).

3.3.3 Electrical Storage Systems (EES)

The electrical energy storage system (EES) is one of the most available ways of storing energy in superconducting systems. The Capacitor is a device consist of two electrical conductors separated by a non-conducting material is used to store energy in the form of an electric field. Their unique characteristics make them suitable for maintaining electricity supplies with transmission standards. There are three types of capacitors; capacitors, supercapacitors, and superconducting magnetic energy storage (SMES).

3.3.3.1 Capacitors and supercapacitor

Electrochemical capacitors (ECs) also known as supercapacitor or ultracapacitors, are devices similar to batteries in design and manufacturing, contain two conductor electrodes, porous membrane separator and electrolyte (Figure 3.7) (Conway, 1999). ECs are capable of storing electrical charge on the surface between the two electrodes and the electrolyte by absorbing and releasing the charge much more quickly (Hall *et al.*, 2010). Depending on the charge storage mechanism, and the active material used (carbon-based materials are usually employed as the main electrode component), ECs can be distinguished into two types: (a) Electrochemical Double Layer Capacitors (EDLCs), where the device can accept and deliver charge rapidly at the interface between an electrode and electrolyte. (b) Pseudocapacitors or redox supercapacitor, where the device can deliver and accept charge through the exploitation of fast redox reaction at an electrode surface (Rennie *et al.*, 2016). The main component of EDLCs consists of electrode immersed in either organic or aqueous liquid electrolyte (Hall *et al.*, 2010).

In recent years, ECs have attracted significant attention due to their long cycle life (>100,000), high power density (> 10 kW Kg⁻¹) (Rennie *et al.*, 2016), and high charge/discharge rate. With respect to their energy density and power density, ECs can be found between classical capacitors and batteries. However, their safety issues including chemical, electrical, fire, and explosion hazards are the main challenge in the development of ECs. There are also environmental concerns due to the lack of recycling of the electrochemical capacitors.

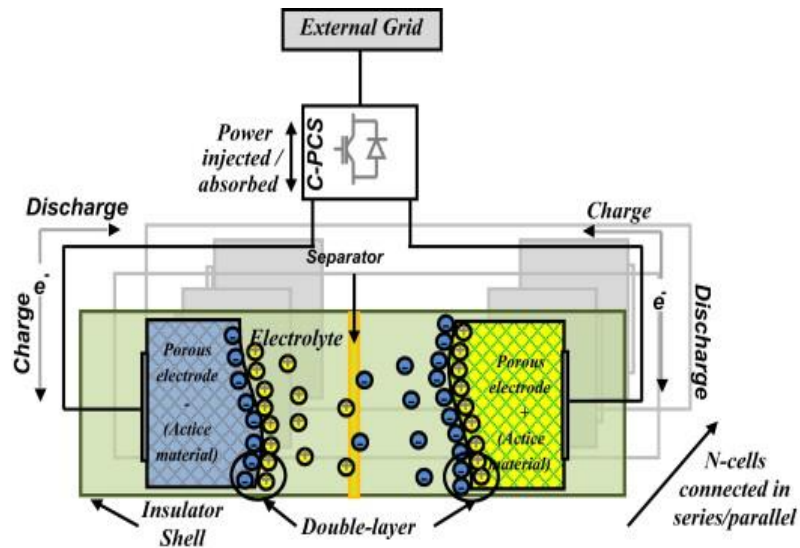


Figure 3.7 The capacitor storage system. Adapted with permission from ref (Kousksou *et al.*, 2014).

3.3.3.2 Superconducting Magnetic Energy Storage (SMES)

The superconducting magnetic energy storage (SMES) is a device that can store energy in the magnetic field, which generated by flowing current through a superconducting coil, without conversion to mechanical or chemical forms (Figure 3.8). The energy can be released by discharge of the coil. SMES can switch from full discharge to full charge very quickly and vice versa. Based on the response to a magnetic field SMES are classified into two types; Low temperature and high-temperature superconductor systems.

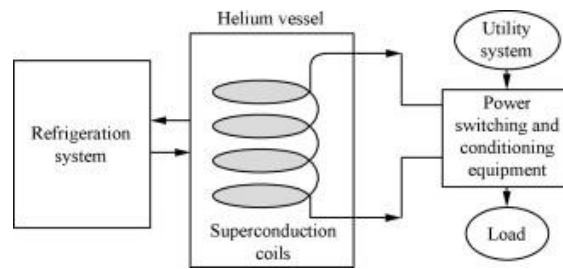


Figure 3.8 Superconducting magnetic energy storage.

Very high efficiency, permanent storage, immediate response and cycling capacity make SMES suitable for use in solving voltage stability and short-term storage power quality applications. However, the high, self-discharge and the high capital costs of the cooling unit are the biggest problems with SMES. Currently, SMES technologies with high-temperature superconductors remain under research with the aim of reducing the cooling demand.

3.3.3.2.1 Research Challenges for prospects:

Enhancing the specific capacitance, costs, and deployment of new electrode materials are the main challenges associated with ECs for further viable use in industrial applications. More research is needed to solve these problems stated above, and cost reduction must, therefore, be adept in the electrode material and electrolyte to make the ECs viable for large-scale applications

3.4 Chemical Energy Storage Systems (CES)

Chemical energy storage (CES) approaches are widely recognised as methods to combine viable renewable sources (RES) into the power grid. There are two major

branches of chemical storage (CES) technologies, electrochemical batteries and hydrogen storage.

3.4.1 Battery Storage Systems (BESS)

Chemical energy stores are the oldest technologies used to store energy from renewables and indeed, are implemented in conjunction with solar and wind power integration. Batteries and hydrogen fuel cells are most commonly known types of CES devices. Batteries systems are one of the conventional storage technologies available for power system applications. Basically, battery storage devices work by directly storing electricity in the form of chemical energy. The cells need to be connected to multiple sets, in parallel or series in order to achieve the desired battery voltage and capacity. Each cell is made of an anode and cathode together with the liquid, paste or solid electrolyte.

There are numerous types of BESSs available and developed for commercial use. Among them, lead-acid (LA) battery, lithium-ion (Li-ion), nickel metal hydride (NiMH) and nickel cadmium (NiCd) are the most widely used for power system applications. In this section, we consider the most common classes of batteries, which have received wide attention as potential candidates for the storage of viable renewable energy. Batteries storage technologies are summarised in Table 3-3 (Rahman *et al.*, 2012).

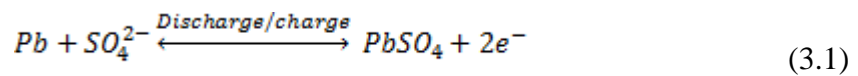
3.4.1.1 Lead-acid (LA) ES

Lead-acid batteries are rechargeable battery devices invented in 1859 by Gaston Plante and are today the most widely used for battery power in electric, hybrid vehicles, and energy storage applications (Kurzweil, 2010). Moreover, this remains an important technology in several commercial applications. Advanced LA batteries are being used in wind integration, peak shaving, and solar PV smoothing application.

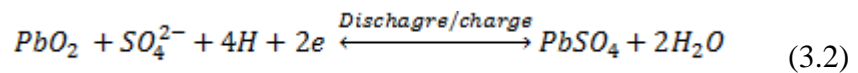
The cell chemical reaction based on a lead dioxide (forms at a cathode electrode), and metallic lead (form at the anode electrode), and sulfuric acid as electrolyte (Figure 3.9).

During discharging, both electrodes are converted into lead sulfate as in the following:-

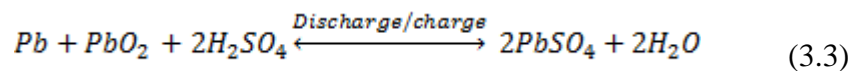
Anode:



Cathode:



Overall:



The reactions at each electrode are reversed during the charging process.

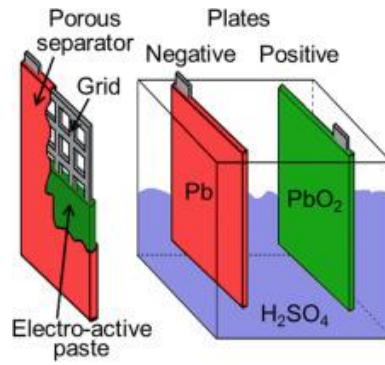


Figure 3.9 Schematic representation of a lead-acid cell (Posada *et al.*, 2017).

In general, there are two main types of LAB: valve-regulated lead-acid (VRLA) battery, and flooded batteries lead-acid (FLA) battery (which the common one). There are a variety of electrode designs, and additives have been developed for the anode and the cathode plates in enhancing the performance of the battery.

The low cost (\$300-600/kWh), high efficiency (65-80%) (Yekini Suberu *et al.*, 2014) and reliability make it a popular choice for power quality and some spinning reserve applications. Nevertheless, LA has been used only a little in commercial and large-scale energy application. However, the relatively poor performances, short lifetime (500-1000 cycles), low energy density (30-50 Wh/kg), and their weight are the main disadvantage of the LA batteries. Moreover, the major concerns about the environment restrained the deployment of this battery and limited the potential in the expanding role of grid applications.

3.4.1.1.1 Research Challenges for prospects:

LA batteries are commercially available, but it should be pointed out that further research on advanced LA batteries is required. However, reducing the weight in the cells is necessary, in order to increase the energy density (about 30 Wh kg⁻¹), The

relatively low charge/discharge efficiency, limited cycle life and the toxicity of the raw materials are another major challenges (Posada *et al.*, 2017).

3.4.1.2 Lithium-ion (Li-ion) ES battery

Lithium-ion (Li-ion) batteries were first proposed in the 1960s. The demand for these types of cells has grown commercially since the 1990s in the field of material technology, power devices, electric vehicles, and stationary storage applications. Moreover, Li-ion batteries are mainly used as a medium and short-term storage. Several demonstration projects with Li-ion battery containers exist nowadays. The anode in this type of battery is made of graphitic carbon. The cathode is made of lithium metal oxide such as lithium cobalt oxide (LiCoO₂). The Anode and cathode are divided by an organic electrolyte solution dissolved lithium salts, such as lithium perchlorate (LiClO₄). A variety of additives have been introduced to stabilise the electrode/electrolyte interfaces.

The battery has low self-discharge, high energy density (75 Wh/kg), and cycle life, great performance. Moreover, the battery can possess good cycle life (500-300), high efficiency, and high power capability (Linden and Reddy, 2002). However, high cost (>\$600/kWh) (Chen *et al.*, 2009), internal overcharge protection and poor safety make the Li-ion battery inappropriate for use in back-up, and large-scale application.

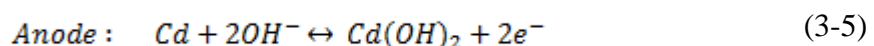
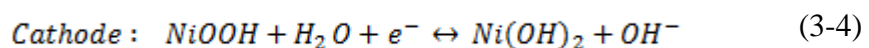
3.4.1.2.1 Research challenges for prospects:

Currently, Li-ion battery technology is widely researched. Several research efforts continue on new cathode materials to reduce the manufacturing cost, enhancing safety, improving the performance of the cell to capture a significant amount of the energy market.

3.4.1.3 Alkaline batteries ES battery

Nickel-based rechargeable alkaline cells such as nickel-cadmium (Ni-Cd) and nickel-iron (Ni-Fe) alkaline rechargeable battery are among the oldest devices developed and have been studied since the 1900s. In the Ni-Cd battery nickel species as the positive and cadmium species as the negative electrodes active materials and an aqueous alkali solution as the electrolyte are the main components. In general industrial applications, this battery is commonly found in two different types: in flooded or sealed form, depending on the application.

The Ni-Cd battery type has good characteristics; they can offer relatively high energy density (50-75 Wh/kg), long cycle life (more than 2000 cycles), a robust reliability and low maintenance requirements (Beaudin *et al.*, 2010). These advantages make the battery favoured for portable devices, and power system. However, the relatively high cost (up to 10 times that LA battery) and the environmental concerns linked to the toxicity of the heavy metals (Cd), are the major drawbacks of Ni-Cd batteries.



In the nickel-metal hydride (NiMH) battery, the cadmium is replaced by alloys that are capable of absorbing the hydrogen atoms. Both Ni-Cd and NiMH batteries have similar charge characteristics. NiMH batteries have been used in widespread applications, such as portable and electronic devices. The battery has almost double the capacity of the nickel-cadmium battery, up to 100 Wh /kg specific energy, and uses safer materials (Posada *et al.*, 2017), and environmentally friendly materials. NiMH,

however, is more expensive than the Ni-Cd battery and suffers from a higher self-discharge rate.

The nickel-iron battery (NiFe) was invented since the 1800s and developed by Thomas Edison in the US. NiFe has been used in various stationary applications until the 1980s when the battery was supplanted by low-cost sealed LAB (Posada *et al.*, 2017). In NiFe is iron used as an anode with nickel oxide hydroxide used as a cathode. Recently, iron-based batteries such as NiFe have attracted the renewed interest, owing it their eco-friendly, robust, inflammable electrolyte and cost-effective, abundant materials, which make them are highly suitable for meeting the emerging need for grid electrical energy storage systems (Posada *et al.*, 2017).

3.4.1.3.1 Research challenges for prospects:

The major challenges that hinder the practical applications of alkaline batteries include : the low charge/discharge efficiencies (30- 60 %), low specific energy. The toxicity of the raw materials of some alkaline batteries is another major challenge (Posada *et al.*, 2017).

3.4.2 Hydrogen based fuel cell energy storage (HES)

Hydrogen is clean and the lightest fuel expected to play a significant role in future power systems. The process of HES involves the electrolysis of water to form hydrogen gas, which is then compressed. Hydrogen can be stored and then can be converted to another energy source. Moreover, hydrogen can be directly used in hydrogen cars with fuel cells or to drive combustion engines or heat generation.

Currently, hydrogen-based fuel cell energy storage is receiving attention, especially in relation to their potential integration with renewables. Fuel cells (FCs) systems, like batteries, are electrochemical devices for the production of energy, and have potential to backup viable renewable energy sources (Oseghale *et al.*, 2015). There are four main technologies for hydrogen-based storage: hydrogen pressurisation, hydrogen adsorption in a metal hydride, the adsorption of hydrogen on carbon nano-fiber and the liquefaction of hydrogen (Kousksou *et al.*, 2014). Nevertheless, despite these advantages, poor efficiency, the high cost of hydrogen fuel at the present and the relatively low round-trip efficiency are the main barriers to the implementation of this type of technology.

3.4.2.1.1 Research Challenges for prospects:

The application of HES in the context of renewables integration at a large scale is expected to become more important for the future power systems. However, increase HES efficiency at low cost is the main challenges for the deployment of HES systems for long-term storage of electricity.

3.5 Technical Comparison of Energy Storages Technologies

This section brings the technical comparison characteristics of the previously discussed storage technologies. Several electrical energy storages (ES) have been discussed in above section. ES technologies can be compared based on several key factors. Some of these key factors (technical, commercial, and environmental) must be considered in order to select a type of storage for a target application:

- **Optimal Power/Energy level:**

The volumetric energy density refers to the stored energy divided by the volume of the whole energy storage system, where power density can be described in gravimetric (W/kg) or volumetric (W/L) terms. Energy storage systems with high power density are suitable for applications which require high power density and adequate fast response time, and they have the ability to provide sufficient energy supporting.

- **Overall Efficiency:** This refers to the fraction of energy removed that is returned to the grid during one charge/discharge cycle.

- **Cycle life or calendar life:** It is definite as the lifetime of storage system subject to repeated discharge-charge cycles. Cycle life for any given energy storage technology plays a significant part in adopting storage technology for any given application. ES systems with long cycle life are usually preferred over those with short cycle life from an investment point of view.

- **Cost:** The cost of ES system is one of the most important factors for commercial deployment of any given storage technology. The capital cost and operating expenses (which cover the cost of maintenance and disposal) should be added to the total cost for any given storage systems. The costs per kW h, per kW, and per kW h per cycle are usually used to calculate the cost of various storage technologies (Chen *et al.*, 2009).

- **Storage Capacity:** The total stored energy defines the ESS capacity, which is measured in Watt-hours (Wh) or Kilowatt-hours (kWh).

- **Response Time/ Discharge duration:** Response time is defined how quickly a storage technology can be charged/discharged, while the discharge duration refers to how long a storage device can maintain output.

The choice of the ideal storage technology option depends on many of factors. These are among the major factors: availability of raw materials, ability to sustain a significant amount of charging, storing and discharging cycles, safety, operating temperature, self-discharge. The discharge time of the ESS is one characteristic that can identify possible option for a given purpose. Hence, ESS with high efficiency and low cost will increase the value of the selected system.

Base on these criteria and for the better understanding of storages characteristics, we intend to make general comparisons between storage technologies that are discussed above by means of; advantage, disadvantages, opportunities, and threats (Yang *et al.*, 2008) presented in Table 3-1. Comparing the performance of various technologies based on different lists of criteria from technical, commercial, and eco-friendliness of the materials is commonly used (Luo *et al.*, 2015, Akinyele and Rayudu, 2014, Guney and Tepe).

ESS can be compared based on how quickly they discharge, and on their power, and energy output. The cycle life, costs and the efficiency of the storage technologies are also used (Chen *et al.*, 2009).

Comparisons of ESS based on; short discharge time (seconds to minutes), medium discharge time (minutes to hours), and long discharge time (days to months) are also can be used. Comparison and assessment of ESS is based on the technical maturity, where ESS can be classified into three groups: mature technologies, developed technologies, and emerging technologies (Chen *et al.*, 2009).

Table 3-1 Comparison of different energy storages types

Storage	Advantages	Disadvantages	Opportunities	Threats
CAES	Low cost per kWh. High capacity. Minor needs for power electronic converters.	Need for underground cavities. Need for fuel	Can prospectively be adopted for distributed storage	Popularity relative to thermal power plants
PHES	Low cost per kWh. High capacity. Minor needs for power electronic converters.	Geographical restrictions. Centralized storage	Can be used for offshore wind parks, with lower reservoir under seabed.	Can become obsolete when distributed storage preferred
BESS	Distributed storage. Good configurability	Cycle life. High investment costs. Temperature dependent.	Emerging technologies	Constant development phase complicates selection. Raw materials limited
FES	Very vast recharge. High capacity. Low environmental impact	Low energy density. Large standby losses	Utility-scale level	Promised increase in efficiency is not reached. Cheaper technologies available
SMES	High capacity. Short access time. High efficiency. Long life time	Low energy density. High production costs. Potential adverse health impact	Power quality	Security requirements due to very low temperatures and high magnetic fields
Supercapacitors	High efficiency. long life cycle. Very vast recharge	Low energy density.	Power quality with very high power demand and cycle load	High power applications by high power Li-ion might be served

Comparison of several typical ESSs is presented in Table 3-2. It is evident from this table that a variety of conventional storage technologies exists with different technical details and characteristics intended for various applications. From the table, we can see that, in terms of energy and power density, FESs, CAES, SMES, and supercapacitors have a lower energy density (Chen *et al.*, 2009). Among the ESSs, the BESSs, TES and CAES have a higher energy density than other ESS, while CAES, and PHS have large storage capacity. When considering ES systems response time, SMES, FES, and supercapacitors have a fast response time, followed by BESS with response time in order of seconds, then CAES, and PHS in the order of minutes.

In terms of costs comparison of ESS technologies, BESS technologies have lower power capacity costs, with higher energy capacity costs, and faster response times. All BESSs, PHS, SMES, supercapacitors and CAES have high cycle efficiency, while TES have an efficiency lower than 60%.

CAES, PHES, and FES energy storage systems have a relatively long lifetime. However, SMES and super-Capacitors are mainly used when we consider ESSs for short-term storage application. For the residential energy storage and vehicles application, batteries energy systems are preferred. All batteries technologies, PHE, and CAES can be used when we consider the storages plants for the daily storage application. The environmental impacts of BESS are also presented in Table 3-2. CAES, PHS, SMES and BESSs have negative influences on the environment.

Table 3-2 Comparison of selected battery technologies

	Lead-acid	Ni-Cd	Li-ion	NaS	NiMH	Fe-air	NiFe
Efficiency (%)	50-70	65-70	60	75-90	70	45	55-65
Energy density (Wh/kg)	30-50	50	75	60-130	30-80	60-80	30-50
Power density (W/kg)	50-100	40-80	130-300	10-90	70-200	20-150	30-110
Cycle life	200-250 300-500	1500	500- 3000	2500	400-500	300	2000+
Operating temperature °C	-10-40	-40-50	-30-6-	300-350	-30-50		-10-40
Self-discharge rate at 20 °C % loss per year	30	28	10-	~0	30	20	20
Cost (\$/kWh)	25-40	70-80	500-700		550	5-10	50-60

Table 3-3 A summary of batteries storage technologies

Technology	Advantage	Disadvantage
Sodium sulfur Batteries (NAS)	High energy and power density, relatively matured, high efficiency and excellent life cycle	High initial cost, safety concerns
Fe-air	Low cost, eco-friendless, abundant raw materials	Low efficiency, low energy density, self-discharge
Regenerative zinc-air	High energy and power density	Relatively new and untested
Lithium metal polymer batteries	High energy and power density, relatively tolerant to temperature extremes	Requires balancing and charge control electronics, high initial cost
Vented Ni-Cd	Mature and well known, high efficiency, high energy and power density, better lifecycle than lead acid, relatively tolerant to temperature extremes	Float effect makes capacity testing difficult, more expensive than lead acid, toxic components (cadmium), low cell voltage
NiMH	Less toxic than Ni-Cd, mature technology, high energy and power density, better cycle life than lead acid	Float effect makes capacity testing difficult, more expensive than lead acid, low cell voltage, intolerant of temperature extremes
Valve regulated Pb acid and Vented Pb acid	Mature and well known, low cost, high reliability and efficiency	Low life, intolerant of temperature extremes
Vented Pb acid		Poor low temperature performance, high maintenance cost, low energy density and cycle life, can't handle temperature extremes

3.6 General Remarks

As indicated in Figure 3.4, several energy storage systems (ESS) have been compared technically, with differing storage methods and essential characteristics. In recent years, several energy storages systems with differing in terms of specifications and characteristics have been developed and new technologies have emerged. Currently, ESS Technology has become the potential and possible solution to energy supply, security, and increasing demand for energy. No one ESS has all the ideal characteristics needed for optimal grid integration of the viable renewable energy. To understand the most widely applied and greatest potential storage technologies, these have been compared in term of energy, power density, cost, self-discharge, cycle life, efficiency, time of storing or releasing the energy, and environmental limitations. The challenges facing the future deployment of the storage types is also presented. Some ES technologies are in the concept stage, such as PHS, CAES, and BESSs have the potential to be employed for large-scale grid applications. PHS, BESS, CAES, FES, and ECs are technically developed, and commercially available. The research on some energy storage systems such as supercapacitors and thermal storage is still at the demonstration or research stage large for storage applications. The relatively high cost of some storage technologies such as FES and SMES, is the major challenge to production scale-up and the commercial deployment of these technologies at grid scale. Additionally, the limited storage capacity of some storage technologies such as FES, ECs, are insufficient to meet the requirements of the power industry. Placement flexibility of ES systems is one of the barriers to development, and widespread use of the ES technologies.

Based on the review above, large-scale batteries electrochemical energy storage are a promising technology and are expected to be gradually implemented for grid applications, due to the fact that BESS can store a significant amount of energy, and

have relatively long discharge times (Posada *et al.*, 2017). For large-scale energy storage to be viable, the cost of materials, safety, and the environmental impact are the most important factors for storage to be viable in use for large-scale (Posada *et al.*, 2017). The durability and reliability of the ESS must be addressed for stationary applications. Moreover, ESS must have a long cycle life (e.g. > 4000 deep cycles), long calendar life (e.g. > 15 years) and minimal maintenance. In addition, how much charging capacity, and how fast the ESS respond to the grid are main parameters for ESS commercial capability.

Among the BESS presented above, Li-ion batteries in terms of energy density, outperform competing technologies such as NiMH, LA, and Ni-Cd batteries. However, the manufacturing cost and safety issues of the cells remain a problem and impede the cell from being used extensively in a large battery energy storage implementation.

For these reasons, batteries energy storage systems, especially aqueous electrolyte ESS systems are a favourable candidate and have the potential to store significant amounts of renewable energy. Recently, considerable interest has been growing in battery technology developed in the past few decades, such as nickel-iron (NiFe) batteries. These batteries are suitable battery technologies to meet the need for the large-scale grid application.

This work proposes the potential of iron-based electrodes alkaline battery such as NiFe, for use in large-scale power applications. The proposed method seeks to tackle the problems associated with the iron electrodes, and thereby enhancing the overall capacity of the cell.

Chapter 4 LITERATURE REVIEW AND RESEARCH PURPOSE

This chapter reviews the recent literature relevant to the studies in this thesis. This chapter provides a brief introduction to the battery fundamental; the iron-based electrode battery will focus on the Iron-based battery, such as Nickel/Iron battery (NiFe) literature.

With efforts to increase the role of renewables sources (RES) such as the wind and solar power, there is a corresponding need for advanced, inexpensive, efficient energy storage system on the small or grid-scale for effective utilisation method of these resources. Among several numbers of energy storage technologies, electrochemical battery energy storage iron-based batteries are promising and have the potential to meet this goal. In order to investigate and to examine, any type of battery and how it stores electric energy, a basic understanding of battery is required.

4.1 Introduction to Batteries

The battery is a device that converts chemical energy into electrical energy by means of an electrochemical oxidation-reduction (redox) reaction (Linden and Reddy, 2002). In the basic electrochemical unit, the term “cell” is used and often referred to by the term “battery”. Thus, the battery consists of one or more of these cells are combined in series or parallel, or both, depending on the desired output capacity and voltage (Linden and Reddy, 2002). Depending on the reversibility of the redox reaction of the electrodes active material, the batteries can be categorised into two types: a primary cell (non-rechargeable) is not capable of being recharged electrically since the electrochemical reaction is irreversible, whereas a secondary (rechargeable)

cell are undergo multiple charge-discharge cycles). Rechargeable batteries are storage devices, and also known as “storage batteries”. Base in their application, rechargeable batteries fall into two main categories: a rechargeable battery used as an energy storage devices, and a rechargeable batteries used as a primary battery which can be recharged after use rather than discarded. The rechargeable battery types are manufactured in various size, forms, and structure, where a unique mix of substances of electrodes and electrolyte are utilised, such as Pd-acid, Ni-Cd, Li-ion, Ni-MH batteries.

4.1.1 Principle of operation

As showing in **Error! Reference source not found.** basically, the battery has three main components: the cathode or positive electrode, anode or negative electrode, and an electrolyte or ionic conductor, which provide the pathway for ionic transport between the electrodes and enables charge balance. Basically, when the battery is connected to an external load, and an electric circuit is completed in the electrolyte, the electron flow causes oxidation and reduction reactions. The amount of current flow during the chemical reaction is proportional to the amount of electricity passed. Faraday’s laws and the rate of current flow govern the charge transfer reaction.

At the anode during the discharge, O, is oxidised and the electrons are delivered to the external circuit:



At the cathode, R, the reduction reaction occurs when the electron accepted from the external circuit (Cho *et al.*, 2015):



In an electrochemical cell, the overall reaction is composed of two independent half-cell reactions at the two electrodes, which can be described as:

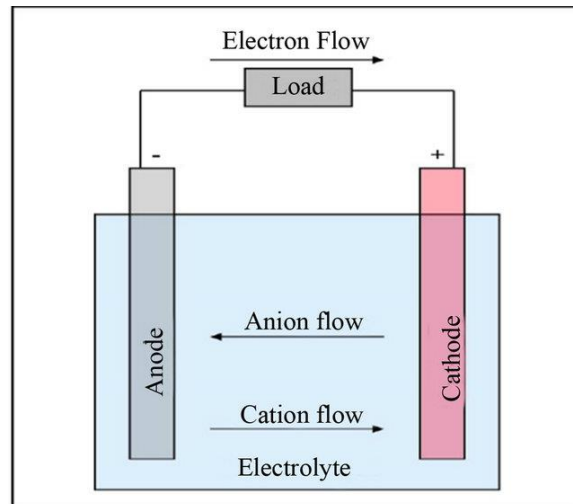
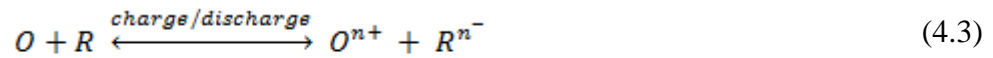


Figure 4-1 Working principle of a battery.

4.1.2 Battery characteristics

There are certain terms used to clarify the battery process, which will be used in this thesis.

Voltage (Cell potential):

The battery potentials are relying upon the free energy changes in overall reaction, which can determine in the Nernst equation;

$$E_{cell} = E_{cell}^{\circ} - \frac{RT}{nF} \ln Q \quad (4.4)$$

Where $E_{\text{cell}} = E_{\text{cathode}} - E_{\text{anode}}$ and Q is the reaction quotient for the cell reaction, E^0_{cell} is the standard cell potential at the temperature of interest, R is the universal gas constant ($8.314 \text{ J K}^{-1} \text{ mol}^{-1}$), F is the Faraday constant.

To simplify the equation, RT/F is treated as a constant, and the Nernst equation can be expressed in logarithmic terms:

$$E_{\text{cell}} = E^0_{\text{cell}} - \frac{0.05916}{n} \text{Log}_{10} \frac{a_{\text{Red}}}{a_{\text{Ox}}} \quad (4.5)$$

The potential difference on the cell can be vary and is reliant on standard electrode potential between the cathode and anode according to the composition of electrodes, concentration of the ions in the cell, and the temperature. When the chemical reaction occurs in the cell, the free energy will decrease due to its transformation into electrical energy. The cell potentials are related to free energy charge, which can determine from the thermodynamic Gibb's free energy charge in Equation (4.6) (Pletcher 1982);

$$\Delta G = -nFE \quad , \quad \text{then } E = \frac{-\Delta G}{n.F} \quad (4.6)$$

Where F is the Faraday constant (96500 C/mol), n is the number of electrons transferred per mole reaction; E is the cell electromotive force (EMF). This relationship between electrode potential and the Gibbs's free energy is the change when the reactants in the cell reaction have unit activity. At equilibrium conditions Gibbs's free energy can be expressed as;

$$\Delta G^0 = -nFE^0_{\text{cell}} \quad \text{then } E^0 = \frac{-\Delta G^0}{n.F} \quad (4.7)$$

Where E^0 is the standard cell potential, which correlated with standard Gibb's free energy charge (ΔG^0). Here, a positive value of E^0 indicates that cell reaction occurs

spontaneously (negative free energy change and a positive E) (Winter and Brodd, 2004). The individual electron potentials are always measured with reference to another electrode that is set as a standard. The standard hydrogen electrode (SHE) is normally used as standard electrode. However, an irreversible energy loss, as waste heat can occur when the current (I) is applied to the cell is induced by the polarised resistance components (overpotential or overvoltage) leading to a decrease of the actual cell potential from ideal potential as shown in Figure 4.2. The overpotential can be classified into three types:

- Activation polarisation: this is linked to the activation energy (kinetics) of the electrochemical reactions at the interface between electrodes and electrolyte.
- Concentration polarisation: This is as result of limited mass transport rates of the reactants, and depends on the current density and the electrode structure.
- Ohmic polarization: This is caused by ionic resistance in the electrolyte and electrode, current collectors within the cell, and is proportional to the current density.

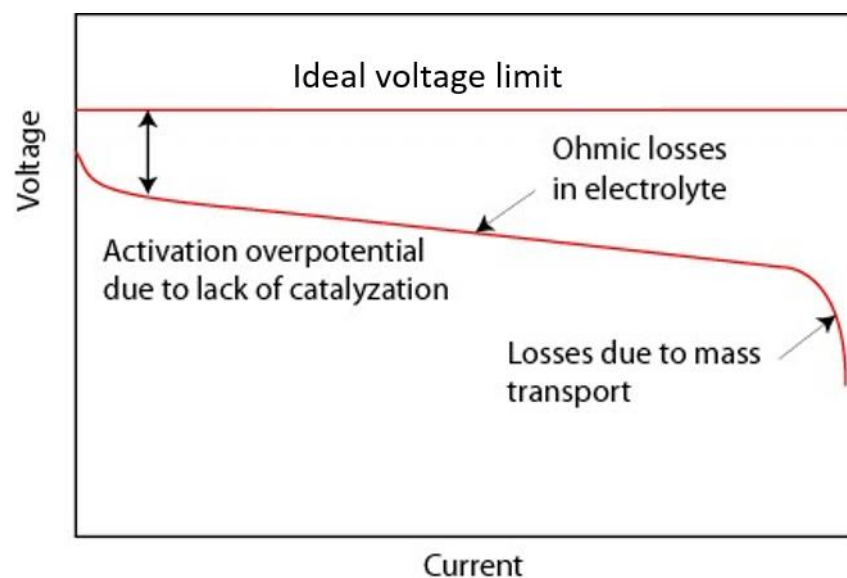


Figure 4.2 The polarisation curve for a typical battery, Adapted with permission from ref (Cho *et al.*, 2015).

The overpotential is given by Equation (4.8) (Winter and Brodd, 2004):

$$\eta = E_{ocv} - E_{op} \quad (4.8)$$

Where E_{op} is the operating voltage, E_{ocv} is the open-circuit voltage (OCV) is the potential difference between the electrodes), and η is the overpotential. Therefore, the available energy can be maximised when the cell voltage is close to operating voltage (OCV¹), since this voltage is related to the cell capacity and average operating voltage. The E_{ocv} , and the capacity of the cell, Q , are very important parameters, which are mainly used for energy determination. The cell overpotential depends on the electrode shape and size, electrolyte composition and concentration, temperature, applied current density, etc. Thus, a cell with an expanded energy can be designed by selecting the anode and cathode materials. Also, a cell with high ionic electrolyte conductivity has a decreased ohmic polarisation. Moreover, the electrode should be designed as a porous structure to reduce the activation polarisation of the cell.

- **Cell Capacity:**

The cell capacity (Q) is the total charge on the electrode for the redox reaction during discharge/charge.

The theoretical capacity, Q_{th} , of an electrochemical cell, is the amount of electricity obtained from the battery. It is relative to the maximum amount of charge (C) in Coulombs that might be transformed between electrodes through the external circuit.

¹ Is the voltage across the terminals flows close to the thermodynamic voltage

More commonly it is expressed in terms of ampere-hours (Ah). Faraday's laws can give the charge capacity in Coulombs that can be defined by the quantities of electroactive components enclosed in the cell:

$$Q_{th} = xnF \quad (4.9)$$

where x is denoted to the number of moles of specific electroactive materials involved in the reaction; F is the Faraday constant; n is the number of electrons transferred.

In a solid-electrode-based electrochemical cell, the capacity is conventionally can be expressed with respect to either the mass of specified electroactive material (as gravimetric capacity) or to overall battery mass , Ah kg⁻¹:

$$Q_{th} = \frac{w \times n \times F}{M} \quad (4.10)$$

where w is the weight of active material, and M is the molar mass.

The actual cell capacity measurement depends on the cell charge-discharge mode. At the constant current mode, Q_a is given by:

$$Q_a = i \cdot t \quad (4.11)$$

where i is the charge-discharge current, t is the charge-discharge time. At the constant voltage mode, Q_a is given by:

$$Q_a = \int_0^t i dt \quad (4.12)$$

At the constant power mode, Q_a is given by:

$$Q_a = \int_0^t i dt = P \int_0^t \frac{1}{U} dt \quad (4.13)$$

The cell specific capacity (Q_s) can be described in terms of gravimetric specific capacity (mAh g^{-1}) or volumetric specific capacity (mAh cm^{-3}) for the charge or discharge process.

- **Specific Energy**

This refers to the amount of energy stored in the specific quantity of mass, that can be expressed in the terms of watt-hour per kg (Wh/kg) or Wh/L , specific gravimetric energy density and specific volumetric energy density respectively. Generally, high energy density battery is preferred.

- **Power density:**

It is the amount of power stored in the battery (volume or weight). The power density can be given by the battery discharge, at current (i) at a voltage (E):

$$P = \frac{iE}{w} \quad (4.14)$$

where w is the weight of the battery.

- **Cycle life:**

This an important parameter for measuring the battery performance. It describes the number of charge-discharge cycles which battery is credible before failure. Different factors can have an influence on the battery cycle life, such as charge-discharge rate, temperature, and depth of charge-discharge.

- **Cell efficiency**

Several factors have a significant impact on the cell efficiency, such as the current density, electrolyte conductivity, and the temperature. In rechargeable battery system efficiency is an important parameter, which defined as how efficient a battery can convert energy from one form to another. Generally, in rechargeable battery, Coulombic efficiency (CE), voltage efficiency (VE), and energy efficiency (EE) are

used. The CE can be defined as the ratio between charge/discharge capacities under a fixed voltage window.

$$CE = \frac{Q_{discharge}}{Q_{charge}} \quad (4.15)$$

Where:

$$Q_{dis} = \int_0^t I dt, \text{ if } I = \text{constant, then } Q_{dis} = I_{dis} t_{dis}, Q_{cha} = I_{cha} t_{cha}$$

The VE is determined by taking the difference in charge-discharge voltage (Wh) into account. The EE value is a derivative of the CE and VE ($EE = CE \times VE$), the VE efficiency can be given by:

$$VE = \frac{EE}{CE} \quad (4.16)$$

It is worth noting that; the essential meaning of efficiency differs for several battery chemistry systems. For example, in iron-based batteries, such as NiFe battery, CE is often an indication of the loss of capacity per cycle.

For the most medium and large-scale BESS, high energy and voltage are required. Moreover, battery safety is a more stringent issue in large-scale battery grid application. Therefore, it is essential to choose the ideal anode and cathode materials that should provide a high electrical conductivity, good mechanical properties, with cost-effective and long cycle life for a specific application; safety and the active temperature are essential for stable and reliable operation.

- **The charge-discharge rate (C-rate)**

The term C-rate is one of the important concepts when comparing battery systems. It describes as the current needed for either a full charge or discharge a battery's nominal

capacity in a certain amount of time, where C denotes the theoretical charge capacity (Ah) of a cell. A C/5 and 1C, for example, stands for a current allowing a full discharge in 5 h and 1 h, respectively.

$$\frac{C}{n} = \frac{\text{Full capacity(Ah)}}{\text{time(hours)}} = \text{current (A)} \quad (4-17)$$

The discharge rate and the delivered capacity are related to each other as following:

$$C = \frac{\text{discharge current}}{\text{nominal capacity}} \quad (4-18)$$

4.2 Batteries Charging Techniques

In general, the charging techniques can be divided into three categories; conventional charging techniques, pulse charging techniques and state-of-the-art charging techniques.

1. Conventional charging technique can be categories into:

- **Constant current (CC):** is a straightforward and inexpensive to design, where the battery is submitted to a very low constant current until it is fully charged. Some CC charging techniques are specific to certain rechargeable battery types that allow the user to modify the charging profile.
- **Fast Constant Current (FCC) charging Techniques :** where the battery receives a large current until it is fully charged. FCC can reduce the battery charging time from ten hours under constant current charge to three hours in fast constant current charge. However, the FCC charging techniques do not take into account the internal electrochemical process of the battery being charged resulting in significant negative long-term effects (ref).
- **Constant Current Constant Voltage (CCCV) Charging Technique :** where

the battery receives a steady current until the cell reaches a predetermined voltage value, at a constant voltage until the charging current drop to near zero value. CCCV charging produces the same negative long-term effects as of the fast constant current charging techniques but to a lesser degree.

In short, constant current charging techniques are simple, low-cost solution, but without taking into account eventual long-term negative effects such as battery capacity reduction and shortened life span.

2. Pulse Charging (PC) Techniques: The concept of pulse charging (PC) techniques relied on delivering a charging pulse current for about a full second followed by resting period in the order of milliseconds. Then the charge charge-rest period will carry out repeatedly until the battery is fully charged.

3. State-of-The-Art Charging Technique

By applying multiple shorter discharging pulses with much greater amplitude, taking into account the battery properties, in order to offer better fast charging of the battery.

4.3 Iron-based batteries

4.3.1 Introduction

The increasing reliance on renewables as a clean and sustainable source of energy has catalysed and renewed great interest in energy storages systems (ESSs) at both small and large scales for the efficient use of energy, and peak shift grid applications. In addition, to sustain the non-renewable resources, reduce greenhouse emission, the only way to sustainable energy (Abdalla *et al.*, 2016). Such ESSs are undoubtedly needed to accommodate the increasing demands of renewables and intermittency of energy generated from renewable sources such as solar and wind-

based electricity. Converting the renewables energy and storing it into chemical fuels using ESS and transported for energy power supply is one of the promising and potential solutions (Cho *et al.*, 2015). Over the last two centuries, a wide variety of energy storage systems (ESS) technologies have emerged, such as batteries, compressed air, capacitors, and pumped hydro have been developed and commercialised for this purpose. Among these various ESSs, electrochemical storage systems such as rechargeable batteries are considered a good candidate for renewable energy based on their energy densities, scalability, efficiency, and flexibility to be sited anywhere (Alotto *et al.*, 2014, Chen *et al.*, 2009, Cho *et al.*, 2015). As an effort to address the issues of the lack of grid-scale storage application, a superior class of rechargeable battery technologies for renewables and grid storage is, therefore, essential. To develop these types of batteries, wide range of different combinations of an anode, and cathode, and electrolyte materials. However, rechargeable batteries need more advanced low-cost, abundant materials design, and new chemical processes and systems integration to be commercially viable.

In the last ten years, advancements have led to better batteries for transportation and utility grid application (Figure.4.3). Among them, lead-acid (LA) battery is the oldest and widely used, especially for renewables storage grid applications (Posada *et al.*, 2017). However, their low density, low cycle life, poor cycle efficiency, the toxicity of raw materials eventually reduce their market adoption (Vela and Aguilera, 2006, Posada *et al.*, 2017). Today, lithium-ion (Li-ion) batteries are one of the most promising technologies in the role of the storage energy, owing to their long-cycling capability, and high energy density. However, the high cost and non-safe electrolyte limited their market adoption applications. Therefore, advanced, efficient, cost-effective, safe, robust, energy storage systems are extremely desired and critical to renewables energy integration and smart grid applications.

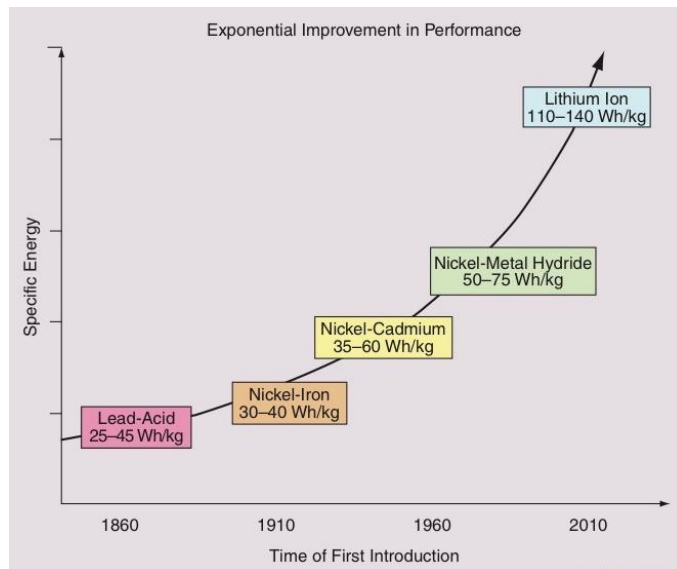


Figure 4.3 The improvement in the battery performance over the last 10 years (Tan *et al.*, 2013).

Of several possible BESSs choices, iron-based rechargeable batteries such as nickel/iron (NiFe) iron/air have attracted renewed attention, especially for large-scale storage, owing to their inexpensive, abundant, and eco-friendly raw material (Wang *et al.*, 2012, Shukla *et al.*, 2001, Öjefors, 1976, Öjefors and Carlsson, 1978). Nevertheless, iron-based batteries are electrically and mechanically rugged (Sarkar *et al.*, 2016), have long cycle life, safety, and high theoretical capacity (0.96 Ah g^{-1}) (Hang *et al.*, 2013). In the most alkaline iron-based (such as NiFe and iron-air), metallic iron is used as anodes, and is globally abundant, inexpensive, and environmentally friendly (Hang *et al.*, 2013). Moreover, the theoretical specific capacity of active metal iron is also very attractive. Besides, with all these advantages, these technologies might afford a safe, cost-effective option to store electricity for the grid network, and have been projected as potential candidates for electric vehicle

applications (Vijayamohan *et al.*, 1991). A comparison and characteristics of various iron-based batteries are shown in Table 4-1 and 4.2 respectively.

Table 4-1 Iron Electrode Battery Systems (Linden and Reddy, 2002)

Type of Battery	Uses	Advantages	Limitations
Iron/nickel oxide	Material handling, vehicles, underground mining, lamps, railway, emergency lighting	Not damage by discharge stand, Long cycle life, Withstand electrical abuse: overcharge, over discharge, short-circuiting	Hydrogen evolution on charge and discharge, High self-discharge, low power density, Low energy density, Poor low-temperature performance, Higher cost than lead-acid, Low cell voltage,
Iron/air	Motive power		Low efficiency, Hydrogen evolution on charge, Poor low-temperature performance, Low cell voltage.
Iron/silver oxide	Electronics		High cost, Hydrogen evolution on charge

Table 4-2 Iron Electrode Characteristics

Technology	Nominal voltage, V		Specific energy Wh/kg	Energy density Wh/L	Specific power W/kg	Cycle life, 100% DOD
	Open-circuit	Discharge				
iron/nickel oxide tubular	1.4	1.2	30	60	25	4000
Developmental	1.4	1.2	55	110	110	>1200
iron-air	1.2	0.75	80	--	60	1000
iron/silver oxide	1.48	1.1	105	160	--	>300

4.4 Rechargeable nickel-Iron battery (NiFe)

4.4.1 Introduction

The nickel-iron (NiFe) battery is a rechargeable electric energy storage (ES) device that invented independently by Waldemar Junger in Sweden and Thomas Edison in the US and successfully commercialised in the early 1900s (Shukla *et al.*, 2001, Posada *et al.*, 2017). NiFe batteries commercially available today are virtually the same as those developed by Thomas Edison, the cell often referred to as the Edison cell (Linden and Reddy, 2002). The battery is produced for industrial traction application in large number in U.S.A and other countries. The 1.15 V cell rechargeable NiFe alkaline battery is mainly used in heavy industry applications such as forklift trucks, railway, electric road vehicles and mines as traction battery at the early industrial stage (Chakkaravarthy *et al.*, 1991). However, this interest fell out of favour in engine starters to a cheaper lead-acid battery. Further development and perfection of NiFe batteries were, however, hindered by the advent of nickel/cadmium system (Thomas, 2000).

The NiFe alkaline battery is similar to nickel-cadmium (Ni-Cd) battery, which was commercialised used in the 1910s. The only difference between NiFe battery and Ni-Cd batteries, that iron is used as an anode electrode in nickel-iron battery, which was replaced by a cadmium anode electrodes (Thomas, 2000).

Iron is the fourth most naturally abundant element in the Earth's crust (Morard *et al.*, 2013). On the other hand, nickel is known as the second most abundant element in the Earth's crust, which can be found in several countries such as Australia, Brazil, Canada, Indonesia, Philippines, Russia, etc. (Oxley and Barcza, 2013). Nevertheless,

iron is cost-effective, eco-friendly, recycled readily, with a large theoretical specific capacity (Shangguan *et al.*, 2015).

The resurrection of attraction of the NiFe battery systems over recent years is due to it being seen as environmentally friendly and cost-effective than the lead-acid batteries. Their compatibility is particularly suited to the potential application where batteries are to be included in a system using photovoltaic (PV) (Chakkaravarthy *et al.*, 1991). This is mainly due to their low-cost per kWh compared to other available technologies (Posada and Hall, 2015). Moreover, the specific energy that NiFe has is 1.5-2 times than lead/acid (LA) batteries, with longer cycle life, and it has ruggedness (Dell, 2000) and Table 4-3. Nickel/cadmium typically offer 1500 cycles, lead/acid usually last 300 cycles, and nickel metal hydride 500-800 cycles (Vijayamohanam *et al.*, 1991). Cycle life up to 4000 deep discharge cycles for NiFe is frequently cited (Halpert, 1984, Shukla *et al.*, 1994), which is far superior to the other types.

Table 4-3 Comparative specific energies of NiFe and Pd-acid batteries at two discharge rate.

Rate (W/kg)	NiFe (Wh/kg)	Lead/acid (Wh/kg)
20	54	36
40	50	26

Additionally, NiFe has enhanced safety and environmental advantages compared with other rechargeable batteries such as nickel-cadmium and lead-acid, which are substantially toxic. Besides, NiFe has a robust physical structure that can withstand mechanical shocks and vibrations, as well over-charge, and over-discharge (Dell, 2000). Owing their relatively low-cost of bulk materials over other cells chemistries,

combined with the global abundance of the raw materials, are the major advantage attractt this technology as an inexpensive option for large-scale power systems (Malkhandi *et al.*, 2013).

Nonetheless, the viable use of this technology has so far been surpassed by other battery chemistries in almost all applications, where a lightweight battery is required. NiFe is limited by relatively poor charge-discharge cycles, with an energy efficiency of 50-60% (Shukla *et al.* 2001, Gil Posada *et al.* 2015). A further drawback is their low energy and power densities: NiFe where can display a specific energy of around 30-50 Wh kg⁻¹ (Shukla *et al.*, 2001, Linden and Reddy, 2002), whereas Lithium-ion batteries at low discharge rate can achieve as high as 200 Wh kg⁻¹. The low specific power, and low discharge capability is related to several factors including self-discharge and the undesirable hydrogen evolution that occurs during the charging of the battery. That results in reduced charge efficiency, and poor utilisation of the active material: that has prevented their use in applications where a sealed, maintenance-free battery is required.

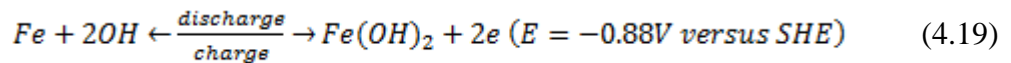
The following section outlines the basic operating principle of NiFe cells, convention production, performance characteristics, and given an indication of current retail and future research in the area.

4.4.2 Operating Principle of Nickel-Iron (NiFe) Batteries

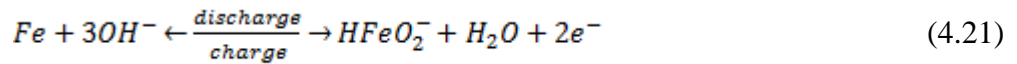
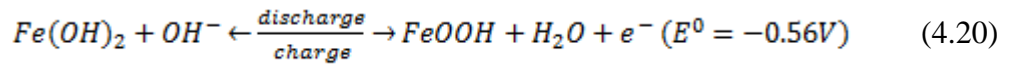
In NiFe cell, the active materials are metallic iron used as a negative electrode or anode, nickel hydroxide serving as the positive electrode or cathode and a solution of potassium hydroxide as the electrolyte. The basic working principle of the NiFe batteries constitutes the following battery chemistry:

4.4.3 Negative Electrode

The negative electrode of the two different transformations during charge/discharge take place, equation (4.19) and (4.20) (Shukla *et al.*, 2001) which represented as:



And

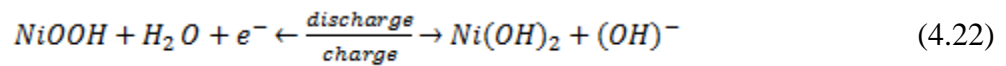


The first oxidation step of Fe to Fe (II), as result of reaction (Equation 4.19) and (Equation 4.20). The second step conversion Fe (II) to Fe (III) can occur under deep discharge in a cell with a negative-limited configuration, although the cells are usually positive-limited to increase cycle life (Shukla *et al.*, 1994). During discharging, the oxidised iron forms small crystallites close to the reaction site, and while charging the low solubility limits the rate of crystal growth of the iron, which helps to sustain the nanostructure of the electrode material. Moreover, the low solubility restricts the cell performance at high rates, and low temperatures, where the discharged species precipitate and prevent access to the remaining active materials.

4.5 Positive Electrode

In the positive electrode, Nickel oxyhydroxide is the active material, which is converted to nickel hydroxide $Ni(OH)_2$ during charging as represented by Equation 4.22.

Nickel oxyhydroxide is the active material in the positive electrode of NiFe cells. The nickel electrode reaction involves the reduction of nickel oxy-hydroxide (NiOOH) to nickel hydroxide; $Ni(OH)_2$ during charging/discharge proceeds respectively as represented by Equation (4.22) as:



It has been proposed that the oxidation state of Nickel has different crystallographic are formed, a different form of nickel species can transform into one another, which be produced during cycling. (Divisek *et al.*, 1989). The usual form of nickel in the positive electrode is β -Ni(OH)₂. During charging the form β -NiOOH will produce as a proton is ejected from the material. The possible transformation relevant for nickel oxide electrode is presented in **Error! Reference source not found.**

As in Figure.4.4, there are two forms of nickel hydroxide, the form β -Ni(OH)₂ and α -Ni(OH)₂. The form α -NiOOH will produce during discharging which has 80% larger molar volume than the β -NiOOH, then the form α converts the β form. The yields β -NiOOH and γ -NiOOH can form during charging (Shukla *et al.*, 2001). The β -NiOOH can transform into the γ -NiOOH form during overcharging, and this form has a molar volume approximately 50e% larger than the forms β -Ni(OH)₂ and β -NiOOH.

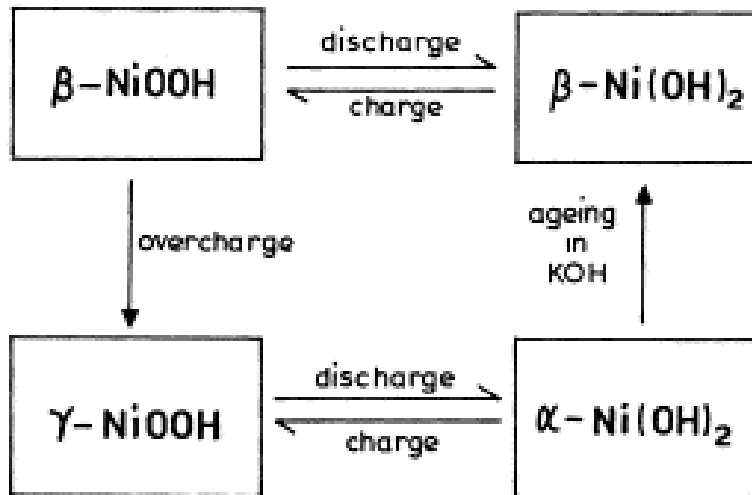
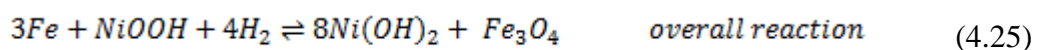
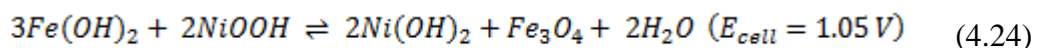
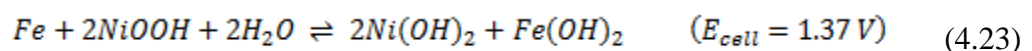


Figure 4.4 Scheme diagram of possible transformations in the positive electrode (Shukla *et al.*, 2001)

Amongst other things, the addition of cobalt (2 to 5 wt.%) in the form of cobalt hydroxide or cobalt sulfate improves the reversibility of the nickel electrode. Cobalt addition has also been said to increase efficiency at higher temperatures, reduce the degree of self-discharge experienced, prevent electrode swelling (*i.e.* formation of γ -NiOOH) and increase the overvoltage required for oxygen evolution (Shukla *et al.*, 2001).

The reactions result from the transfer of oxygen from one electrode to another as shown in the cell reactions below (left to right shows the reaction where the discharge reaction taking place):



These cell reactions are highly reversible in alkaline electrolyte, especially if only the first discharge plateau is exploited, which is normally the case when cells are positive-defined limited.

4.6 Electrolyte

The cell is normally flooded with an aqueous electrolyte, which consists of 25-30%wt potassium hydroxide (KOH). The addition of distilled water to the electrolyte is required periodically as the water is electrolysed during cell charging. Alkali ion electrolyte can provide conduction and act as a transport medium between the anode and the cathode. 6-8 M KOH solution is the normally used in NiFe cells. The additives are added to the electrolyte to achieve a functional electrolyte. Adding 50 g/L⁻¹ of lithium hydroxide (LiOH) is the most widely used additive to improve the cell capacity and prevent capacity loss during cycling (Linden and Reddy, 2002).

4.7 Conventional Cell Construction

Traditionally, NiFe cells are produced in a pocket or tubular plates are filled with the active materials. The negative plate is made of nickeled steel grid contains powdered iron, the positive plate is made of nickel tubes contain nickel oxides and nickel hydroxides, and the electrolyte is a solution of concentrated potassium hydroxide (Linden and Reddy, 2002). The group of plates are connected to form a common terminal using a bus bar and assembled into cells (Figure.4.5). To ensure best cycle life, usually the single cell includes one or more negative plates more than the number of those positive plates.

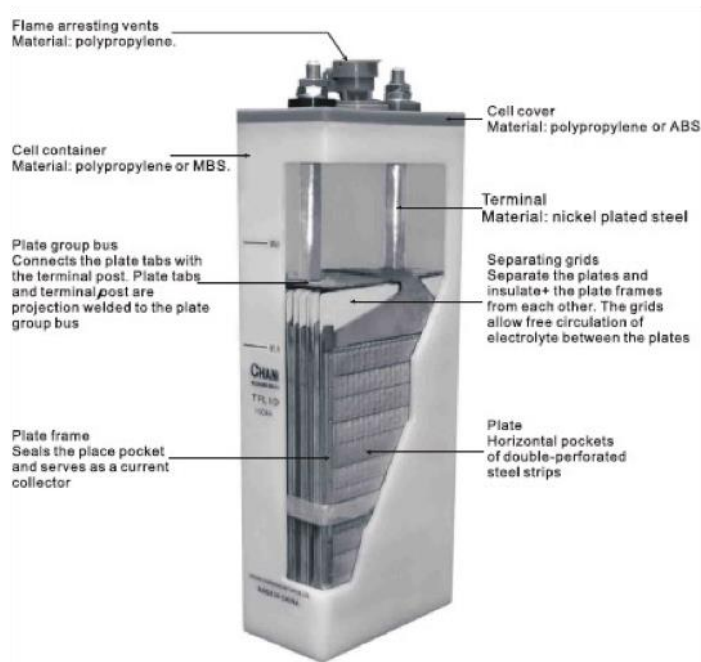


Figure.4.5 Conventional pocket plate type NiFe cell, available from :(Changhongbatteris, 2013).

4.7.1 The Negative Electrode

4.7.1.1 Pocket plates

This is made by dissolving pure iron in sulfuric acid to form FeSO_4 , which will be dried and heated in air at $800\text{-}850^\circ\text{C}$ to produce Fe_2O_3 . Then the material is washed, and dried under hydrogen at $750\text{-}800^\circ\text{C}$. The Fe and Fe_2O_3 , which is the resulting mixture, is blended with small amounts of additives such as FeS or copper that can be added to reduce gas evolution and to increase the life of the battery or increase the conductivity (Vijayamohan *et al.* 1991, Balasubramanian and Shukla 1993, Ravikumar *et al.* 1995, Thomas 2011).

4.7.1.2 Pressed electrodes

The resulting mixture of active materials and additives are blended with a polymer binder (*e.g.* PTFE), and then hot-pressed, rolled with a nickel-plated steel screen. The resulting pore former is leached out using boiling water to leave a porous plate as a result (Vijayamohanan *et al.*, 1990).

4.7.1.3 Sintered electrodes

Iron powder is mixed with additives (*e.g.* Zn, As, Mn, Cu). The resulting mixture is then pressed and sintered on a nickel plate steel grid at temperature range 700-800°C for 60 min under a hydrogen atmosphere (Jayalakshmi and Muralidharan, 1990). A carbonyl iron powder can be mixed with a binder and a pore former and sintered. The sintered electrodes can improve the power density of the battery and increase the iron electrode utilisation.

4.8 Performance

The NiFe specific performance characteristics are very dependent on the cell design. The typical NiFe cell open circuit voltage is 1.4 - 1.5V, and the nominal cell voltage is 1.2V. The voltage required to charge the cells is between 1.6 and 1.7 volts. The capacity of the NiFe cell is limited by the capacity of the positive electrode (NiOH), which is normally rated at the 5h discharge rate. Discharge capacity is also depended on temperature (Shukla *et al.*, 1994).

NiFe cells are usually charged galvanostatically at 15-20 Ah per 100 Ah of its rated capacity. The typical charging regime is C/5 for 7h and C/3 for 4h (battery charged to certain final charge where the cell has accepted an amount of charge current defined as its charge capacity) (Shukla *et al.*, 1994). At higher rates, more replacement

of electrolyte will be required due to increased gas evolution. The Ampere-hour (Ah) should return about 25-40% overload of the previous discharge, to ensure the complete charging process. The constant current (CC) charging method has usually preferred a method of charging in practice in the laboratory, because calculating Ah is more convenient, and charging with constant CC can be done with simple equipment. Typical charge/discharge profiles of NiFe are shown in (Figure 4-6).

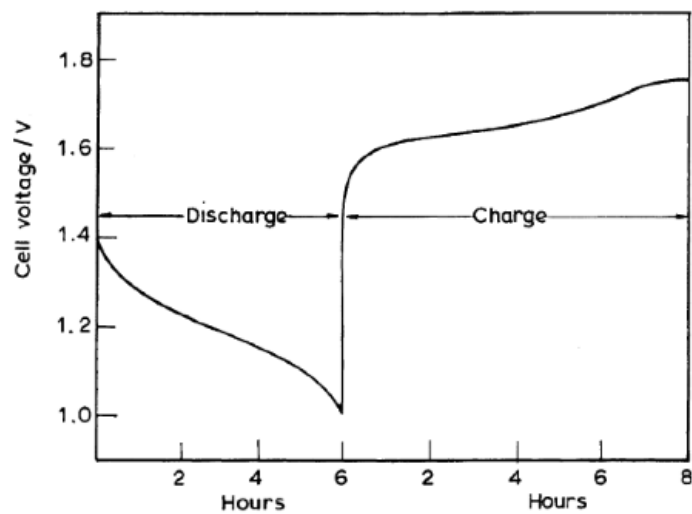


Figure 4-6 Typical Charge - discharge curves for a Ni-Fe cell (Shukla *et al.*, 2001).

The discharge of the battery can be done at any current rate. However, this discharge cannot be sustained beyond the point where the battery nearly about to be exhausted (1 to 8 hours). The discharge voltage of the NiFe cell battery might vary from 1.23 V at C/1 to 0.85V at C/1 (Linden and Reddy, 2002). The NiFe cell is best suited to a low rate of discharge. The NiFe delivered capacity decreases with increasing discharge rate. Hence, the high internal resistance of cell can lower the terminal voltage, where high rates of discharge are required as illustrated in Table 4-4, and Figure 4.7.

Table 4-4 Variation in capacity with discharge rate (Linden and Reddy, 2002).

Discharge Rate	Delivered Capacity [%]
C/10	105
C/8	105
C/6	101
C/5	100
C/4	97
C/3	90
C/2	73
C	50

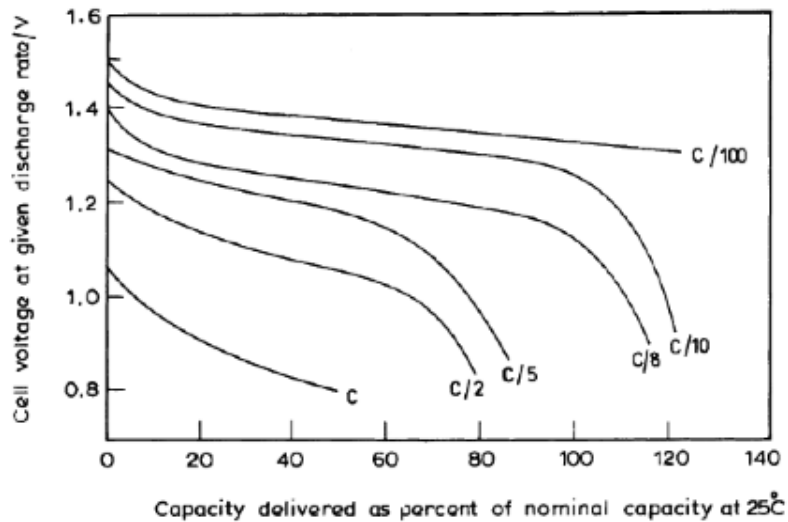
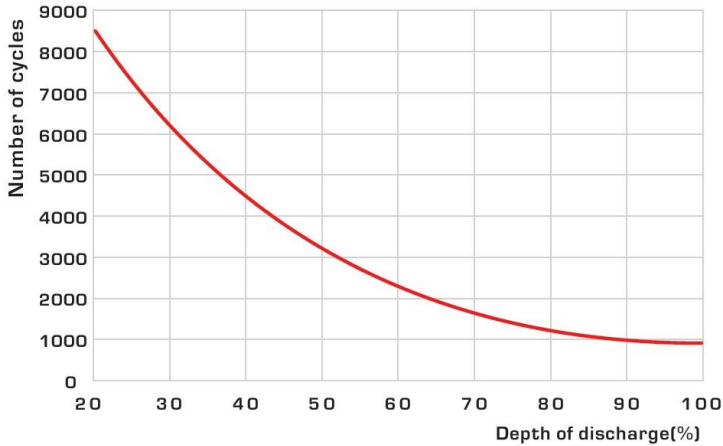


Figure 4.7 Discharge curves at various rates for a NiFe cell

(Shukla *et al.*, 2001).

Details concerning the cycle life of NiFe cells have been approached with some caution as reliable data over the period quoted are not available. 2000 cycle life can be expected with moderate care and limiting temperature to below 35°C. Nevertheless, it is generally accepted that 3000-4000 cycles can be achieved when pocket plate type cells at C/5 rates are used (Chakkaravarthy *et al.*, 1991).

Figure 4.8, present the data from NiFe manufacturer shows that the expected cycle life can be significant decreased with increasing depth of discharge, and nearly 1000 full charge-discharge cycle can be achieved.



Typical cycle life versus DOD(20°C)

Figure 4.8 Expected cycle life against depth of discharge (DOD) for NiFe cells, available from: (Changhongbatteris, 2014).

The discharge capacity of a NiFe cells is also dependent on temperature. It has been the cell performance decreases at lower temperatures, which is typically attributed to the passivation of the iron electrode. NiFe cells are rarely employed at operating temperatures lower than -15 °C. The upper operating temperature of NiFe battery is 45-50 °C; at higher temperatures increased solubility of iron influences the operation of the nickel electrode and exacerbates self-discharge.

4.9 NiFe Battery Application and Developments

The recent developments of the iron-based alkaline battery began several decades ago (Öjefors and Carlsson 1978, Vijayamohanan *et al.* 1991, Inc Annual Report for 1983).

In the US, development of iron-based batteries for electric vehicle was primarily undertaken by The Eagle-Picher Industries and the Westinghouse Corporation (Vassie and Tseung 1976, Bryant 1979, Corporation *et al.* 1980, Inc Annual Report for 1983).

In addition, the development of NiFe and iron-air batteries has been undertaken by several institutions worldwide from 1970-190 (Öjefors and Carlsson, 1978, Vijayamohanan *et al.*, 1991). Different techniques and strategies have been used to fabricate and improve the performance of the iron electrode are described in several reports (Bryant, 1979, Vassie and Tseung, 1976, Ravikumar *et al.*, 1995, Balasubramanian *et al.*, 1993, Ravikumar *et al.*, 1996). Several reports in the previously literature on the performance of iron-based electrode batteries recognised the robustness of the iron electrode and the possibility of achieving up to 3000 cycles (Öjefors and Carlsson, 1978). The NiFe battery was analysed in various stationary and mobile applications in the USA and Europe until the early 1980s (Manohar *et al.*, 2012). After this time, the research on this type of batteries was sharply discontinued, except for some fundamental research by Shukla *et al.* during the period 1986-1992, then the interests in these batteries reduced and supplanted by cheaper sealed lead-acid batteries (Manohar *et al.*, 2012).

Table 4-5 The NiFe characteristics (Chakkaravarthy *et al.*, 1991).

Cell voltage (OCV)	1.37 V
Working voltage	1.00-1.2 V
Theoretical energy density	267 W h kg ⁻¹
Attained energy density	82.5 W h kg ⁻¹ at C/5 rate (Japan) 50 W h kg ⁻¹ at C/2 rate (USA) 50 W h kg ⁻¹ at C/5 rate (Germany) 26 W h kg ⁻¹ (USSR)
Charge/discharge efficiency	50%
Cycle life	>1000
Calendar life	15-20 years

Table 4-6 Nickel-iron battery performance (Thomas 2000).

	1980 to present state of the art	Goal
Specific energy at battery level (Wh/kg)	50	60
Energy density at battery level (Wh/l)	102	120
Specific peak power at battery (W/kg)	110	125
Deep discharge (100%) cycle life	1000	2000

4.10 Motivation for the Research on NiFe Batteries

Since the introduction of the first NiFe batteries 100 years ago by Edison, the focus of both academia and industry has been placed on extending the battery system viable for a big market. Only the nickel /cadmium system, the nickel /metal hydride system (NiMH) have reached the stage of large volume production (Köhler *et al.*, 2004). In this work, we propose the potential of Nickel-Iron battery system of meeting the needs of large-scale storage. The recent growth interest for energy storage technologies has derived and motivated to this study.

Despite the tremendous promise that Iron-based electrodes batteries such as NiFe batteries hold advantages for large-scale grid applications. The cost-effective materials, long-lasting, safety and environmentally friendly, compared with other battery electrode materials such as nickel, cadmium, zinc, and lead (Wen *et al.*, 2011). The promise of NiFe battery for large-scale grid application has encouraged renewed attention in their development (Manohar *et al.* 2013, Posada *et al.* 2017b).

The objectives of this study is the technical problems with this battery and an attempt to solve them in the effort to improve the overall battery performance. Traditionally, iron as anode materials has been desirable for batteries because of various positive factors: a low cost, abundant, and environmentally benign material. However, their developments have been hindered by numerous limitations and problems. Those limitations are poor discharge capability and charge efficiency.

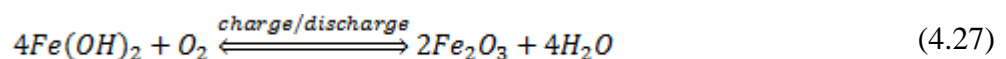
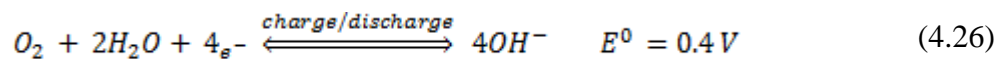
Therefore, in order to realise the benefits of NiFe battery, improving the overall NiFe technology, it is necessary to understand the problems associated with specific component; iron anode, the electrolyte. In general terms, the main issues in alkaline

NiFe batteries are the following: the high dissolution of iron, hydrogen evolution as a side reaction and the electrolyte dissociation.

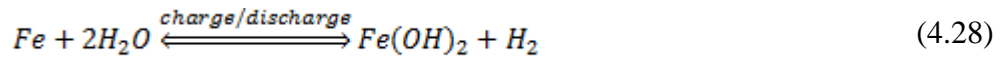
4.10.1 Problems and Challenges Facing NiFe Batteries

4.10.1.1 Problem Associated to the Iron Anode

Over recent years, the iron electrode has received considerable research attention (Vijayamohanan *et al.*, 1991, Shukla *et al.*, 1994, Andersson and Öjefors, 1976, Öjefors, 1976). In iron-based battery systems such as the NiFe battery, iron is the primary raw material. Thus, the iron dissolution in the aqueous electrolyte occurs in two steps, which utilises iron in three oxidation states (Fe, Fe (II), and Fe (III)) Equation.4.19, Equation.4.20 and Equation.4.21. This first step of reaction involves oxidation of metallic iron to iron(II) hydroxide. The second step of reaction results in further oxidation of iron(II) hydroxide to form iron(III) hydroxide. Consequently, iron is unstable thermodynamically, and the battery needs to be overcharged by 60-100% to reach its full capacity (Manohar *et al.* 2012). The major problem of iron electrodes is passivation during the discharge process caused by iron hydroxide, which prevent further anodic utilisation. The passivation of the iron electrode could be due to the dissolved oxygen and form of passive corrosion products as flows (Ravikumar *et al.*, 2015);



Due to a side hydrogen evolution reaction, ferrous hydroxide could also be produced as shown below:

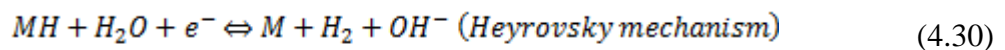
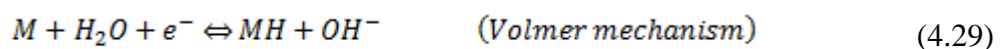


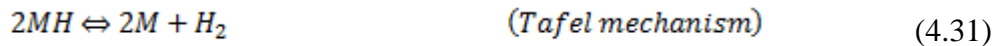
The low charging efficiency of iron electrodes (about 60-70%), poor discharge capability, and also corrosion, are as a consequence of hydrogen evolution reaction. However, the factors that affect the rate of formation, mechanism of formation, and the capacity are not completely understood (Manohar *et al.*, 2012).

4.10.1.2 Problem Associated to the Hydrogen Evolution Reaction (HER)

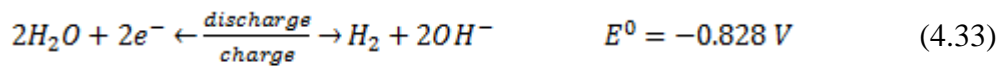
The hydrogen evolution reaction (HER) is a half reaction of water electrolysis that takes place on the surface of an electrode that reduces protons into hydrogen in alkaline medium (Gong *et al.*, 2015). The basic water electrolysis unit is consisting of an anode, a cathode, and an electrolyte, as illustrated in Figure.4.9. Several researchers have extensively studied the mechanism of HER. Depending on the catalytic surface, there are general two mechanisms can be applied to the HER in both acidic and alkaline media (Gong *et al.*, 2015). Generally accepted reaction mechanisms in alkaline media proceed in three steps (Gong *et al.* 2015, Wang *et al.* 2016):

- (1) Adsorption of hydrogen and reduction of water (Volmer mechanism Equation.4.29) (Gong *et al.*, 2015).
- (2) The adsorbed hydrogen atom can either be combined with another adsorbed hydrogen atom to form a hydrogen molecule that leaves the surface (Heyrovsky mechanism Equation (4.30)).
- (3) Chemical desorption (Tafel mechanism Equation.4.31).





This reaction occasionally takes place on negative electrodes in iron-based batteries leads to a decrease in current efficiency and deposition rate. The HER occurs, because the hydrogen has more positive standard potential than those of metals such iron (Equation 4.29), and the reversible potential of the iron electrode reaction (Equation 4.28) is more negative than that of the potential for hydrogen evolution.



However, the resistance of the electrolyte is one important factor when considering the overpotential and the energy efficiency of a cell. Strong acids, base or some solid electrolyte, is necessary. Figure 4.9; illustrate the principle of alkaline water electrolysis.

Figure 4.10; illustrate the charge-discharge half-cell potential for the iron electrode.

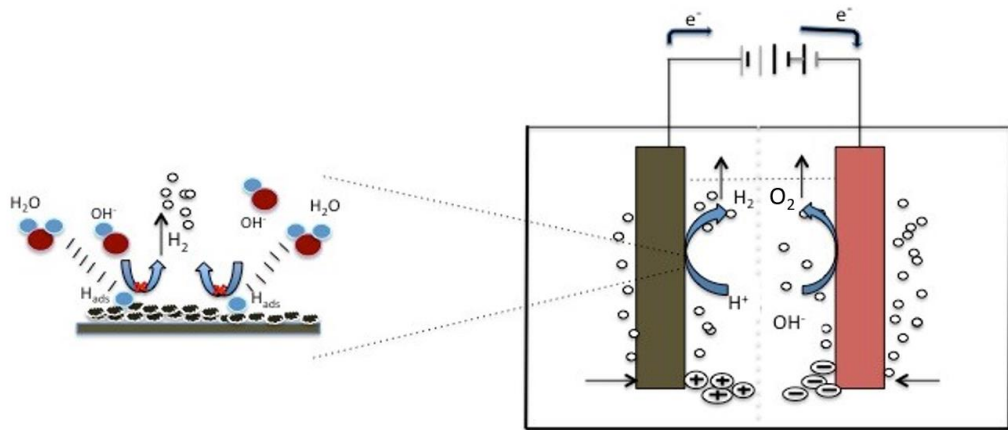


Figure 4.9 Illustrate the principle of alkaline water electrolysis and hydrogen evolution reaction.

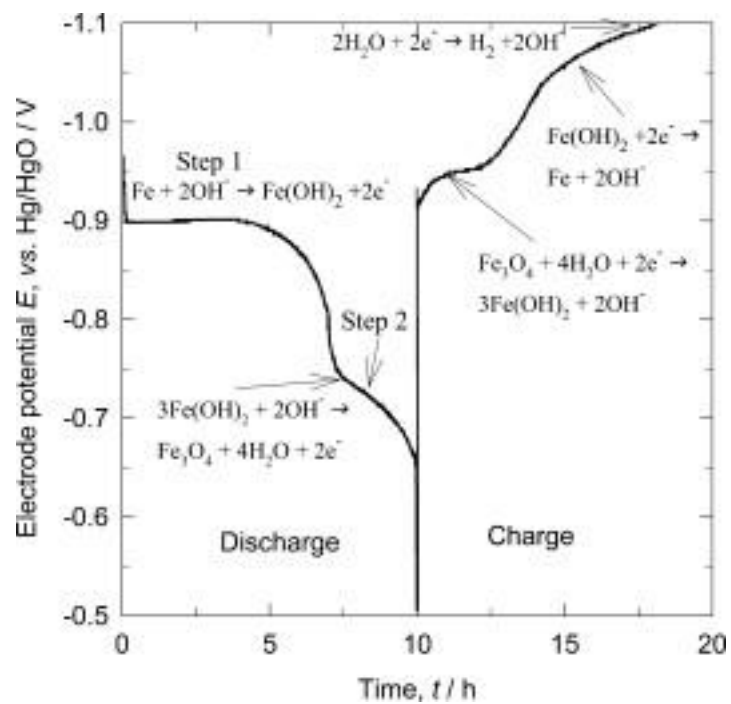


Figure 4.10 Typical charge-discharge curves of the iron electrode (McKerracher *et al.*, 2015).

The suppression of hydrogen evolution at the iron electrodes is essential and critical to the commercial exploitation of iron-based batteries. Consequently, suppressing hydrogen evolution will (1) enhance the round-trip energy efficiency; (2) reduce the loss of water from the battery during charging, and increase the overall performance of the battery.

4.11 Approaches for improving the performance of iron electrodes for NiFe batteries.

Considerable efforts have been made to overcome these problems toward practical iron-based electrodes. The two major concerns in such a battery are; (i) hydrogen evolution (HER) causing water electrolysis to increase the internal pressure of the battery, and (ii) dendrite formation during repeated charge/discharge processes.

The HER over the iron electrode reduces the reversibility of the iron anode, results in the water electrolysis and increases the internal pressure of the battery. However, all of these disadvantages need to be solved before they are commercially viable. In this regard, several promising approaches to suppress the wasteful evolution of hydrogen at the iron electrode have been proposed, including:

(1) Using Additives: depositing or physical mixing high HER overpotential metal impurities or metal oxide to the electrode or electrolyte has been identified to have a positive effect by occupying the reactive sites. Recently, Manohar *et al.* has demonstrated, that using metal sulfide and bismuth additives had a significant effect on electrodes during charging, and achieving a tenfold reduction in the hydrogen evolution rate. With an overall efficiency of 96%, with discharge a capacity of 0.3 Ampere-hour/g⁻¹, and has been reported the effect of using bismuth additives in reducing hydrogen evolution (Manohar *et al.* 2012). Ravikumar *et al.*, reported the

benefits of in situ electrodeposition of carbon grafting into the active iron material with and without bismuth additives on iron in suppressing the evolution of hydrogen (Ravikumar *et al.*, 2015). Yang *et al.*, identified the benefit of using a small quantity of compounds as electrolyte additives to improve the performance of iron electrodes (Yang *et al.*, 2014). Caldas *et al.*, reported, that the hydrogen evolution was inhibiting with the addition of iron sulfide to the electrode, and a small amount of bismuth to the electrolyte (Caldas *et al.*, 1998). Malkhandi *et al.*, demonstrated that the addition of long chain thiols to the electrolyte are very effective in suppressing hydrogen evolution on alkaline iron-based electrode batteries (Malkhandi *et al.*, 2013).

(2) Electrode design: the influence of electrode design and fabrication method on the rate of formation and utilisation of the performance of iron-based electrodes has been recognised. For example, Manohar *et al.* demonstrated, that iron electrode containing differently formulated additives fabricated by pressed-plate type electrode showed increase charging efficiency (Manohar *et al.*, 2015). Periasamy *et al.* described the performance of sintered iron electrodes in NiFe batteries (Periasamy *et al.*, 1996). Gil Posada and Hall reported enhancement on the charge/discharge process of the Fe electrodes prepared by hot-pressing of an iron-polyethylene base on different iron electrode formulations (Posada and Hall, 2014). Bryant, demonstrated, that iron electrodes fabricated by a sintering method can deliver maximum capacity near 0.4 Ah g^{-1} , and the discharge capacity found to be highly depended on the electrode's density (Bryant, 1979).

(3) Structure modification of iron materials: several studies have been reported, that iron electrode based on nano-sized materials can deliver an excellent electrochemical performance. For example, Manohar *et al.* have demonstrated, that iron electrode made from carbonyl iron can deliver a high charging efficiency of 92% and excellent rate

performance (Manohar *et al.*, 2012). Recently, Shangguan *et al.*, demonstrated that synthesised FeS/C as anode material using simple calcination method followed by a co-precipitation process exhibits high charge efficiency, high discharge capacities, superior rate capability and excellent cycling stability (Shangguan *et al.*, 2015). Lei *et al.* reported, enhancement in NiFe batteries based on synthesised coupled nanoFe/multiwalled carbon nanotube and nanoNiO/MWCNT nano-composite materials (Lei *et al.*, 2016). Also, Liu *et al.*, proposed NiFe cells designed and fabricated based on Graphene foam/carbon nanotubes hybrid film are able to deliver high energy/power with up to 270 mAh g⁻¹, and excellent cycling stabilities (Liu *et al.*, 2014). Rajan *et al.*, suggested that improved electrode conductivity base on F-carbon nano-composites enhanced and improved the performance of NiFe cell with a specific capacity value in excess of 400 mAh g⁻¹ (Rajan *et al.*, 2014). Wang *et al.*, proposed a NiFe battery based on inorganic nanoparticle/graphitic nano-carbon hybrid materials and showed increasing in charging and discharging rates by near 1,000-fold over conventional NiFe batteries (Wang *et al.*, 2012).

Table 4-7 Different types of selected anode materials for NiFe cells

Iron materials	Particle size [μm]	Support materials	Type of Additives	Electrode design	Discharge specific capacity [Ah g^{-1}]	Percentage charging efficiency	Ref
Commercial Iron electrode	1-3	None	None	Pressed pocket-plate	0.12 at C/5 rate	70 at C/20 rate	(Chun, 2006)
Fe+Fe ₃ O ₄	5-10	PVA + carbon black	1 % Bi ₂ S ₃	Powder spread with PTFE	0.4 at C/5 rate	80	(Moura <i>et al.</i> , 2013)
Carbonyl iron	0.5-3	none	10% Bi ₂ O ₃ +FeS	Pressed powder + PE binder	0.22 at C/5 rate	93 at C/20 rate	(Hariprakash <i>et al.</i> , 2005)
Carbonyl iron	0.5-3	none	5 % Bi ₂ S ₃	Pressed powder +PP + K ₂ CO ₃	0.24 at C/5 rate	30 at C/5 rate	(Haddad <i>et al.</i> , 2008)

The addition of hydrogen evolution inhibition additives to the electrolyte have been proved to be an effective way and most commonly strategy to reduce the HER by forming adsorbed layers at the iron electrolyte and increasing the hydrogen overvoltage (Yang *et al.*, 2014).

4.11.1 Hydrogen evolution inhibitors

Using additives is one of the effective strategies to suppress or reduce the hydrogen evolution reaction (HER). For instance, it should take into the consideration when choosing the electrode/electrolyte materials as corrosion inhibitors include; conductivity, catalytic effect, and noble metals, as electrode materials are either costly or easy to be corroded in the alkaline environment. Metal sulfide currently is popular electrode material owing to its better corrosion resistance to alkaline environment compared with other transition metal compounds. Iron is responsible for the hydrogen formation in the presence of water. However, in highly concentrated alkaline solution, there is a high amount of dissolution with causes a problem if high hydrogen evolution occurs. So it can be concluded that the suppression of the HER may be achieved by excluding water from the surface of the iron electrode.

In this regard many anodes additives materials have been proposed and examined. Some additives to anode materials, such as bismuth sulfide, cobalt, copper, and carbon black are considered as promising anode additives. In the literature, Liao, Lei *et al.* (Liao *et al.*, 2013), reported the most common additives materials. Mahela and Shaik showed that metal sulfide is commonly used as additives for HER in alkaline solution (Mahela and Shaik, 2016). However, use of some additives in large-scale system is limited due to low-abundance and high cost. In an effort to develop NiFe batteries, and to overcome the problems of the iron electrode and reduce the HER, two main approaches have been proposed:

(1) The use of inhibitors such as bismuth, carbon black, metals sulfide etc.;

Our choices of additives will be using :

- (1) cost-effective, eco-friendly materials
- (a) Additives for the iron electrode

(b) (b) Additives for aqueous alkaline electrolytes

(2) Electrode design method;

(a) paste-type electrode

(b) hot-pressed electrode

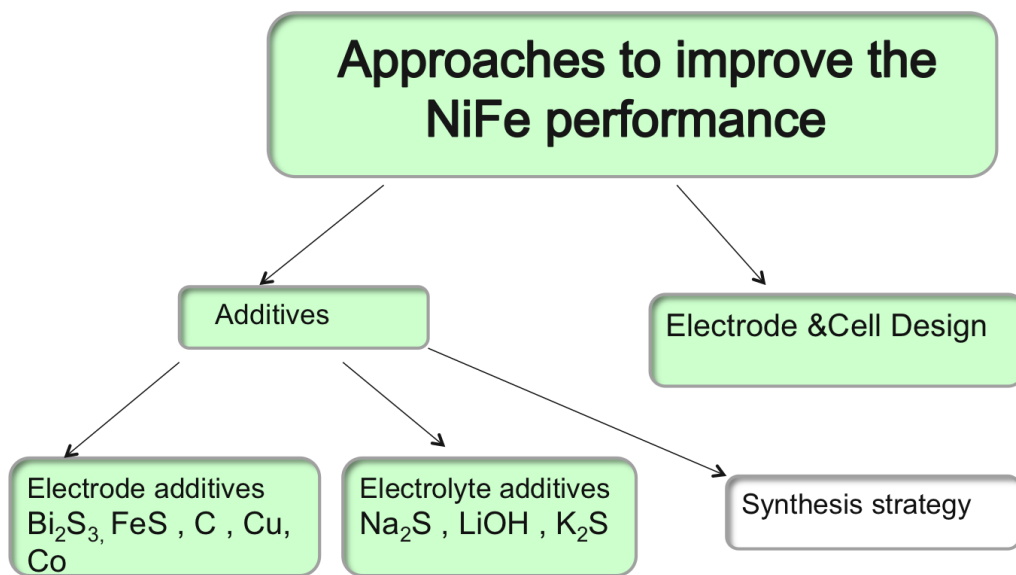


Figure 4.11 Approaches for improving the performance of the iron electrodes.

The present work aims to investigate the use of such additives and the utilization of electroactive materials for suppressing the hydrogen evolution and improve the overall performance of the iron electrode.

Chapter 5 EXPERIMENTAL SECTION

In this section, a brief introduction to the general experimental conditions and some of the techniques that are commonly used, which are related to the work reported and applied in this thesis.

5.1 Introduction

In order to study electrode reactions, experimental methods and conditions must be created and used which enable study and minimize all unwanted factors. Electrochemical techniques are concerned with the measurement of electrical quantities such as potential or charge, current, or other relationship to chemical parameters. The next section describes the methods employed to prepare the electrode samples; the electrochemical and physical methodologies are used practically to characterise the electrodes. The electrochemical techniques are mainly used to investigate the electrochemical performance of the prepared electrodes, while physical characterizations are used to explore and understand the crystal structure and morphology properties of the electrode materials prepared that used in this study.

5.2 Materials and Electrolyte

Aldrich chemical company supplied most of the materials and chemical used in this work. Lists of materials and chemicals used in this study and their stated characteristics are presented in Table 5-1.

Table 5-1 Descriptions of materials and chemicals used in this study.

Materials or Chemicals	Formula & weights	Purity (wt.%), supplier
Potassium hydroxide	KOH, 28.5 w/v%	≥ 85.0%, pellets, Sigma-Aldrich
Bismuth sulfide	Bi ₂ S ₃	99.5% ≤ 5μm, Sigma-Aldrich
Bismuth	Bi	Powder, Sigma-Aldrich
Iron	Fe	99% ≤ 10μm, Powder, Sigma-Aldrich
Iron (II) sulfide	FeS	99.5% ≤ 10μm, Sigma-Aldrich
Copper sulphate	CuSO ₄ 5H ₂ O	98% ≤ 10μm, Sigma-Aldrich
Polytetrafluoroethylene (PTFE)	(C ₂ F ₄) _n	Teflon 30-N, 59.95% solids, Alfa Aesar
Nickel foam	Ni	99.0%, density 350 g/m ² , Sigma-Aldrich
Potassium carbonate	K ₂ CO ₃	99.0%, Sigma-Aldrich
Polyethylene powder (PP)	(C ₂ H ₄) _n	99.0%, Sigma-Aldrich

5.3 Preparation of Active Material

5.3.1 Electrode samples preparation

Paste-type electrodes have been advanced quickly and used extensively for electrochemical application, due to reduced complexity in mass production (Yang *et al.*, 2003). These electrodes can be fabricated under mild condition consisting of mixing an iron powder with a binder, then coating slurry of active mass into porous Ni foam, the highly porous Ni foam used as a substrate and current collector. The highly pre-size and porosity (400-700 μm pore size) allow easy access, a high packing density of the active mass slurry during the coating process (Yang *et al.*, 2003). A brief description of paste electrode processing is described by (Oshitani *et al.* 1989, Bernard and Bouet 1999). In this study primary paste-type electrode samples were investigated.

5.3.2 Paste-type electrode

The respective iron paste-type electrodes samples were fabricated in two steps as follow:

1. Slurry preparation

Mixing the required amount of dry iron powder with different concentration of additive and active material, a certain volume of Polytetrafluoroethylene (PTFE) binder (60% suspended solution) was added to the electroactive powder to form the slurry (certain amount of binder is necessary to avoid shedding or removal of active materials from the electrode during the electrochemical testing, the binder can produce fibers structure that holds the active materials) (Chang *et al.*, 1999). The mixture was agitated in ultrasonicated water for 15 minutes.

2. Electrode coating

The electroactive slurry was then dip coated consistently onto a Nickel-foam, where the Ni-foam was cut to dimensions of 10 x 40 x 1.5 mm. The nickel foam used as a current collector. The pasted electrodes were vacuum dried at 80 °C for 4-5h. The coating steps repeated 2 to 3 times until approximately 0.3 g of electroactive material (iron) were loaded on an area of 1 cm². The content of active iron material the resultant electrodes was determined by weighing the electrode before and after water absorption during a certain time. Then the electrodes dried under vacuum at 80 °C for 24h.

The packing density of the iron in the electrode samples is calculated through the iron loading from the total pore volume of the Ni-foam. For comparison, control iron electrode samples without additives using pure iron powder as active material are also prepared. In this work, all electrodes were prepared for similar iron loading and capacity when iron powder was added in the electrodes, and to ensure that the observed electroactive mass added on the Ni foam, were not exceed the active mass required. The actual electrodes thickness varied from 0.44 to 0.50 mm.

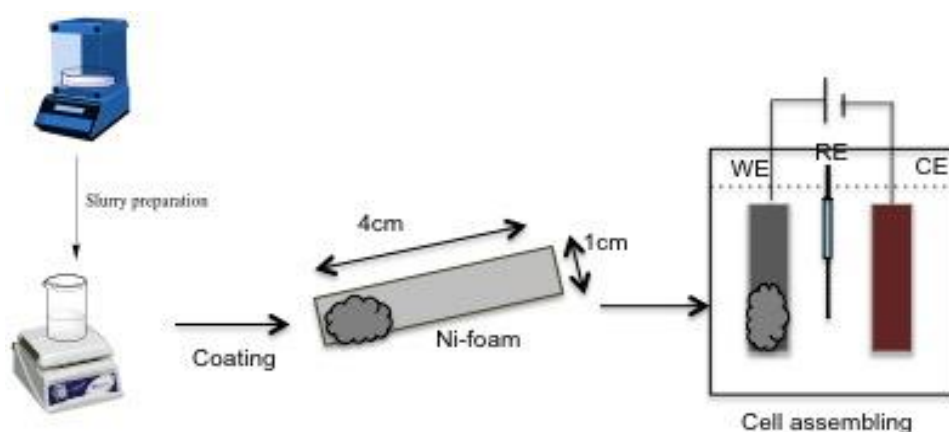


Figure 5.1 Electrode samples preparation.

5.3.3 Hot-pressed type electrode

The electrodes were prepared by mixing the required amount of dry iron powder with different concentrations of electroactive additives, a certain amount of potassium carbonate (K_2CO_3) and polyethylene powder (PP). The PP and K_2CO_3 were used as the binder and pore former. Then the mixture was hot-pressed on onto strips of nickel foam (10 mm x 40 mm x 1.5 mm) at 140°C, a pressure of 10 kg cm⁻². The process was repeated until a constant amount of iron was reached (approximately 0.2- 0.3 g). Then the electrodes dried under vacuum at 80 °C for 24h. The procedures for the hot-pressed type electrode preparation have been described in previous studies (Manohar *et al.* 2012)

5.4 Experimental Procedures

The experimental procedure in this work is illustrated in Figure 5.2. Initially, after choosing the electrode/electrolyte additives, Fe-based active composites electrode samples with different concentration are prepared by paste-type, hot-pressed methods, then cycled up to 60 times to measure their electrochemical performance. Then the electrode samples were characterised using series of techniques, such as X-ray diffraction (XRD), scanning electron microscopy (SEM), transmission electron microscopy (TEM).

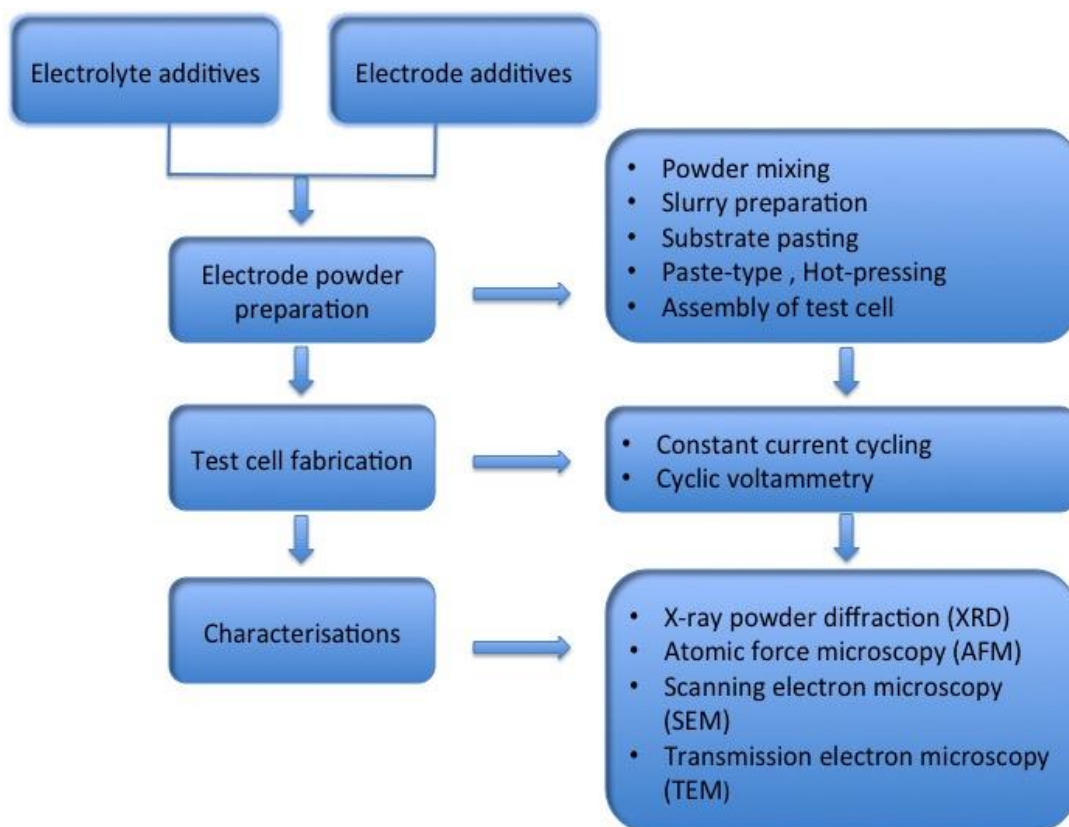


Figure 5.2 Schematic diagram for experimental procedure.

5.4.1 Data analysis

In order to investigate the effect of different concentration of additive on the electrochemical performance of our electrode samples with a reasonable number of experiments, a designs of experiment approach were used. Experimental design is an effective commonly used tool to study and identifying important variables, and time, cost-effective way for studying the effects of two or more factors (vander Heyden, 2006).

A factorial design is a most common and very effective way for studying two or more factors. Full factorial design at two and three levels can be used for the optimisation and interaction effects for two level designs, to determine the effect of

different concentration of substance (Bezerra *et al.* 2008). The mixture design can allow us to choose the optimum formulation for the mixtures (Bezerra *et al.*, 2008).

In the present work, full factorial and simplex were used in order to study the effect of several additives on the electrochemical performance of our electrode samples. Design Expert® (DX7) software was used for building, finding out the optimum condition, parameters and analysing of the experimental design.

For statistical analysis, data have to be validated by analysing the following statistics:

- The adjusted coefficient of determination and the higher R^2 , the better the model fits the data.
- The p -values, which used in hypothesis tests to decide whether to reject or fail the hypothesis for the models is, should be less than 0.05. The smaller the p -value the better probability of making a mistake of rejecting the null hypothesis.
- Analysis of variance (ANOVA) is a typically used to analyse the data and has to be carried out in order to determine and judged the effects of the interaction terms. Three replicates per formulation were used in this work, to ensure consistency, bearing in mind that the mixing rules in a 3-dimensional composition space.

5.5 Electrochemical Techniques Principles of Equipment

5.5.1 Electrochemical testing

5.5.1.1 Electrochemical cell set-Up

In this section, the process of cell fabrication is described. The electrochemical properties of the iron electrodes were investigated in a three-electrode type cell configuration used in the study. Symmetrical cells consist of one commercial nickel electrode (referred to as the Counter electrodes) (CE) fabricated on one side, prepared pasted electrodes (also referred to as working electrode) (WE) fabricated on other side of the reference electrode (RE) (mercury/mercury oxide (MMO) was used as reference electrode, $E_{\text{Hg}/\text{HgO}} = + 0.098\text{V}$ vs. normal hydrogen electrode (*NHE*). An aqueous solution of KOH (28.5 w/v%) was used as an electrolyte. Figure 5.3 showed a schematic illustration of the cell test arrangement.

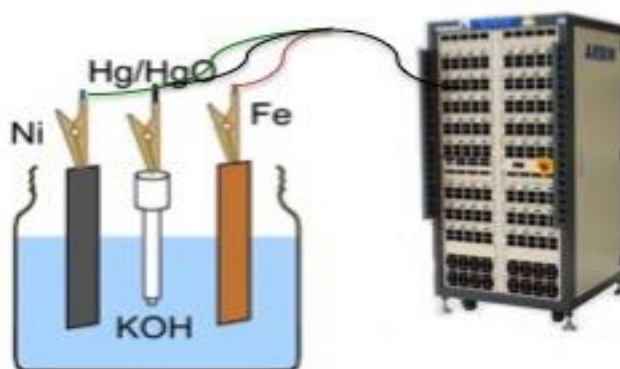


Figure 5.3 Schematic of the Cell configuration.

All electrochemical baseline experiments in this research were carried out in 60-Channel Arbin-SCTS169395 electrochemical battery testing (Figure 5.4), operating in a galvanostatic mode.

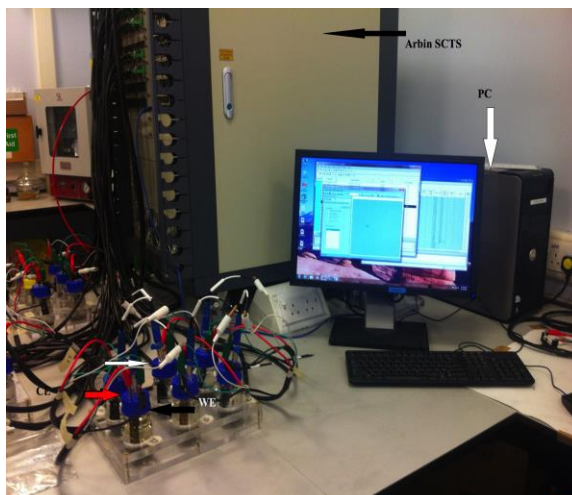


Figure 5.4 Photo of 60-channel Arbin electrochemical battery tester (SCTS169395).

5.5.1.2 Start-Up Procedure

The Arbin electrochemical battery testing provides a direct measurement of current (A) and voltage (V). Also the machine can automatically calculate energy flow (Wh), power (W), voltage response (dv/dt), and current response (dI/dt). In order to determine the battery performance metrics, a series of charge/discharge cycle need to be performed.

5.5.2 Galvanostatic charge- discharge cycling

Galvanostatic charge-discharge cycling is an important technique for electrochemical evaluation of battery cycling performance, capacity, and estimates the rate of the capability of the electrode materials in a certain voltage window. The

instrument used for this technique is called a galvanostat. A constant-current method here applied to the cells, where the potential (E) is recorded as a function of time (t). The total amount of charge passed per unit mass (m) of electrode material. The specific capacity C, during complete discharge, is given by:

$$C = I \cdot \frac{t}{m} \quad (5.1)$$

5.5.2.1 Testing protocol

The testing protocol performed was as follows:

Discharge the cell at desired current rate (C-rate C/5), record voltage every 0.01V over time (recording signal every 5 minutes), halt discharging when the battery reaches cut-off voltage 0.7V (battery safety parameters), then go to next step when voltage reach $\leq 0.7V$. Charging the to a potential of 1.4v, record voltage every 0.01V, go to step one when the voltage reaches $\leq 1.4V$. Allow cell to rest 5minutes, then repeat steps (1) and (2) for 60times then stop the test. The battery capacity will be recorded as the total charge can be delivered for the duration of step (1).

5.5.3 Voltammetric technique: Cyclic voltammetry

Voltammetric methods are based on controlled-potential while monitoring of current response to an applied potential. Of all the electrochemical methods for study electrode processes, cyclic voltammetry (CV) is one of the most widely used techniques. This technique is used to examine different redox processes, quickly it provides useful information about a potential range of activity, kinetics, electron transfer, the reversibility of a redox reaction and coupled electrochemical reaction of electrode/electrolyte in a solution (Jean-François and Patrice, 2009, Allen and Bard,

1980). Where the potential is applied between the working electrode (WE) and the current electrode (CE) from initial potential (E_1) to final (E_2) and then the potential swept back to the initial potential, with the current and time of the potential are recorded with each scan (the voltage changes with a defined scan rate). The reference electrode (RE) is used to adjust the potential on the WE. The full potential cycle (plotting the current versus the voltage) is known as a voltammogram as shown in Figure 5.5.

The main parameters in a CV trace are:

- The anodic (oxidation) peak current (I_{pa}), which is the highest peak in the anodic branch of the current trace.
- The cathodic (reduction) peak current (I_{pc}), the highest peak in the cathodic branch of the current trace.
- The anodic peak potential (E_{pa}), which is the potential where the anodic current is maximum.
- The cathodic peak potential (E_{pc}), the potential where the cathodic current is maximum.

The anodic ($\frac{E_{pa}}{2}$), or cathodic ($\frac{E_{pc}}{2}$), half-peak potential, which the potential where the current is at the half of the peak current and can be obtained by drawing a vertical line from the point at which the current is at its high down to the baseline. Then we measure the half the distance of this vertical line and draw a perpendicular horizontal line dividing the vertical line (Figure.5.5). The vertical line where the point crosses the CV is the half-peak potential. The anodic ($\frac{E_{pa}}{2}$), or cathodic ($\frac{E_{pc}}{2}$), half-

peak potential is related to half-wave potential ($E_{1/2}$), and for a reversible couple, the separation between peaks as following:

$$E_{p/2} = E_{1/2} \pm \frac{0.028}{n} V \quad (5.2)$$

The ($E_{1/2}$) can be calculated using the following equation:

$$E_{1/2} = \frac{1}{2} (E_{pc} + E_{pa}) \quad (5.3)$$

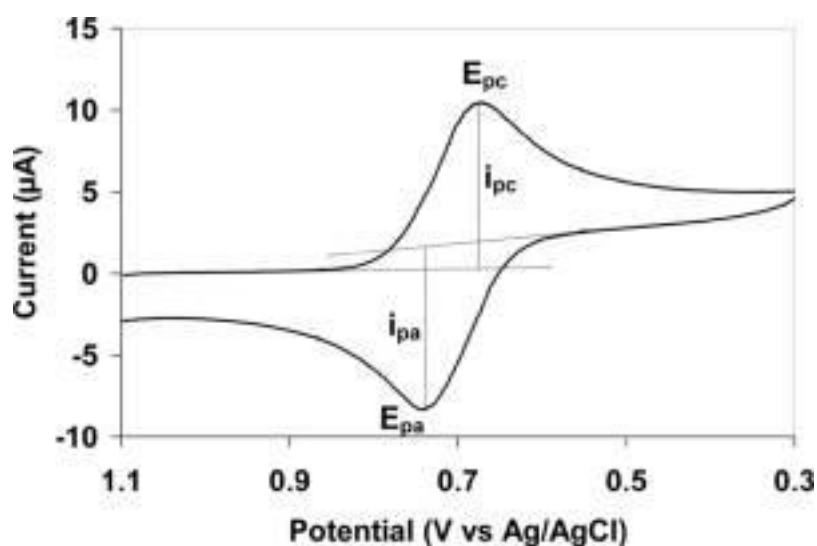


Figure 5.5 A typical cyclic voltammogram curve showing the important peak parameters.

The electron transfer rate, the rate of diffusion, migration, and electrode surface and scan rate and more factors have an influence on the cyclic voltammogram peak separation.

In order to characterise the CV of a sample electrode transfer reaction three cases must be understood:

A. **Reversibility:** the concept of reversibility that the Nernst equation is obeyed locally, and that the ratio of $\frac{[O]}{[R]}$ at the electrode is given by the Nernst equation.

The electron transfer process is faster than the rate of diffusion and always maintains equilibrium at the surface of the electrode is another way to express the means of reversibility. The correlation between peak current and scan rate represent the mechanisms of electron transfer at the surface of the electrode. The theoretical analysis of the wave shape leads to the Randles-Servcik equation for peak current voltammetry (Allen and Bard, 1980);

$$i_p = 2.69 \times 10^5 n^{3/2} A D^{1/2} C v^{1/2} \quad (5.4)$$

I_p is the peak current, n is the number of electrons transferred, A is the electrode area (cm^2), D is the diffusion coefficient ($\text{cm}^2 \text{S}^{-1}$), C is the concentration of the redox active species in the solution (mol cm^{-3}), and v is the scan rate (mV s^{-1}) and it is the proportionality between peak current against $v^{1/2}$ for a reversible system. This equation usually gives a diffusion coefficient D for a redox couple of known concentration C , electrode area, from the slope of the I_p against $v^{1/2}$, and then determined D at 25°C. This process corresponds to the rate of reaction at the electrode surface. The electroactive layers halted on the surface of the electrode can lead to the CV. It can be seen from the equation above that, the peak currents depend

on the square root of the scan rate, and the peak current ratio $\frac{i_{pa}}{i_{pc}} = 1$ for the reversible voltammetric couple (Allen and Bard, 1980).

Peak separation is another criteria for the reversible system. The potential peak separation ΔE_p is the difference in potential between the anodic and cathodic peak potential:

$$\Delta E_p = E_{p,a} - E_{p,c} = \frac{0.059}{n} V \quad (5.5)$$

If the exchange involves two electrons ($n = 2$), it means that the process has a peak distance of 30 mV.

- B. **Irreversibility:** It is the opposite case of the reversibility, this means that the rate of electron transfer is low or slower than the rate of electron diffusion, and the ratio of $\frac{[O]}{[R]}$ in Nernst equation is not obtained during the measurement.
- C. **Quasi-reversibility:** it is the intermediate case of the cyclic voltammetry. These processes can occur when the rate of electron transfer is inadequate to maintain Nernstian equilibrium.

5.5.4 Equipment/Instrumentation for cyclic voltammetry measurements

5.5.4.1 Working Electrode pre-treatment procedure

Glassy-carbon working electrodes (GCE) were prepared in two steps as follow:

1. Electrode Polishing

The glassy carbon electrode surface was rinsed with deionized water to flush any encrusted material on the surface. Follow this with an acetone rinse. Then the electrode is dry with a fresh lab tissue. The GCE was polished with alumina suspension 0.5 and 0.05 μm buffing pad. Following sonication, the electrode was rinsed with a flash of ethanol, acetone and deionized water and sonicated for 15 minutes, sequentially, and then the electrode was dried in air.

2. The electrode coating

A certain amount of iron powder and Polytetrafluoroethylene (PTFE) binder were measured. After mixing the required amount of dry iron powder with different concentration of additives, active material and a certain volume of PTFE binder to form the slurry, the slurry was sonicated for 20 minutes. Next, the slurry was pipetted and spread on the surface of the glassy-carbon working (the surface area of GCE is 0.07 cm^2). Then the electrode was dried in an oven overnight at 80 $^{\circ}\text{C}$. The amount of active materials paste was determined to be 3 mg/ml.

5.5.4.2 Electrochemical Cell set-up

All voltammetric measurements (CV) were made under potentiostatic mode using a Solartron 8-channel 1470E/1455A potentiostat/galvanostat. The equipment was supplied with software to control the experiment via a PC.

Cycle voltammograms were conducted using a three-electrode cell assembly (working, reference, counter electrodes), which are immersed in the sample solution Figure 5.6. A three electrodes cell is preferred for the electrochemical analysis. The glassy-carbon working electrode (WE) (OD 6 mm ID: 3.0 mm) is the electrode at which the reaction of interest takes place, while the reference electrode (RE) provides a stable potential against which the potential of WE is compared. The reference electrode (RE) was Hg/HgO, and the counter electrode (CE) was a platinum wire (0.25 mm radius) : sometimes the reference electrode can be used as auxiliary and reference electrode at room temperature, aqueous solutions of potassium hydroxide (KOH, 28.5 w/v%). The KOH solution was prepared using distilled water. The scan parameters were adjusted depending on the type of the experiment performed.

Before all CV measurements the cell was bubbled with nitrogen gas for 20 minutes, to maintain the inert gas and to expel any gases that might generate during the electrochemical experiments. All electrochemical experiments measurements were carried out at room temperature. The CV profiles were collected using the Zview software.

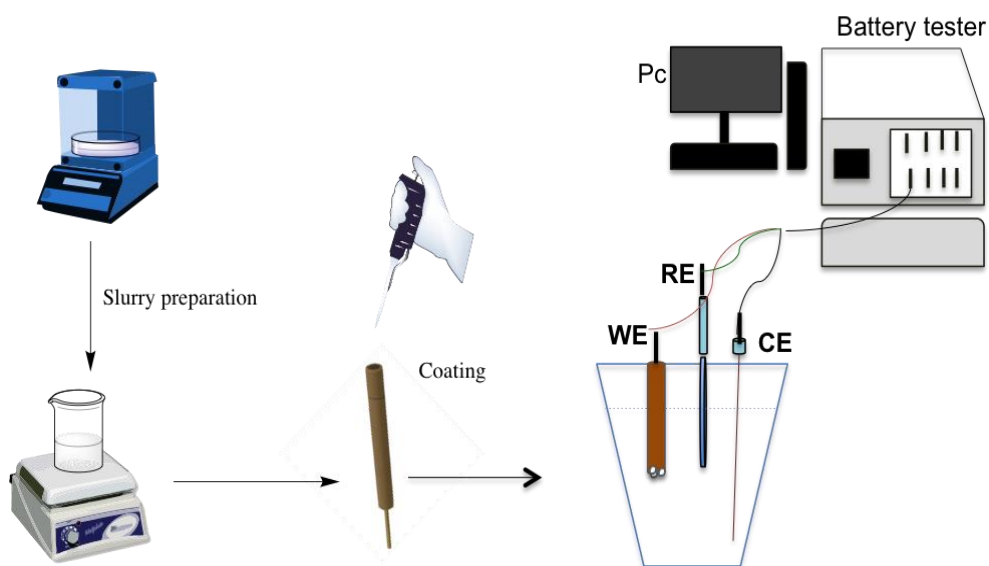


Figure 5.6 Schematic diagram of working electrode preparation and the cell assembly for voltammetric measurements

5.6 Physical Characterization Techniques

The prepared and discharged anode electrodes were thoroughly characterised by a variety of physical methods. The phase structure of the iron electrode samples was identified by X-ray diffraction (XRD). The surface imaging of as prepared iron and after cycling formulated electrode samples were performed by atomic force microscopy (AFM). Scanning electron microscopy (SEM), and transmission electron microscopy (TEM) were used to observe the surface morphology of the electrode, X-ray energy dispersive spectroscopy (EDS) was used to analyse the chemical composition of the electrode samples.

5.7 Principles of characterization methods

5.7.1 X-ray powder diffraction analysis (XRD)

There are several techniques to analysis our electrode samples, including Raman spectroscopy, Fourier transform infrared spectroscopy (FTIR), X-ray powder diffraction (XRD), and so on.

XRD technique is a powerful technique for the characterization of structural properties, crystal structure, and size for single and mixtures of a crystalline phase of the materials. Moreover, XRD technique can provide qualitative and quantitative identification information and the percentage in a mixture of two compounds. XRD is based upon the unique diffraction pattern for electromagnetic radiation for each crystalline substance. When the X-ray radiation collides with a crystal lattice surface, the incident beams will scatter and form a reflected beam makes with the plane of atoms in a consistent manner by assigning Miller indices represented by (hkl) family of the plane. Respectively, reflection of each an x-ray from a crystal is assigned with a unique hkl value. The wavelength of an X-ray is very small which allows the X-ray to interact with the sample atoms. Bragg's law can describe the diffraction of X-ray, in which will scattered at unique angles for each set of lattice planes (Equation 5.6):

$$n\lambda = 2d \sin \theta \quad (5.6)$$

Where λ is the wavelenghts, n the order of reflection, θ is the angle of incidence beam of X-ray, and d is the distance between the crystal planes. The diffraction angle 2θ can be calculated from a distance between the two crystal planes, which is denoted d . The position of the diffraction peak depends on the wavelength and the separation of the crystal planes of the incident beam of X-rays. Each solid crystalline compound has its

unique X-ray diffraction pattern. The theoretical diffraction pattern calculated from the crystal planes can be compared to the diffraction pattern at specific angles obtained by XRD to help identify the sample materials. Figure 5-7 illustrates the principle of XRD. The average particle size (d) can be calculated from the X diffraction plane using the Scherrer equation (Equation 5.7) (Oseghale *et al.* 2015).

$$d = \frac{0.94\lambda}{\beta \cos\theta} \quad (5.7)$$

d is the mean particle size, λ is the X-ray wavelength; θ is the angle of the incident beam, and β is the full width at half-maximum in radians (FWHM). Sample preparation is extremely important in producing good X-ray diffraction results.

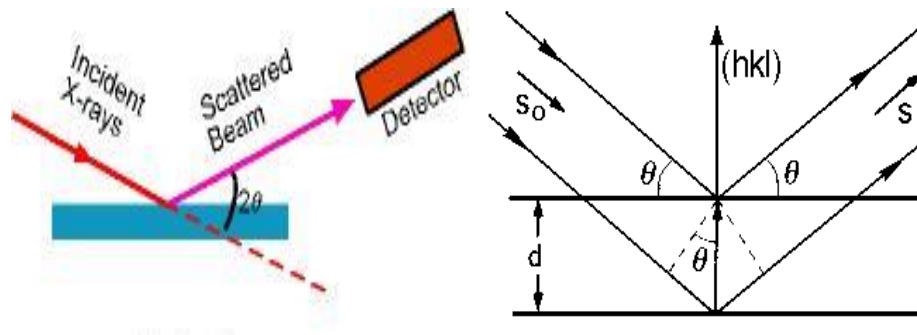


Figure 5-7 X-ray diffraction and Bragg's law

5.7.1.1 Equipment/Instrumentation for X-ray powder diffraction analysis

X-ray diffraction (XRD) was used to characterise the prepared and cycled electrode samples. The X-ray diffraction measurements data were conducted on a STOE PSD system, radiation ($M_o k_{\alpha 1}$, $\lambda = 0.74$ nm, the voltage and current used were 40 kV and 30 mA) and Bruker D2 Phaser system, the radiation used was $Cu k_{\alpha}$, $\lambda =$

1.5406 nm. The XRD data analysis was performed by ICDD PDF-4+ and Sieve+ software.

5.7.2 Atomic force microscopy (AFM)

Atomic force microscopy (AFM) is one of the leading techniques used for the indefinite identification of the layer of electrode samples. AFM is a very useful technique for high resolution imaging of the topography of surfaces and electrode size structures. AFM allows both imaging of surface and interactions with surface of interest, which help to explain the crystal lattice structure and surface chemical at a nano scale.

AFM consists of a probe, scanner, controller, and signal-processing unit. AFM works by proving a sharp probe across the surface (rather than use electrons or beam) to obtain a three-dimensional surface topography. As the probe proves, it characteris the highs and lows surface topography.

Then these signal are sent back via a laser reflected back from the probe surface to a photo-detector. The feedback signals are sent to a signal processing software, which generates a three-dimensional topography of the surface (Figure 5-8).

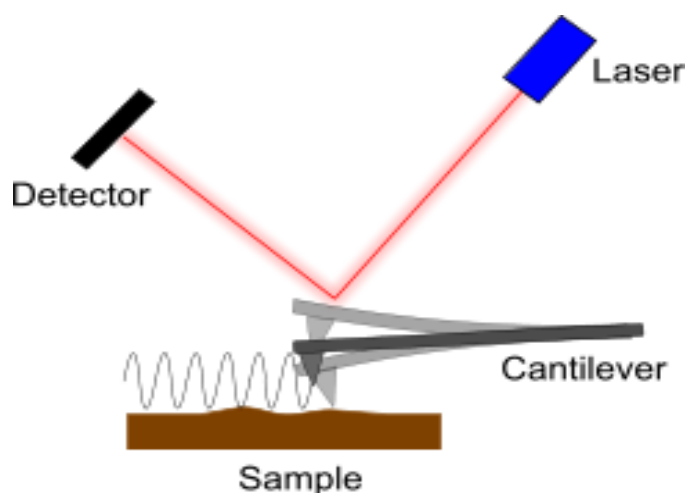


Figure 5-8 Atomic force microscope block diagram

The operating modes of AFM can be divided into a static mode (DC)- in which the probe does not vibrate during imaging, and dynamic mode (AC)- in which the cantilever is excited to vibrate at or off its resonant frequency. The imaging could be conducted by manipulating the repulsive interaction between a probe and surface, which is referred to as contact mode imaging.

AFM has been implemented as a structural characterisation technique for examining the surface morphology at the iron electrodes before and after cycling formation, where the electrode sample electrodes after been subjected to charge/discharge cycling are immediately rinsed with deionised water, followed by drying under a stream of nitrogen. The surface imaging was performed on a Bruker Dimension Icon, operating with the ScanAsyst system in soft tapping mode in air , with the nominal force constant of 40 N m^{-1} and a resonant frequency of 300 kHz.

5.7.3 Scanning Electron Microscopy (SEM)

Scanning electron microscopy (SEM) is an important technique, which can be used to study the material's morphology in high-resolution images of micro and nanostructured materials. In SEM, electrons of a certain energy are focused on and

scanned over a surface of a sample to elucidate its morphology and topology. The operation principle of SEM is based on the interaction of the electrons with the sample; electrons emitted from the surface can be used to create a surface image. SEM images are used in this work in combination with other techniques, to characterise the electrode samples.

SEM images were obtained using an equipped. The samples were prepared by casting 5 μ L suspension of iron electroactive composites or pre-cycled iron electrode samples on a clean carbon type surface followed by drying on air.

5.7.4 Transmission electron microscopy (TEM)

Transmission electron microscopy (TEM) can provide information on crystal structure, high-resolution images of a sample's morphology, similar to SEM. The principle of the TEM technique works similar to the traditional light microscopy, this light has a wavelength of 0.50.2 μ m. The technique is based on using electron beams for imaging and magnetic lens to focus electron beams where electrons are generated in the gun chamber and then accumulated by magnetic lenses and passed through the specimen resulting in a diffraction pattern, which will then imaged below the specimen on a fluorescent screen. Moreover, these diffracted beams can be magnified as an image on the viewing screen. TEM magnification can reach 100,000 times with a resolution of about 0.2 μ m. TEM was adopted to investigate samples' morphology, and crystal structure with lattice information. Moreover, this technique performs compositional analysis by addition of an X-ray detector. High resolution TEM images (HRTEM) were examined by JEOL-2010, 40kV, 45mA. EDS is a good technique for qualitatively to detect the presence of an element, where the resolution can reach until 0.5 nm. The iron electroactive materials samples were drop-caste from ethanol

dispersions of iron electroactive materials and dried in air onto copper coated TEM grids.

5.7.5 Energy dispersive X-ray spectroscopy (EDS)

Energy dispersive X-ray spectroscopy (EDS) is a technique, which is used for the elemental composition of the materials. EDS is a method, and the work is an integral part of SEM and TEM. When the surface is stroked by electrons, some electrons in the material are removed from their quantum shells. When higher electrons drop into those previous shells, energy is released in the form of X-rays. Every element were have it own X-ray wavelength elemental-map

This thesis aims to investigate the potential of the iron-based electrode battery such as Nickel-Iron battery for large-scale energy implementation. Aiming to improve the overall performance of NiFe battery, several anode materials have been used and investigated.

6.1 Bismuth sulfide (Bi_2S_3) as an anode additives materials

6.1.1 Introduction

There is an urgent demand for efficient, clean and sustainable sources of energy as fossil fuel reserves deplete and environmental pollution increase. Renewable energy is the pathway to sustainable energy future and one key challenge in materialising this vision is developing effective electrical energy storage systems (EES). However, renewable sources are not always available on demand, and energy storage is needed to balance the electric grid. Therefore, large-scale storage systems for effectively integrating alternative and renewable energy sources to the modern electrical grid are required. Owing their high-energy efficiency and stability, Nickel-Iron (NiFe) is one promising technology that attracted significant attention in recent years (Posada *et al.* 2017b).. Nevertheless NiFe, there is two technical problem limit the use of NiFe for large-scale grid application; poor discharge rate and low discharge efficiency due to the high evolution of hydrogen on iron electrode take place during charging process (Yang *et al.*, 2014, Manohar *et al.*, 2012). Therefore, mitigation of the hydrogen evolution at the iron electrodes is essential and crucial to the large-scale commercial implementation of iron-based energy storage systems.

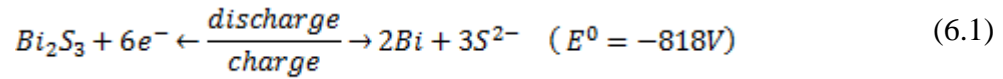
The present work aims to investigate the use of bismuth and sulfide additives for suppressing the hydrogen evolution and improve the performance of the NiFe battery.

The benefit of bismuth additives for different rechargeable alkaline batteries has been recognised and reported widely in the literature (Haddad *et al.*, 2008, Manohar *et al.*, 2013, Greaves *et al.*, 1984, Maja and Penazzi, 1988). The reason for choosing bismuth sulfide:-

Bismuth is an ideal choice for it is eco-friendly (non-toxic), highly conductive, and does not have an effect on eco-friendliness of the iron electrodes materials. Moreover, bismuth has additional advantages of having a high overvoltage towards hydrogen evolution (Mikkelsen and Schroder 2000). Batteries with electrode/electrolyte based on bismuth have been used in several electrochemical stripping analysis studies (Mikkelsen and Schroder 2000, Hočevár *et al.* 2005, Skogvold and Mikkelsen 2008). Rice, reported the effects of bismuth additive on the electrochemical performance of lead/acid (LA) batteries (Rice, 1989). The unique behaviour of bismuth is related to the fact that multicomponent or binary alloys or mixing small amounts of bismuth with several heavy metals such as lead, zinc and cadmium have been reported to substantially reduce the rate of the HER (Yano *et al.*, 1998, Rice, 1989). Maja and Penazzi tested the addition of small amounts of bismuth materials to the electrolyte in fully charged negative plates of lead-acid batteries, which can improve the cycle performance and significantly decrease the HER (Maja and Penazzi, 1988).

As various reports have demonstrated, using metal sulfide and bismuth additives had a significant effect on electrodes during charging, and achieving a tenfold reduction of hydrogen evolution rate, and overall efficiency of 96%, with a discharge capacity of 0.3 A.h.g⁻¹ (Manohar *et al.*, 2012). Then we hypothesised that using sulfide and bismuth additives could improve the charging efficiency of the iron electrode.

In addition, the reduction of bismuth sulfide (Bi_2S_3) has a more positive electrode potential than iron (Equation 6.1), with electrode potential equal to the hydrogen evolution (Equation 6.2).



6.1.2 Materials and electrode samples preparation

6.1.2.1 Materials and solution

All chemicals and solutions used in this study, which purchased from Sigma Aldrich, were of analytical grade and used without further purification. The chemicals and materials used were of the following specifications: iron powder (Fe, 99% \leq 10 μm , Sigma-Aldrich), Bismuth sulfide (purity 99.5%) from Sigma Aldrich, Potassium carbonate (purity 99.0%) from Sigma Aldrich, Potassium carbonate (purity 99.0%) from Sigma Aldrich, nickel foam (Ni, purity 99.0%, density 350 g/m², Sigma Aldrich), Polytetrafluoroethylene (PTFE) (60% suspended solution) was used as binder, Potassium hydroxide (28.5 w/v% KOH, Sigma Aldrich) was used a electrolyte. The solutions were prepared with deionized water and potassium hydroxide.

6.1.2.2 Preparation of the working electrode samples

6.1.2.2.1 Paste-type electrode samples

In this study, paste-type iron electrode samples were used to evaluate the performance of active iron materials. The pasting electrode preparation process was detailed in Chapter 5. Iron electrodes from this active material are obtained as follows; strips of Ni foam (10 mm x 40 mm x 1.5 mm) were coated with differing amounts of electrode materials as shown in Table.6.1.

Table 6-1 Experimental determinations of factors and levels

Factors	Components weight fraction	
	Low	High
Fe	60	90
Bi ₂ S ₃	0	15
PTFE	5	15

6.1.2.2.2 Hot-pressing type electrode samples

For comparison, and to study the effect of electrode type and binder, another type of electrode samples using a hot-pressed route was used. Iron electrodes under strong alkaline conditions were examined by means of galvanostatic charge/discharge, cyclic voltammetry and X-ray diffraction (XRD). In this study, the chemicals and materials used were of the following specifications: iron powder (Fe, 99% ≤ 10μm, Sigma-Aldrich), Bismuth sulfide (purity 99.5%) from Sigma Aldrich, Potassium carbonate (purity 99.0%) from Sigma Aldrich, Potassium carbonate (purity 99.0%) from Sigma

Aldrich, copper sulfate ($\text{CuSO}_4 \cdot 5\text{H}_2\text{O}$, 98% $\leq 10\mu\text{m}$, Alfa Aesar), potassium hydroxide (KOH, purity $\geq 85.0\%$, pellets, Sigma Aldrich). Ni foam (Ni, purity 99.0%, density 350 g/m^2 , Sigma Aldrich),

To prepare the working electrode samples, an active material is obtained as follows:- strips of Ni foam (10 mm x 40 mm x 1.5 mm) were coated and hot pressed (140 °C, at a pressure of 10kg cm^{-2}) with differing amounts of electrode materials as shown in Table 6-2. A required amount of electroactive paste, consisting of Fe powder, Bi_2S_3 powder, and a mixture of polyethylene powder (PP) and potassium carbonate (K_2CO_3) used as a binder. The coating process was repeated until a consistent mass of paste was reached (approximately 0.3 g).

Table 6-2 Experimental determinations of factors and levels

Factors	Components weight fraction	
	Low	High
Fe	60	90
Bi_2S_3	4.5	5
PP	3	5
K_2CO_3	3	5

To investigate the effect of the additives on the performance of iron electrode, reduce the cost and the number of runs, an experimental design (DOE) approach was used. Design Expert® (DX7) software was used for building, finding out the optimum condition, parameters and analysing of the experimental design. A 2^3 full factorial

DOE with three replicates runs used. The significant factors were determined using ANOVA analysis of variance, and 0.05 *p*-values as the limiting value.

6.1.3 Electrochemical testing methods

The electrode samples were assembled into a conventional three electrode cells, the cells were 100 ml glass that had been treated with H₂SO₄ – HNO₃ solution and washed with distilled water before each experiment. In this study, commercial nickel electrodes were used as counter electrodes (CE), our in-house as prepared electrode samples were used as the working electrodes (WE), Hg/HgO was used as reference electrodes (RE), ($E_{MMO} = +0.098V$ vs. the normal standard electrode). An aqueous solution of potassium hydroxide (28.5 w/v%) was used as electrolyte. All the cells was cycled up to 60 cycles, where the electrode samples charged galvanostatically at *C*/5 and discharged to cut off voltage of -0.6 vs. Hg/HgO reference electrode to a potential of 1.4V, at room temperature. The electrochemical testing was carried out using an Arbin 64-Channel (Model-SCTS) cycling system operating in galvanostatic mode.

The CV measurements were performed under potentiostatic control using a Solartron Cell Test System. The electrochemical CV measurements were conducted by Solartron 8-channel battery testing System (1470E/1455A potentiostat/galvanostat) in fresh 28.5% w/v% KOH solution. A conventional 3- electrode assembly was used in the test, with Hg/HgO as reference electrode, a platinum wire as counter electrode, and the as prepared electrode as a working electrode. The electrolyte was. The CV was scanned from -1.6 to -0.2V; the scan rate was 10mV/s, at room temperature. Before every CV measurement, nitrogen gas is bubbled for 20 minutes, to maintain the inert gas and to expel any gases that might generate during the CV experiments. The CV

profiles were collected using the Zview software that provided with the battery testing system.

The X-ray diffraction (XRD) technique was used to characterise the crystal phase of materials. STOE PSD X-ray powder diffraction model with (Mo $k_{\alpha 1}$, $\lambda = 0.74 \text{ \AA}$) radiation source was used. The Bragg angle range between 0° and 40° (θ) (were used.

The XRD data analysis was performed by ICDD PDF-4+ and Sieve+ software.

Transmission electron microscope (TEM) was adopted to study the mixed iron bismuth-sulfide coating electrode samples. Images of HRTEM was studied on a JEOL-2010 model, 40KV, 45mA.

6.1.4 Results and Discussion

6.1.4.1 Charge-discharge Cycling Performance

In this study, two types of pasted electrode samples were tested; iron electrode free of additives, and modified electrode with additives. The charge-discharge of the iron electrode is shown in Figure 6.1. Cycle performance was significantly improved when a bismuth sulfide additive was used.

Figures 6.1a, 6.1b shown the charge/discharge curves of 17th and last (30th) cycles , the cells demonstrate a good cycling over the 60-charge/discharge. In the potential versus time charge/discharge curves for NiFe cell, at a C/5 rate in constant current mode, the graphs presented an increased in cells efficiency by cycles, which found to be stable over at least charge/discharge of the 30th cycles.

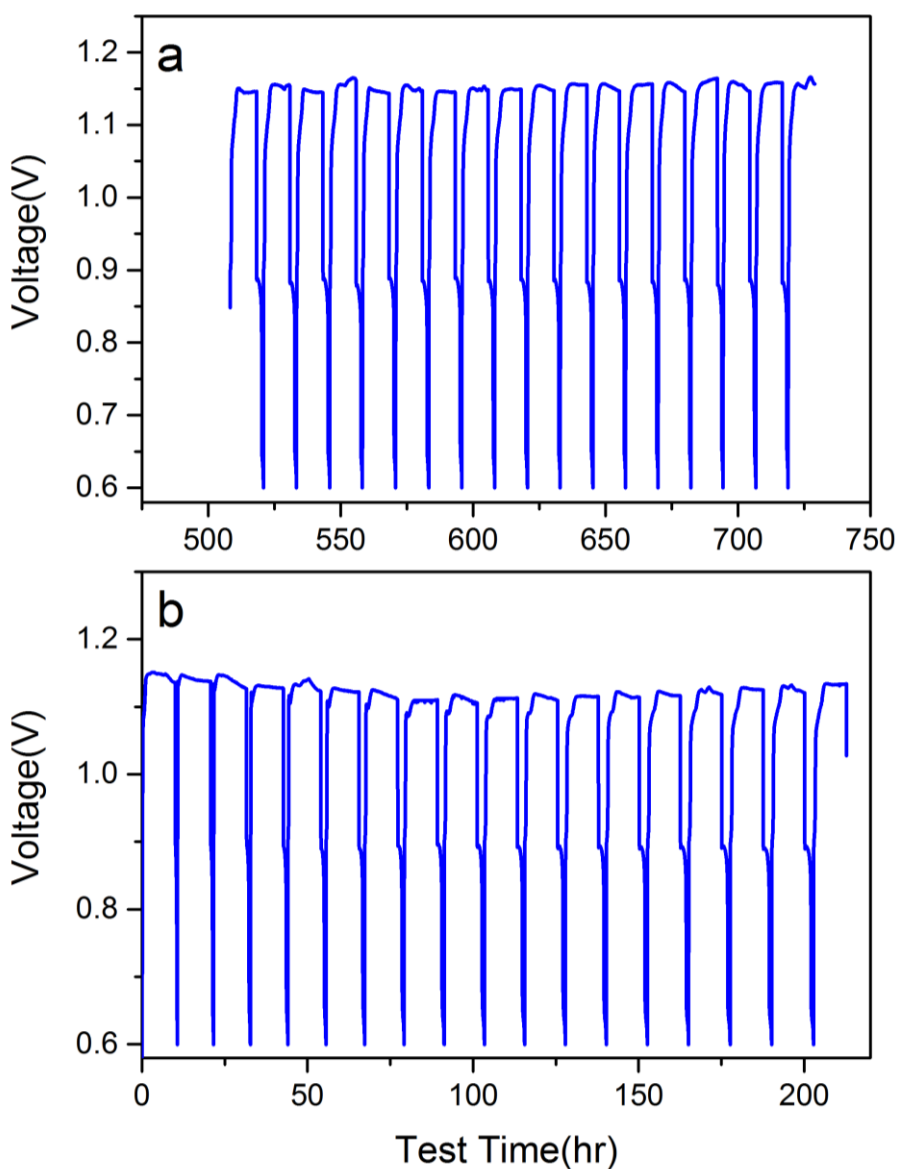


Figure 6.1 Charge/discharge constant current curves of the iron electrodes vs. Hg/HgO reference electrode of 17th and the last (30th) cycles.

Figure 6.2 a, and b - demonstrated the charge efficiency of the cells. The discharge capacity curves for 2nd, 5th, 10th, 15th, 20th, 25th, 30th, 35th, 40th, 45th, 50th, 55th, 60th, and 60th cycles, and the electrode samples with different quantities of Bi₂S₃ additives;

0.0wt%5wt%, 10wt%, 15wt%, 20wt% in iron electrodes as a function of cycle number, are presented in Figure 6.2 a-b.

It can be concluded, that the discharge capacity of iron electrodes gets better with the addition of 4.5-10wt% Bi₂S₃ additives, and the optimum percentage of Bi₂S₃ additive in iron electrodes is 4.5% wt with higher discharge capacity. Results showed, that the iron electrodes with lower Fe, has a lower discharge capacity, than that with adequate Fe in iron electrodes. This effect could be due to the adsorbed sulfide ion, which interacts strongly with Fe(II) or Fe(III) Eq.6.4), or the effect of both Bi or Bi₂S₃ Equation 6.4, which will be investigated.



6.1.4.2 Coulombic efficiency (CE)

Figure.6.2a-b shows, that the coulombic efficiency of cells with various iron electrode samples with a number of different ratio of Bi₂S₃ additives of 0%, 5%, 10%, 15%, 20 additives at a C/5 rate. The CE calculated is on average $\eta_Q \approx 30\%$ (Table 6-3). In comparison, the coulombic efficiency of the hot-pressed type with the same additives ratio is on the average $\eta_Q \approx 25\%$. The decrease in the cell efficiency might be related to the lower porosity of the Ni foam with the hot-pressed type.

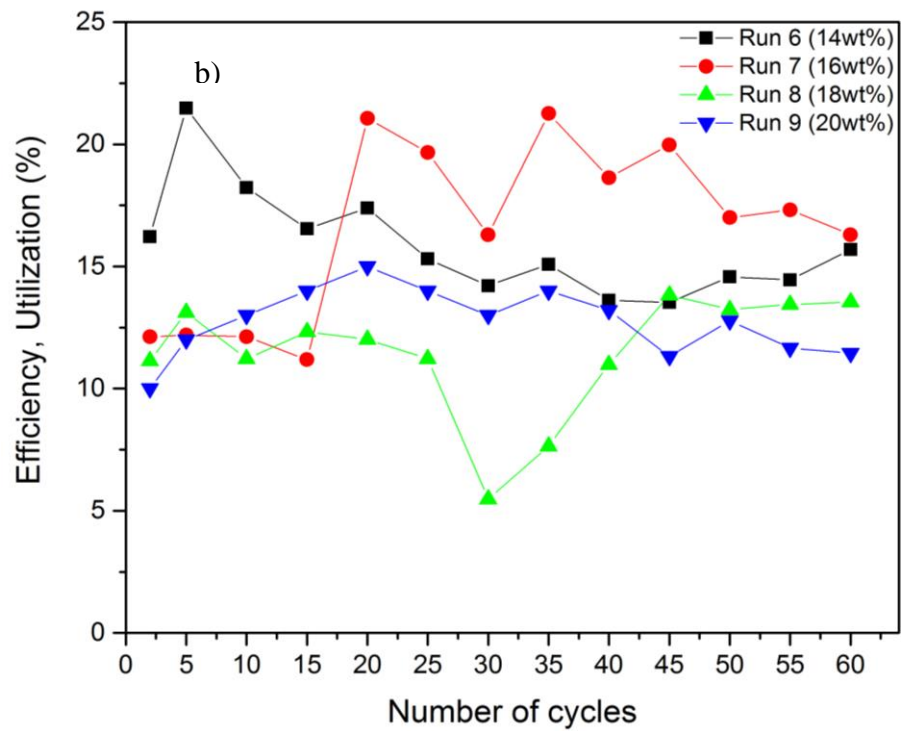
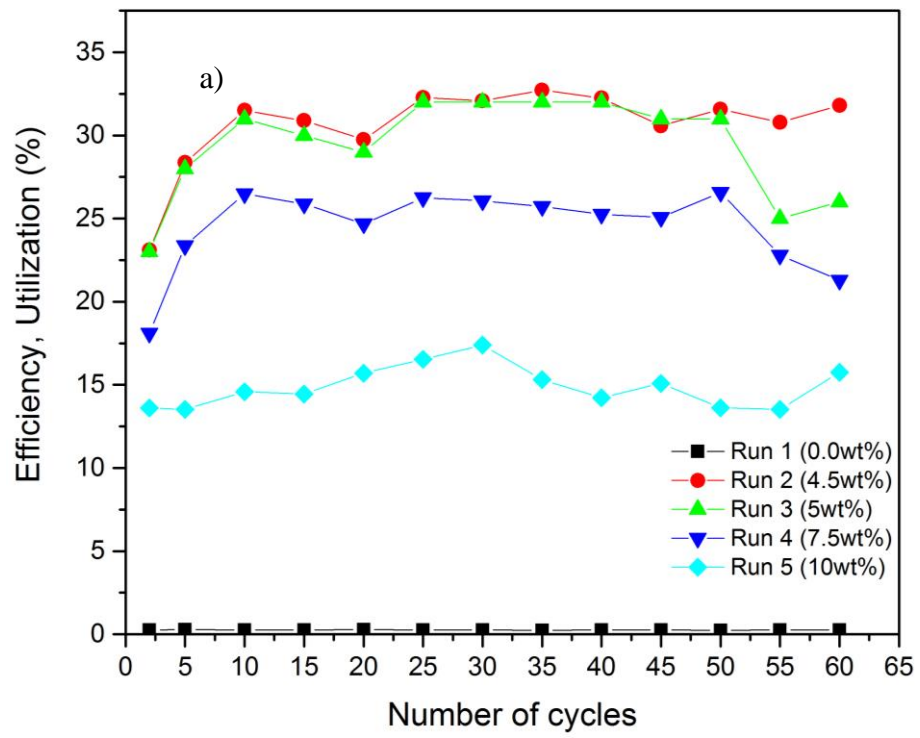


Figure 6.2a-b Constant current charge-discharge capacity curves for the 5-60 cycles with different quantities of bismuth sulfide (0-20wt.%).

Table 6-3 Example of proposed composition.

Components weight fraction				
Sample	W [Fe/g]	W [Bi ₂ S ₃ /g]	W [PTFE]/g	η_0
S1	0.9	0.0	0.1	≈ 0.25
S2	0.829	0.051	0.12	≈ 34.7
S3	0.783	0.097	0.12	≈ 18.5
S4	0.879	0.041	0.08	≈ 29.5
S5	0.74	0.18	0.08	≈ 24.4
S6	0.808	0.093	0.099	≈ 18.8
S7	0.9	0.0	0.1	≈ 0.25
S8	0.74	0.18	0.08	≈ 23.7
S9	0.846	0.072	0.082	≈ 28.6

6.1.5 Cyclic voltammetry study of iron electrode samples

6.1.5.1 Effect of Scan Rate

The effect of scan rate variation on the anodic and cathodic peak currents has been investigated. Using slow scans rate means less current flowing and the electron transfer process is faster than required for reversible reaction comparative to the diffusion rate, and can help to reduce the depletion of the reacting species at the electrode surface.

The cyclic voltammetry measurements were performed under potentiostatic control using a Solartron 8-channel testing System. An in-house three-electrode glass cell assembly was used for recording the CV measurement. The as prepared electrode was used as working electrode, Hg/HgO as reference electrode, and the counter electrode

was a platinum wire. The electrolyte was 5.1M KOH solutions. Cycling the potential within a potential range of -1.4 to -0.2 made the CV measurements at various scan rates of 2, 5, 10, 20, 50, and 100mV s⁻¹ for 10 cycles.

As described in chapter 5 section 6.4.1, the glassy carbon (GCE) surface was polished and rinsed with distilled water, and electrolyte solution purged with nitrogen for 20 minutes before each measurement.

The plots of representative CV result of the iron electrode in 5.1M KOH at various scan rates (2, 5, 10, 20 and 50mV/s) are illustrated in Figure 6.3. The voltammograms showed that both anodic and cathodic peak current linearly increases with the increase of scan rates. With the increase in scan rate, the anodic peak position slightly shifts towards the positive direction, while the cathodic peak moves a little towards the negative potential, primarily to the resistance and polarisation of the electrode materials. In Figure 6.4, peak current versus square root of scan rate of 2, 5, 10, 20, and 50mV for the iron electrode in KOH solution showed the linear increase in the anodic and cathodic peak currents with the increase in the square root of the scan rate suggesting that the electrode process is reversible.

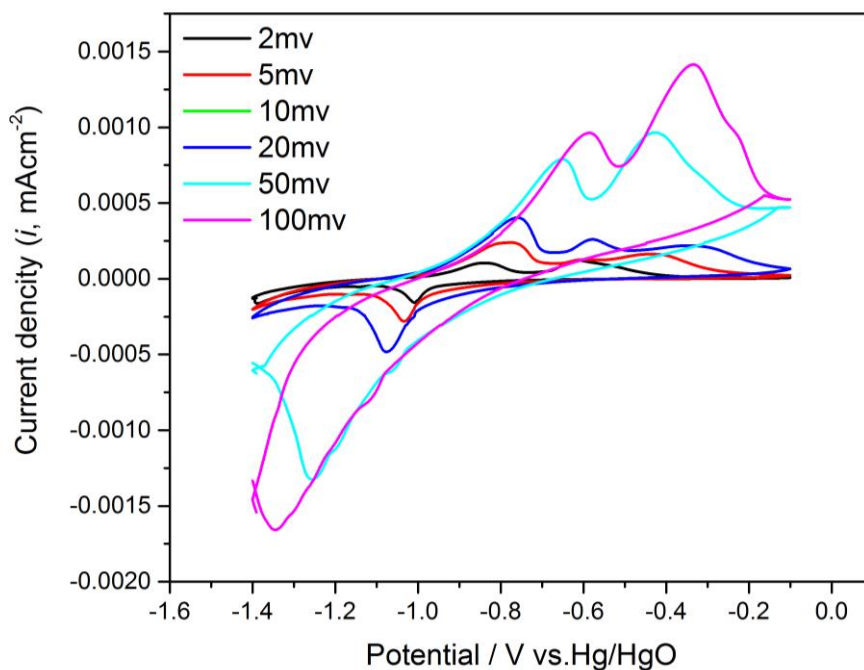


Figure 6.3 Cyclic Voltammetric of Fe in 5.1M KOH with a scan rate of 2, 5, 10, 20, 50, 100 mV s⁻¹.

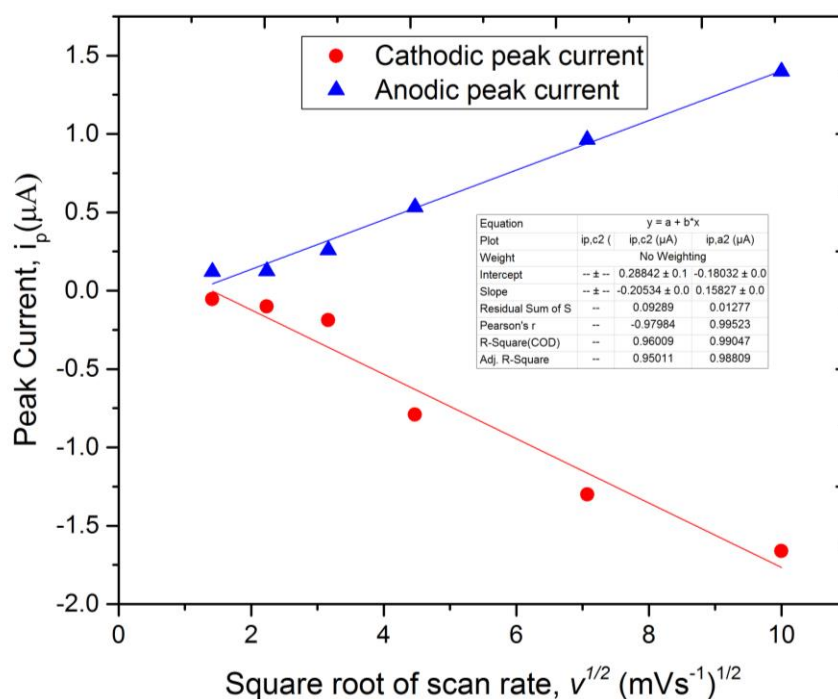


Figure 6.4 Peak current dependence with square root of scan rate of Fe in 5.1M KOH solution.

6.1.5.2 Effect of KOH Concentration Variation

The effect of electrolyte concentration on the redox behaviour of the iron electrode at GCE was also investigated. An electrolyte solution of KOH with different concentrations (0.1, 0.5, 1, and 5.1M) was used. The electrolyte contains a various concentration of KOH; the aim was to study the activity changes with increasing KOH concentration (Figure 6.5).

The diffusion coefficients were evaluated for different KOH concentration from the slope of the plot of anodic peak current versus the square root of the scan rate. Figure 6.6 indicates that the anodic peak current increased linearly as the concentration of KOH increased, which indicates that the electrode process was diffusion controlled, and showing a favourable response at higher concentrations.

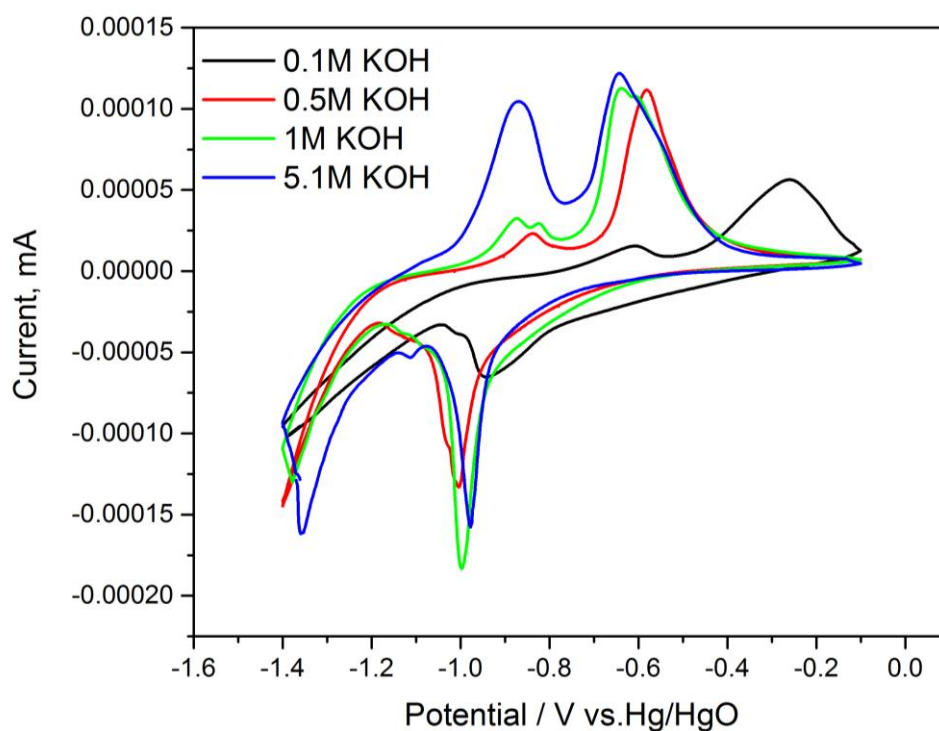


Figure 6.5 Cyclic voltammetry of Fe in 0.1M, 0.5M, 1M, 5.1M KOH with scan rate of 10mV s^{-1} .

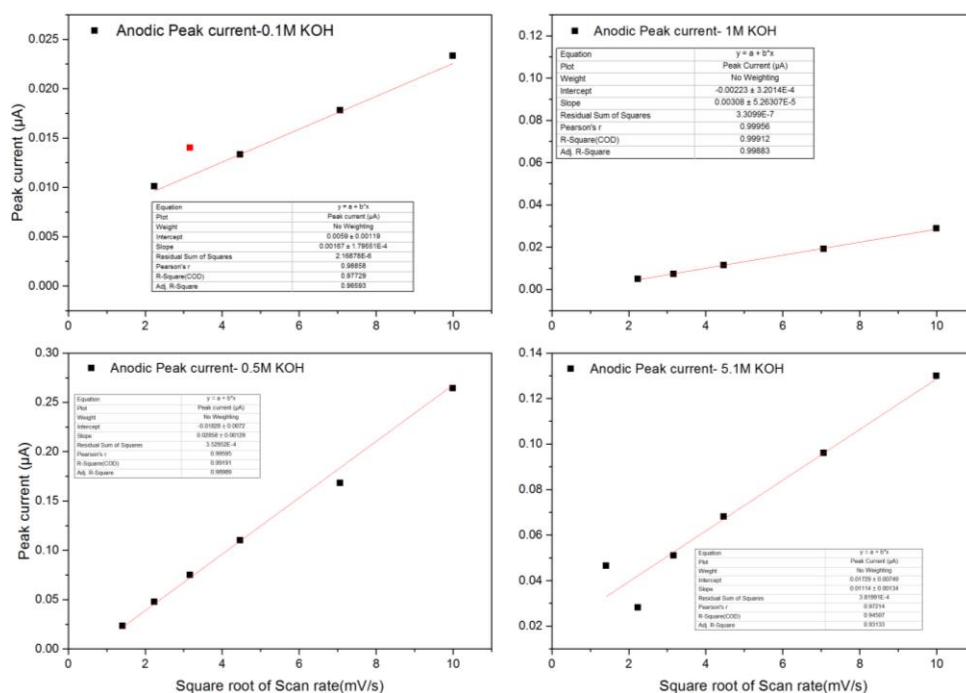


Figure 6.6 Anodic peak current vs. square root of scan rate of Fe, in 0.1, 0.5, 1, and 5.1M KOH and anodic regressions equation.

6.1.5.3 Effect of additives

To evaluate the electrochemical performance of iron electrode samples, the electrode samples with different additives are initially subjected to cyclic voltammetry measurement on the different iron electrode formulations as shown in Figure 6.7. Cyclic voltammetry of the pasted iron powder electrode in 28.5% w/v KOH solution was used to explore the electrochemical properties of the iron electrode samples. As is showing in Figure 6.7a, (electrode additives free), two oxidation peaks -0.81 V (ox₁), -0.6 V (ox₂) (vs./HgO). Those peaks related to the oxidation of Fe⁰ to Fe^{II} and Fe^{II} to

Fe^{III} , and reduction peaks -0.91 V (Red_1), -1.07 V (Red_2) corresponding to the reduction of Fe^{III} to Fe^{II} and Fe^{II} to Fe^0 .

The effect of Bi_2S_3 on the redox behaviour of $\text{Fe}/\text{Bi}_2\text{S}_3$ is presented from CV profiles (Figure 6.7b). Oxidation peaks at -0.78 V (ox_1), and -0.64 V (ox_2), which are related to the oxidation of Fe^0 to Fe^{II} and Fe^{II} to Fe^{III} , and reduction peaks -0.9 V (Red_1) corresponding to the reduction of Fe^{III} to Fe^{II} . The reduction peak (Red_2), which corresponding to reduction of Fe^{II} to Fe^0 is not visible, possibly because it was swamped by the hydrogen evolution reaction, as was suggested in several other studies (Černý and Micka, 1989, Bednarkiewicz and Kublik, 1980, Černý *et al.*, 1993, Caldas *et al.*, 1998).

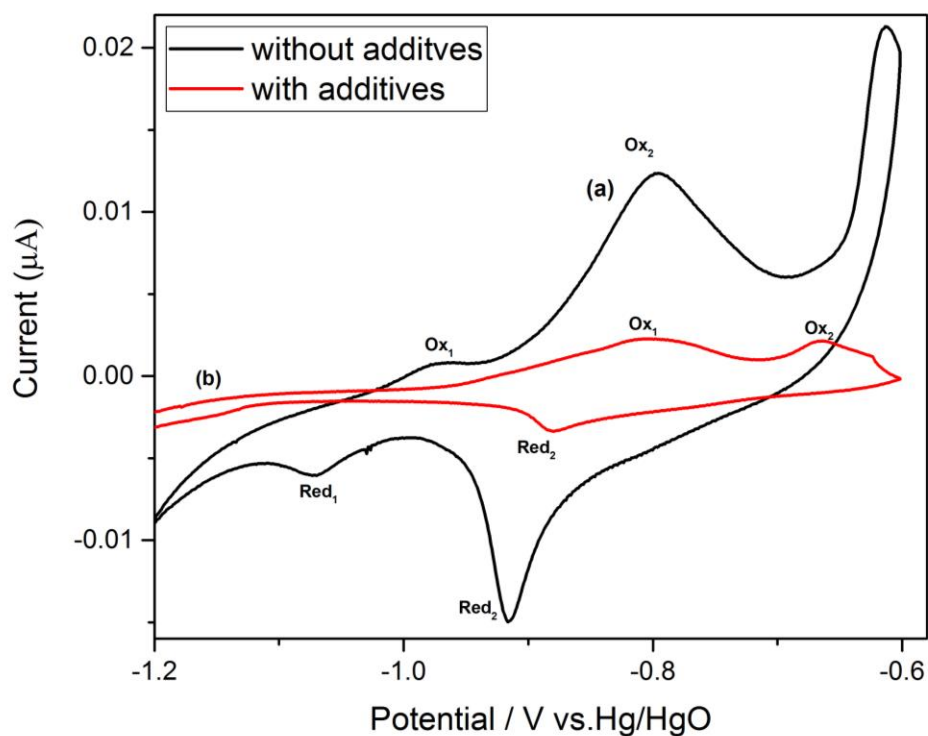


Figure 6.7 Cyclic voltammetry for the pasted iron powder electrode with Bi_2S_3 , and without Bi_2S_3 additives.

Table 6-4 shows the ratio between anodic peak current (i_{pa}) to the cathodic peak current (i_{pc}) for iron electrode samples with and without additives. The peak separation potentials $\Delta E_p = E_{pa} - E_{pc}$ is 32mV for electrode free additives, and 26mV for the electrode sample with additives, while the ratio between i_{pa}/i_{pc} is approximately equal to 1 for both electrode samples. This phenomenon indicates a diffusion-controlled process for both electrode types.

Table 6-4 The peak current and peak potentials for the iron electrode with and without additives.

Sample	i_{pc} (μA)		i_{pa} (μA)		E_{pc} (V)		E_{pa} (V)	
	$\times 10^{-2}$		$\times 10^{-2}$					
	$i_{pc1} (-)$	$i_{pc2} (-)$	i_{pa1}	i_{pa2}	E_{pc1}	E_{pc2}	E_{pa1}	E_{pa2}
Additive Free	3.8	1.2×10^{-2}	2.1	4.4	-0.93	-1.08	-0.8	-0.6
With additive	--	2.5×10^{-3}	1.8×10^{-3}	1.4×10^{-3}	--	-0.9	-0.76	-0.65

For further detailed investigations, CV for an iron electrode modified with 4.5% Bi_2S_3 additives was carried out with different potential windows from -1.4 V to 1.6 V, at a scan rate of 10 mVs^{-1} . Figure 6.8 illustrates the Cyclic Voltammogram for the Fe- Bi_2S_3 -mixed electrode during the initial ten cycles at a scan rate of 10 mVs^{-1} . From this profile, it is clear that the mixed Fe electrode with 4.5% Bi_2S_3 additives strongly affects the redox behaviour of the Fe electrodes. In this case of the Fe electrode (Figure 6.8) three oxidation peaks are observed, (Oxidation peaks (Ox_0), (Ox_1), and (Ox_2)),

and two reduction peaks were observed. The first oxidation peak in this voltammogram may be attributed to the formation of the α -Fe(OH)₂ layers or oxidation of adsorbed hydrogen atoms. Shangguan et al., indicate that the appears of both (Ox₀) and (Ox₁) peaks, which involve the electro-oxidation of iron to adsorbed Fe(II)_{ads}, only with the addition of S²⁻ ion (Shangguan *et al.*, 2015). Nonetheless, further investigation is required to understand this phenomenon better. This result is consistent with results of charge-discharge cycling measurements. Moreover, the voltammogram showed, that only hydrogen evolution proceeded when the potential was below -0.8. Where the reduction of Fe(II) to Fe⁰ will not occur because the potential of hydrogen evolution is higher than that of the reduction of the reaction of (Fe(II) to Fe).

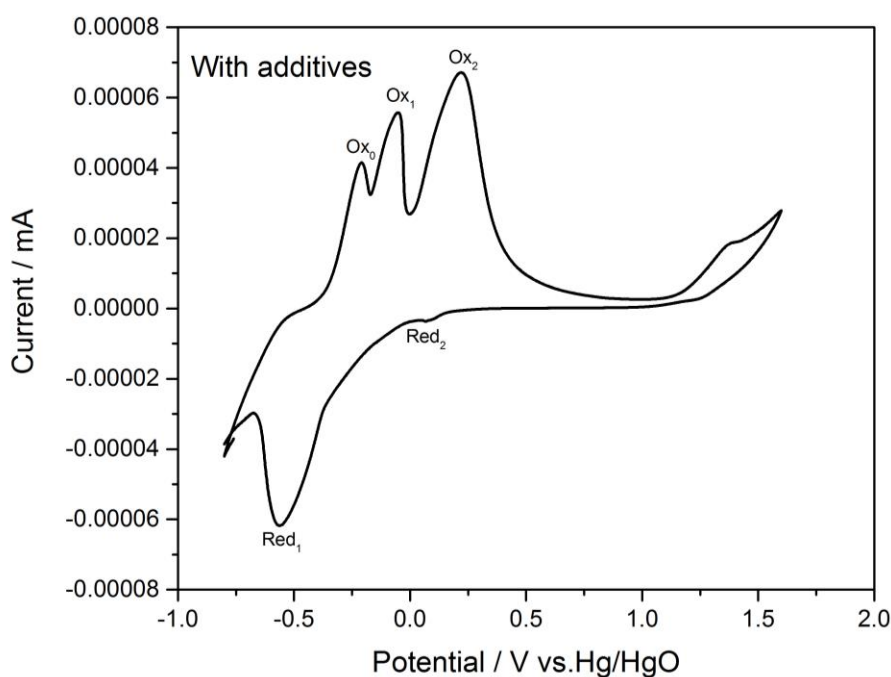


Figure 6.8 Cyclic Voltammogram of iron electrode in 28.5% KOH at scan rate of 10mV s⁻¹, with 4.5% Bi₂S₃ additive, for -0.8 V to 1.6 V potential window.

6.1.6 Characterisation of the electrodes

The morphology of the iron electrode with additives (as prepared) was observed by X-ray diffraction (XRD), and high-resolution transmission electron microscopy (HRTEM), together with X-ray energy-dispersive spectroscopy (EDS). X-ray measurements were also carried out on these electrodes to confirm the present of these materials.

6.1.7 X-ray powder diffraction results

The X-ray diffraction patterns (XRD) are in agreement with for the prepared electrode samples. Figure 6-9, 6.10, and 6.11 showed the powder XRD patterns for the as prepared electrode samples with; bismuth-sulfide of as received of Fe/Bi₂S₃, powder XRD patterns of the sample;

(S1) contain the diffraction lines of two phases: approximately (90% Fe), and (10% Bi₂S₃). Powder XRD patterns of the sample (S2) contain the diffraction lines of two phases: approximately (80% Fe), and (20% Bi₂S₃). The XRD patterns of the sample (S3) contain the diffraction lines of two phases: approximately (70% Fe), and (30% Bi₂S₃).

The XRD confirm the present of Bi₂S₃ in iron electrode samples. The diffracted lines of (ICDD-Fe 00-006-0696 card) and (ICDD-Bi₂S₃ 00-006-0333 card) in figures 6.9, 6.10, 6.11, were found between the angle $2\theta = 9$ and 29. XRD pattern of iron electrode indicates a weak peak at Fe (200) and a broad peak at Fe (110). Few peaks with a relatively weak peak intensity of Bi₂S₃ at (101), (220), (310), (320), (041), (640) were detected and show good matching.

Table 6-5 Conditions for the diffraction acquisitions

<i>hkl</i>	Standard position ($^{\circ}2\theta$)	Step size ($^{\circ}2\theta$)
110	20.17	0.05
200	28.65	0.05
101	10.8	0.05
220	10.28	0.05
310	11.4	0.05
320	13.06	0.05
041	17.66	0.05
640	26.39	0.05

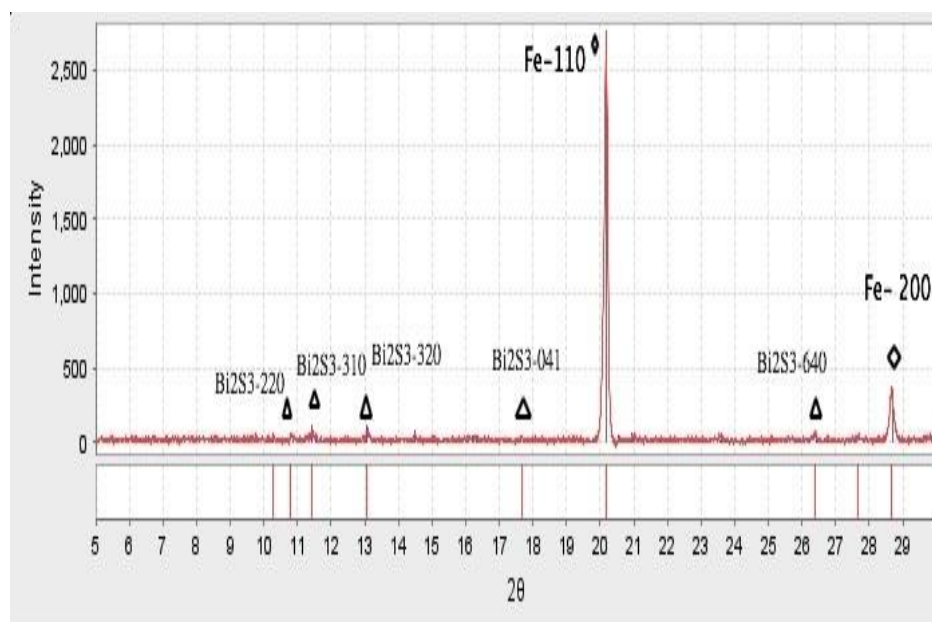


Figure 6-9 XRD powder pattern (sample S1) for iron electrode with bismuth-sulfide.

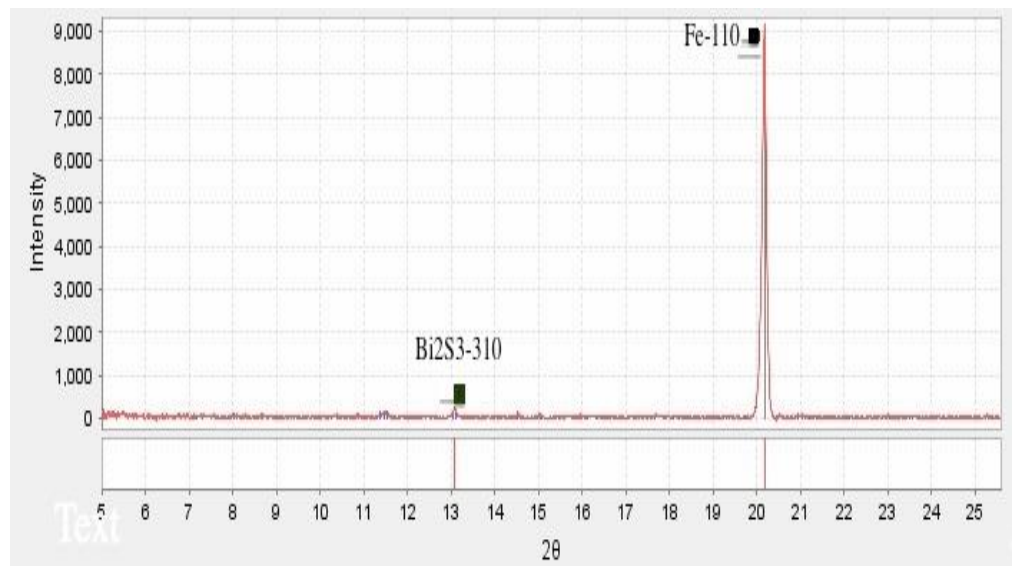


Figure 6-10 Powder XRD pattern (sample S2) for iron electrode with bismuth-sulfide.

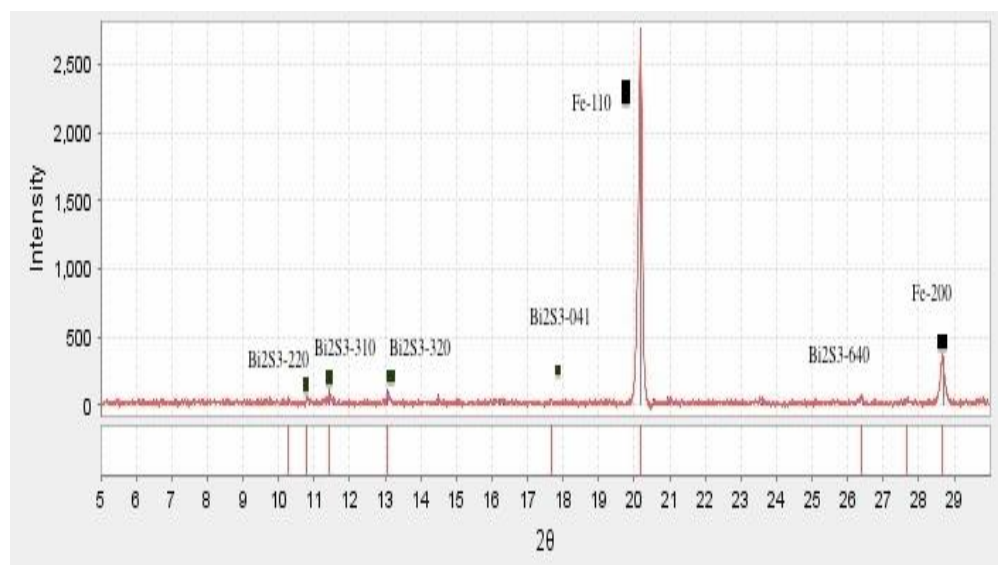


Figure 6-11 Powder XRD pattern (sample S3) for iron electrode with bismuth-sulfide

6.1.8 HRTEM analysis

Figure. 6.12a, 6.12b, represents the HRTEM images and the distribution of iron with the energy dispersive spectroscopy (EDS), in order to confirm the nature of the Bi_2S_3 present on the Fe. Energy dispersive spectroscopy EDS was performed to check and define the chemical composition of the image features Figure 6.12c and 6.12d. HRTEM images of as-prepared Fe-loaded Bi_2S_3 are shown in Figure 6.12b; the dark particles in this figure are Fe. The HRTEM images revealed that fine Fe particles were spread on the surface. Such a distribution of Fe is expected to improve the cycling ability of the Fe-loaded Fe/ Bi_2S_3 electrodes during cycling. Further, the active materials of the Fe/ Bi_2S_3 -mixed electrodes consist of relatively large iron particles Figure 6.12a. Figure 6.12b; confirm that particle is a Bi and S phase. The peaks diffraction are labelled as an orthorhombic phase of Bi_2S_3 according to standard data pattern JCPDS file (card No-43-1471) (Balducci, 2008).

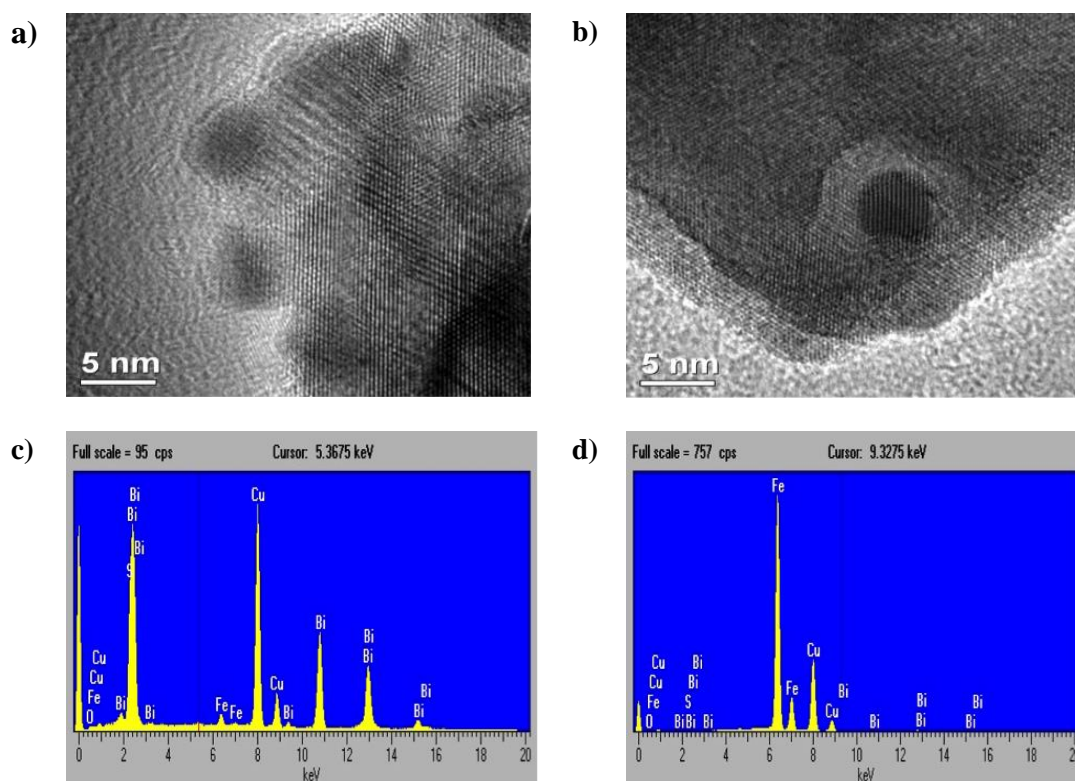


Figure 6.12 a-d, HRTEM images of Fe-Bi₂S₃ electrodes, EDS results of Fe-Bi₂S₃ electrodes.

6.2 Summary

Aiming to meet the challenge of the low charging efficiency of the rechargeable NiFe batteries. A paste electrode with Fe/ Bi₂S₃ loaded as iron electrode material was prepared. After charge/discharge cycling of the iron electrode samples with additives, analysis results shows improvement with a plain electrode and electrode with additives. Overall it was seen that addition of bismuth sulfide additives to iron electrodes led to an improvement in chargeability during cycling. The best charge efficiency of an iron electrode of Fe-loaded Bi₂S₃ electrodes can be observed for a Fe / Bi₂S₃, with 4.5%wt bismuth sulfide additive, with coulombic efficiency on average of $\approx 30\%$ ($\eta_Q \approx 30\%$). The Galvanostatic charged and discharged electrode was

investigated by X-ray diffraction and HRTEM, together with EDS. The presence of Fe, Bi, and S, confirmed by XRD, HRTEM with EDS.

6.3 Iron-Copper as anode materials

6.3.1 Introduction

Lowering the global energy consumption and reduce the depending on the fossil fuel reserves has encouraged the need for efficient, clean, sustainable sources of energy. The utilisation of energy from renewable sources such as the wind and solar power is the pathway to the sustainable energy future. However, renewable sources are not always available on demand, and energy storage is needed to balance the electric grid (Huang and Ehrman, 2006). In fact, long cycle life, high efficiency, scalability, and low-cost, are the principal requirement for the implementation of large-scale energy storage. Moreover, storage base on cost effective, safe, abundant raw materials, eco-friendly, and reduced running management costs are also required (Marini *et al.*, 2013). Recently, there is renew interest on alkaline rechargeable batteries such as Nickel-Iron batteries, because of their inherent long cycle life, safety, low cost, and environmental friendliness of raw materials compared to other competing technologies (Dang *et al.*, 2011, Pumera, 2010, Nguyen *et al.*, 2012). However, some technical issues such as low efficiency and poor utilisation of the electro-active material related to the parasitic evolution of hydrogen (HER) at the iron electrode have hindered the successful commercialization of this type of battery (Thomas 2000). Electrolyte decomposition results in poor charging efficiency and loses the water from the electrolyte (Thomas 2000). Consequently, mitigation of hydrogen evolution is a major challenge for commercial deployment of NiFe cell technology.

The suppression of hydrogen evolution and electrolyte decomposition has been successfully achieved by utilizing the electrode or the electrolyte with additives such as bismuth, bismuth sulfide, cobalt, copper, iron sulfide, carbon black, etc. (Maja and

Penazzi 1988, Haddad *et al.* 2008, Manohar *et al.* 2013, Sharifi-Asl and Macdonald 2013, Jorge Omar Gil Posada and Peter J. Hall 2014, Huo *et al.* 2014). Undoubtedly, bismuth sulfide is one of the most effective additives to reduce the evolution of hydrogen under strongly alkaline conditions (Haddad *et al.*, 2008, Manohar *et al.*, 2013, Greaves *et al.*, 1984, Maja and Penazzi, 1988). Moreover, The metal sulfide such as iron sulfide has also been effectively used (Maja and Penazzi, 1988, Caldas *et al.*, 1998). Adding additives, the electrolyte such as Na₂S, Li ions is another strategy. This strategy has been effectively adopted and used not only for controlling the reduction of Fe(II) to Fe(III) but in increasing the capacity of the iron electrode as well (Ujimine and Tsutsumi, 2006, Maja and Penazzi, 1988).

In this study, the effect of metal sulfide additives such as Bi₂S₃ and Cu on the electrochemical performance of the iron electrode is reported. Paste-type electrodes with different additives, such as Bi₂S₃, are used as a means to tackle the problem mentioned above. The formation of highly conductive materials such as copper powder to improving the reversibility of the iron electrodes active material were investigated (Kao *et al.*, 2011, Kitamura *et al.*, 2012). Copper has good mechanical properties, high electrical conductivity, and high corrosion resistance (Rosalbino *et al.*, 2012, Kao *et al.*, 2011). Iron electrodes under strongly alkaline conditions were examined. The electrode samples were investigated by galvanostatic charge/discharge cycling method and electrochemical voltammogram technique. The morphology of the electrode sample was characterised by X-ray diffraction (XRD) method. Coulombic efficiency was measured using the following:

$$\eta_Q = \frac{Q_{disch}}{Q_{ch}} \times 100\% \quad (6.5)$$

Where η_Q is the coulombic efficiency, Q_{disch} is the discharge capacity, and Q_{ch} is the charge capacity.

6.3.2 Materials and Solutions

6.3.2.1 Preparation of iron electrodes

Iron-paste type electrode was prepared as it described in chapter.3. In the dry coating process, iron powder (Fe , $99\% \leq 10\mu\text{m}$) mixed with differing amounts of electrode materials and PTFE (Teflon) binder to form the slurry as shown in Table 6-6. A strip of foam nickel (10 mm x 40 mm x 1.5 mm) was coated with the slurry. The electrodes were dried under vacuum for 4h. The process of the coating was repeated 2 to 3 times until a constant amount of electroactive paste was reached (about 3g). Then the electrodes were placed in the vacuum oven at 110°C for 24 hours to ensure consistency. Two type of iron electrode sample were used. The experiments were carried out using the following electroactive formulations; (A) iron powder at various levels of copper powder and PTFE; (B) iron powder at different levels of bismuth sulfide, copper powder, and PTFE. The electrolyte was an aqueous solution of KOH (28.5 w/v%).

Table 6-6 The experimental design determinations of factors and levels.

Group A			Group B		
		Level			Level
Factors	Low (% _w)	High (% _w)	Factors	Low (% _w)	High (% _w)
Fe	60	90	Fe	60	90
Cu	0	10	Cu	0	10
PTFE	8	15	PTFE	8	15
			Bi ₂ S ₃	4.5	5

6.3.3 Characterization techniques

6.3.3.1 X-ray powder diffraction (XRD)

The cycled electrode samples were removed from the cell, washed with distilled water and stored in the oven under vacuum. Then the electrodes sample either cut into 1 cm squares or carefully removed from the Ni foam manually by scraping with a spatula and ground up with a mortar for XRD analyses. The XRD method was used to characterise the phase structure of the samples. Bruker D2 Phaser X-ray diffraction model with (Cu-K α , $\lambda = 1.5406 \text{ \AA}$) radiation source, at a 2θ range between 5° to $85^\circ(2\theta)$ with a 0.02° scanning step size. The XRD data analysis was performed by ICDD PDF-4+ and Sieve+ software.

6.4 Electrochemical measurements

6.4.1 Charge-discharge cycling

For the charge-discharge cycling measurements, three-electrode cell configuration was used. In our in-house the commercial nickel electrodes were used as CE, as prepared electrode samples were used as WE, Hg/HgO were used as reference electrodes (RE), ($E_{\text{MMO}} = +0.098\text{V}$ versus. the standard hydrogen electrode). KOH (28.5 w/v% KOH) was used as electrolyte.

The electrochemical cycling measurements were taken with Arbin 64-Channel Model-SCTS battery charger system operating in galvanostatic mode. The cycling protocol consisted of a several steps procedure where the cell was cycled up to 60 cycles; cells were charged galvanostatically to their rated capacity, discharged to the

cut off voltage of -0.8 versus. Hg/HgO, (RE), to a potential of 1.4V at a C/5 rate. All measurements were taken at laboratory temperature.

6.5 Results and discussion

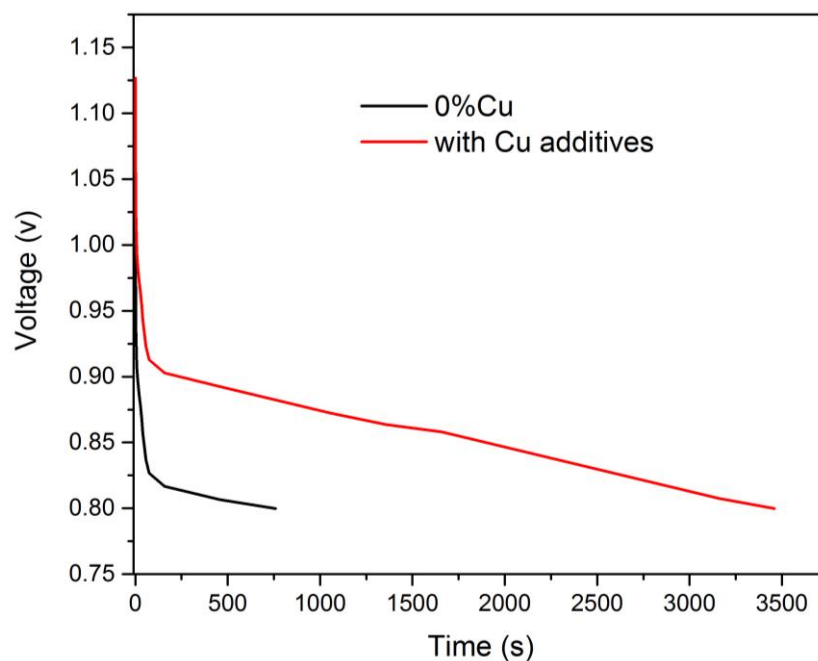
6.5.1 Cycling performance

The first discharge for iron-based electrode samples with and without additives is illustrated in Figure 6.13. The results reveal that while electrodes of the A type exhibit one single plateau, electrodes of the B type exhibit two plateaus, the first of which would correspond to the conversion of Fe to Fe(OH)₂. The second plateau would suggest the presence of bismuth sulfide.

It is also interesting to compare the additives usage per rated efficiency of the electrodes. It was observed that electrodes lacking copper-based additives always underperformed their copper loaded counterparts. In addition, the presence of bismuth sulfide did also increase the overall performance of the cell. Some authors believe that this improvement might be due to the adsorbed sulfide ion, which interacts strongly with Fe⁰ or Fe^{II} or Fe^{III} (Moura *et al.*, 2013).

Under the light of our experimental results, it is clear that coulombic efficiency (η_Q) is enhanced by the presence of both bismuth sulfide and copper. Given the definition of coulombic efficiency (Equation 6.5), it follows that bismuth sulfide and copper would increase the hydrogen overpotential barrier, thus preventing the electrolyte from electrolysis.

The best charge efficiency of the iron electrode of Fe-loaded Bi_2S_3 electrodes can be observed for a Fe / Bi_2S_3 , with 4.5% wt. bismuth sulfide additive. Copper additives showed a positive effect on charge efficiency of the iron electrodes.



Figure

6.13 Voltage-time discharge curves of paste-type iron electrodes with and without additives at a $C/5$ rate.

The discharge capacity for additives free and with additives iron electrodes versus cycle number are shown in Figure 6.14. From this profile, it is clear that electrodes of the group B showed increasing in the discharge capacity from the initial 10 cycles. Moreover, within 15 cycles, with small amount of Cu-containing electrode rendered the best cycling performance among all electrodes. Similar cycling performance characteristics can be found for electrodes of the group A; however, during the first 15 cycles, electrode capacity decreases faster than with B type

electrodes and this could be due to the dropping of electro-active material into the electrolyte.

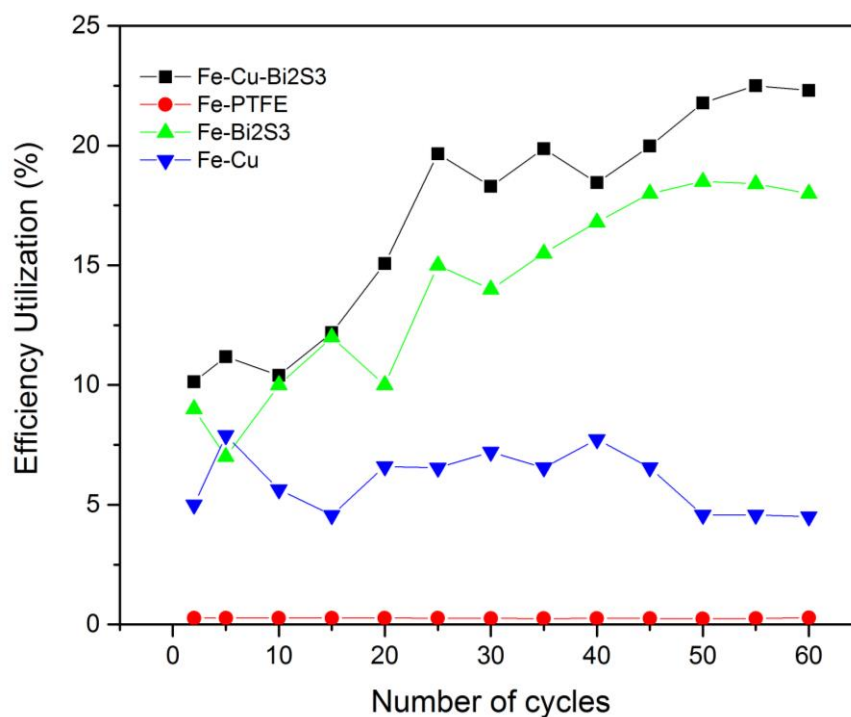


Figure 6.14 Discharge capacity for the iron electrode versus cycle number.

Cyclic voltammograms of the mixed electrode samples of Fe/Bi₂S₃, and Fe/Bi₂S₃-Cu at a scan rate of 5 mV s⁻¹, during are shown in Figure.6.15a-b. From these profiles, the Fe electrode with Cu additives shows not effect on the redox behaviour of the Fe/Bi₂S₃ mixed electrode additives. In comparison, using metal sulfides such as bismuth sulfide and copper additives did enhance the performance of iron electrodes, however, further investigation in needed, because XRD results does not detailed any evidence of reactions between iron and copper.

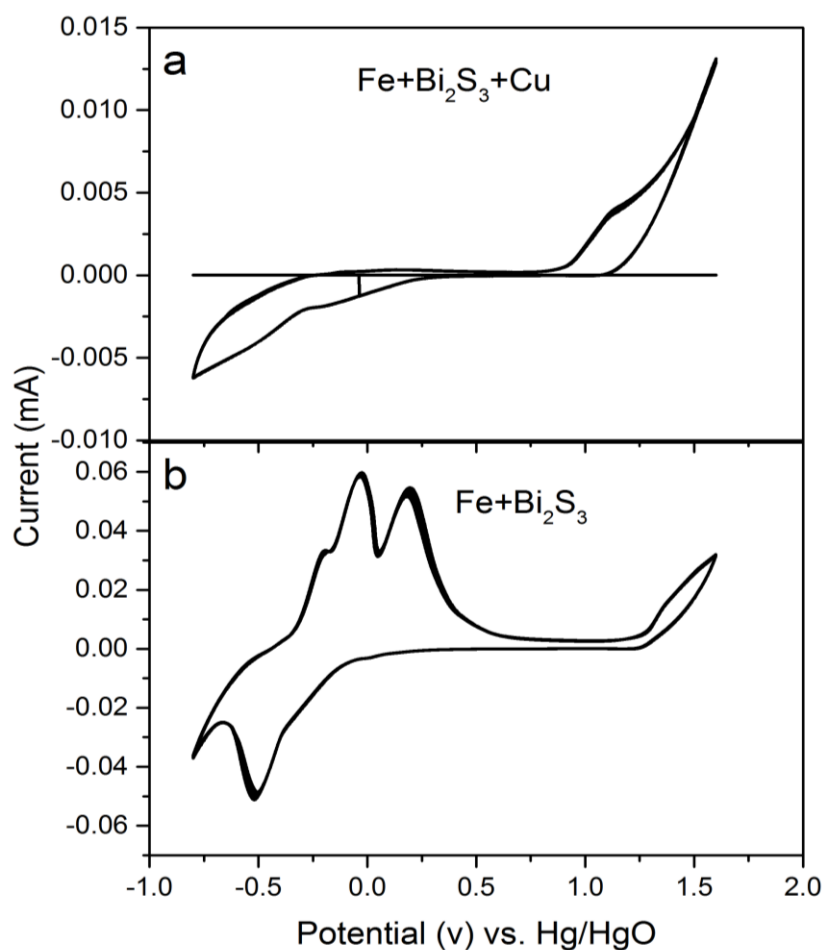


Figure 6.15 Cyclic voltammograms of the (a) Fe/ Bi₂S₃-Cu mixed electrode (b) Fe/Bi₂S₃ mixed electrode additives, at scan rate of 5 mV s⁻¹.

6.5.2 X-ray powder diffraction results

Figure 6.16a-b shows the XRD diffraction pattern for the Fe electrode samples with bismuth-sulfide, copper as received Fe/Bi₂S₃Cu. The XRD confirm the presence of Bi₂S₃ and Cu in the iron electrode. The diffracted lines of (ICDD-Fe 00-006-0696 Card) and (ICDD-Bi₂S₃ 00-006-0333 Card) were found between angle 2θ = 9 and 29. The XRD pattern of iron electrode shows a weak peak at Fe reflections (200) and the broad peak at Fe(110). Fe peaks with a relatively weak intensity where the Miller

indices (*hkl*) of Bi₂S₃ with the reflections of; (101), (220), (310), (320), (041), (640) were detected and show good matching.

Figure 6.16, indicated the powder XRD pattern for the electrode samples with bismuth-Sulfide, copper of as received of Fe/Bi₂S₃-Cu. The X-ray samples as prepared contain the diffraction lines of two phases: approximately 95% Fe, and 5% Bi₂S₃ and approximately 3% Cu. The iron electrode obtained was identified to be Fe+ Bi₂S₃ and copper by X-ray diffraction (XRD). The XRD confirm the present of Bi₂S₃ and Cu in iron electrode.

The diffracted lines of Fe, Cu, and Bi₂S₃ were found between angle $2\theta = 9$ and 95. The XRD pattern of iron electrode shows a weak peak at Fe(200) and a broad peak at Fe(110). Fe peaks with relatively weak intensities of Cu with the reflections of (111), (200), (220), (311), (222), and Bi₂S₃ at (101), (220), (310), (320), (041), (640).

Figure 6.16b, shows the powder XRD pattern of the electrode sample after extended cycling. The powder XRD pattern for the electrode sample modified with bismuth sulfide and copper sulfide after cycling showed the present of Fe, Fe₃S₄ and Cu₂O, and elemental bismuth. The cycled electrode samples exhibited a small shift of reflection peak of Fe(200) and high intensity of the reflection Fe(110) and new replication of the peak of Fe(300), where this reflection is not seen in the prepared electrode samples. The XRD analysis reveals that no definite evidence of reactions between iron and copper.

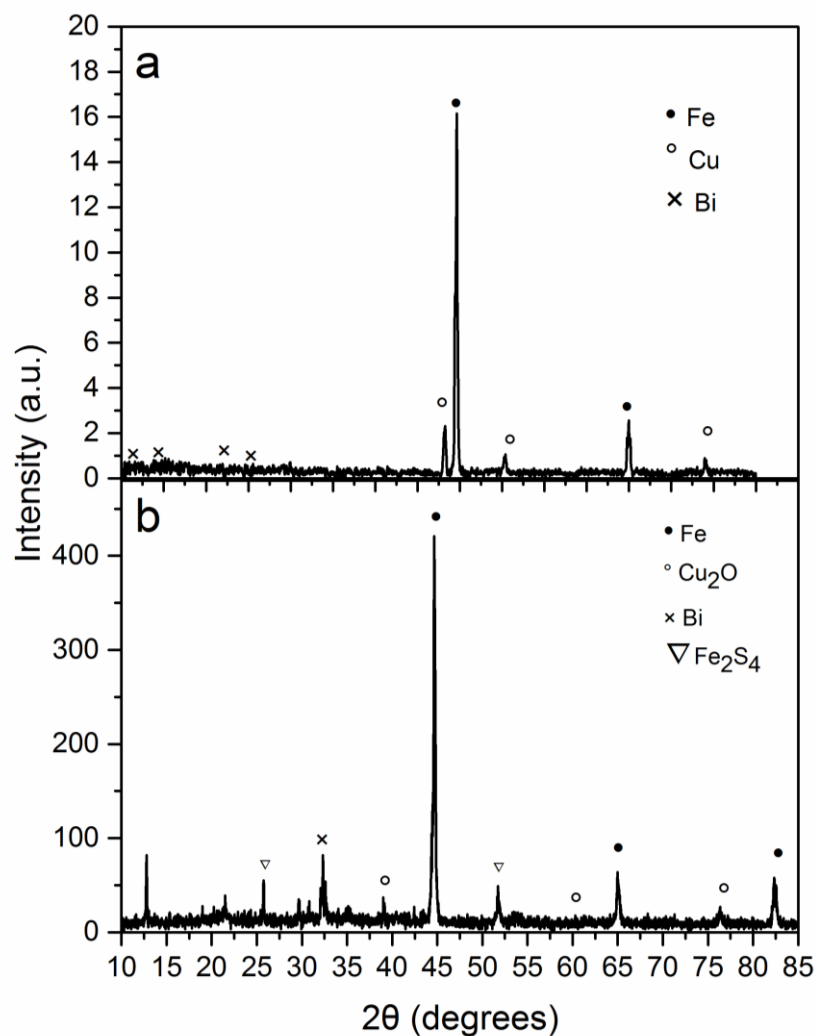


Figure 6.16 XRD powder pattern for the: (a) as prepared iron electrodes, (b) the iron electrode after extended cycling.

6.6 Summary

In this study, iron with copper as an anode additives was investigated. A paste electrode with $\text{Fe}/\text{Bi}_2\text{S}_3$ and Fe/Cu was prepared and electrochemically characterised with the Galvanostatic charged and discharge. The electrode was studied by the cyclic voltammetry technique and X-ray diffraction. Overall it was seen that addition of

bismuth sulfide additives to iron electrodes resulted in an improvement in chargeability over cycling.

The effect of using metal sulfide such as bismuth sulfide and copper additives to enhance the performance of iron electrodes has been examined. Our experimental results confirm that the addition of both bismuth sulfide and copper significantly improves the performance of the electrode. By contrast, the utilisation of copper-alone electroactive additives materials shows no improvement.

6.7 Iron sulfide and copper sulfide as anode materials

Some of this section have been published, and have been quoted verbatim from the following source, "Title; Abdalla, A. H., et al. (2016). "Rechargeable nickel-iron batteries for large-scale energy storage." IET Renewable Power Generation 10(10): 1529-1534.

6.7.1 Introduction

With depletion of the coal, oil, and other fossil fuels, increasing the demand for energy, and rising concerns over environmental pollution has encouraged the development and use of alternative, sustainable, clean and renewable energy resources (Sarrias-Mena *et al.*, 2014, Warren, 2014). The renewable sources such as the wind and power energy have the potential to reduce greenhouse gas emissions (GHG), due to its natural environmental friendliness, abundance, offering a practical way of reducing our reliance on fossil fuels resources (Zhao *et al.* 2015, Hollister-Short 2016). Unfortunately, the intermittent nature of these resources restricts their use. Fundamentally, energy generation from renewables and demand are not easily matched. Amongst numerous energy storage technologies currently exist, electrochemical energy storage systems (ESS) emerge as a possible solution to the problems mentioned above. In fact, considerable efforts have been made in order to develop highly efficient, robust and safe energy storage (Rajan *et al.*, 2014, Zhao *et al.*, 2016). Of course, the intended solution would also require abundant, non-toxic and eco-friendly materials (Marini *et al.*, 2013).

Recently, there is renewed interest on nickel-iron (NiFe) battery that left out of favour with the advent of cheaper lead acid (LA) batteries. Due to their durability,

environmentally friendliness, compatibility with renewable sources (such as wind power), low cost of raw materials, long life-cycle, low cost and good resistance to electrical abuse (overcharge and deep discharge) (Linden and Reddy, 2002, Anani *et al.*, 1991). Further, iron as negative electrode, is known as non-toxic, cost-effective and eco-friendly safe materials. Thus, the relative abundance of chemicals and raw materials required to build these cells, indicate this technology could provide a cost-effective solution to store energy for grid system applications. Unfortunately, the commercial deployment of these batteries has been limited by the poor charge efficiency (50-60%) related to the hydrogen evolution that takes place during charging of the battery. Considerable effort and different effective approaches have been adopted to counteract these issues, including using anode additives. Therefore, Mitigation or even prevention of hydrogen evolution is, essential to achieving large-scale commercial employment of NiFe cells.

The suppression of hydrogen evolution and electrolyte decomposition has been traditionally achieved by utilising electrode additives. By deployment additives to the electrode such as carbon-black, bismuth, bismuth sulfide, cobalt, copper, iron sulfide, etc. (Haddad *et al.*, 2008, Huo *et al.*, 2014, Maja and Penazzi, 1988, Manohar *et al.*, 2013), electrolyte additives (Ujimine and Tsutsumi 2006, Posada and Hall 2015), and nano-sized of the electrode materials (Kao and Chou 2010, Kao *et al.* 2011, Manohar *et al.* 2012, Huo *et al.* 2014, Shangguan *et al.* 2015b). Undoubtedly, metals sulfide is one of the most effective additives to reduce the evolution of hydrogen under strongly alkaline conditions (Haddad *et al.*, 2008, Manohar *et al.*, 2013, Greaves *et al.*, 1984, Maja and Penazzi, 1988).

Several researchers have made considerable efforts on sulphur containing additives. Such as bismuth and bismuth sulfide (Posada and Peter J. Hall 2014), iron sulfide (Hang *et al.*, 2006), lead sulfide (Balasubramanian and Shukla, 1993), sodium sulfide (Kalaignan *et al.*, 1987). These studies indicated that the addition of these sulfur-containing substances significantly suppresses hydrogen evolution and increase the performance of the batteries.

The role of sulfide additives has been attributed to several factors (Shangguan *et al.*, 2015):

- (1) Improvement of the Fe/Fe(OH)₂ reaction rate, and improve the high-rate ability.
- (2) The adsorption of sulfide ion at the electrode/electrolyte can have an effect of the modification of the iron electrode form and morphology.
- (3) Prevention of the rapid electrode passivation and improve the battery cycle ability.

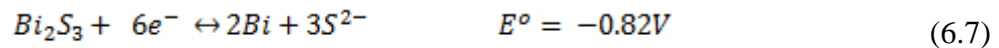
Iron sulfide has been intensively studied and has drawn particular interests. Besides, the beneficial of iron sulfide in increasing the ionic conductivity of the passive film on iron have been reported (Caldas *et al.*, 1998). Several studies have indicated that FeS was mainly used as anode additives to mitigate the hydrogen evolution and the electrode passivation (Jiang *et al.*, 2014) in alkaline batteries.

Thought, one of the less studied electrode additives with the potential to reduce the activation energy barrier for water decomposition on the surface of the iron electrode is copper. Copper is also well known for its high electrical conductivity, chemical activity and good corrosion resistance (Kim *et al.*, 2003, Paixão *et al.*, 2006, Shan *et al.*, 2008, Chou and Kao, 2009, Jayalakshmi and Balasubramanian, 2008, Lv *et al.*, 2014). It has been observed that when employing together with elemental iron

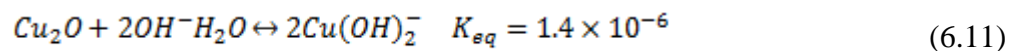
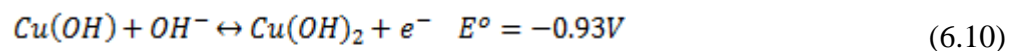
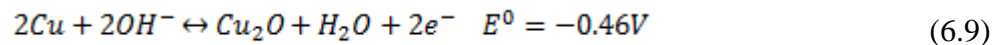
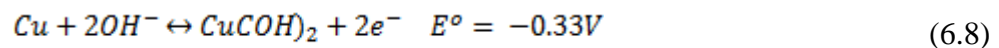
in a solution of copper sulfate, then a single replacement reaction as indicated by Equation 6.6 would occur.



The formation of a protective layer of copper would act in a similar manner than the layer of elemental bismuth that was formed by Equation 6.7



Furthermore, the electrochemical behaviour of the Cu(II)/Cu(I) pair is reported to be similar to the Fe(III)/Fe(II) pair, as illustrated in Equations (6.8-6.11) (Giri and Sarkar, 2016, Paixão *et al.*, 2006, Jayalakshmi and Balasubramanian, 2008).



Giri and Sarkar proposed that as the potential is increased beyond -0.4V the formation of Cu₂O (Equation (6.9) dominates over its dissolution (Equation 6.11) (Giri and Sarkar, 2016).

Electrolyte additives have also been used to enhance the performance of the battery. It has been reported that electrolyte systems based on Na₂S and LiOH would significantly improve the capacity of the iron electrode. It has been recently demonstrated that sulfide ions could suppress the electrolyte decomposition (Burke and Nugent 1997, Burke and Nugent 1998, Kessler *et al.* 2015).

In this study, we aim to explore the use of different forms of copper (metallic and copper sulfate) and iron sulfide as electrode additives for suppressing the evolution of hydrogen; likewise, we shall also use potassium sulfide as an electrolyte additive to further improve our in-house made NiFe cells.

These studies investigate and clarify the effect of iron sulfide and copper composites in suppressing the evolution of hydrogen and improving the electrochemical performance of NiFe batteries.

6.7.2 Experimental Methods

6.7.2.1 Electrode Preparation

For more details, see Chapter 5.5.4.1. Paste-type electrode of anode current collectors was developed and tested. Strips of nickel foam was coated with the electroactive slurry consisting of differing quantities of iron powder (Fe, 99% ≤ 10μm), that mixed with FeS (99.5% ≤ 10μ), CuSO₄ 5H₂O (98% ≤ 10μm) and Polytetrafluoroethylene as a binder (PTFE) used primarily to hold the mixture together. Then the mixture was then homogenised placed in an ultrasonic bath for 10 minutes to form the slurry. Afterwards applied to the Ni foam (10 x 40 x 1.5 mm), was coated with the slurry to form the paste, and vacuum dried for 5h at 100°C. The coating process was repeated until a constant weight of iron was achieved (about 0.3 g

cm⁻²). Then the electrodes were vacuum dried one final time overnight at 80 °C to ensure consistency. The solutions were prepared with deionized water and potassium hydroxide. Table 6-7 shows the experimental factors and level used during the experiments.

Table 6-7 Main factors and levels used in experiments

Factors	Level (% _w)	
	Low	High
Fe	82	89
FeS	0	5
CuSO ₄	3	5
PTFE	8	8

The extraction of data was automated by using an in-house developed C/C++ program that interrogates all files produced by the battery cycles. To investigate the effect of the mixed sulfide additives on the performance of iron electrode samples, reduce the cost and the number of runs, experimental design (DOE) approach was used. Design Expert® (DX7) software was used for building, finding out the optimum condition, parameters fitting, analysing and visualizing the estimated response surface of the experimental design. A full factorial DOE with three replicates runs used. The significant factors were determined using ANOVA analysis of variance, and 0.05 *p*-values as the limiting value.

6.7.3 Charge-discharge cycling

The electrochemical cycling tests were taken using Arbin 64-Channel SCTS battery testing system and MITS Pro software. A sketching illustration of the cell test configuration can be found in Figure 6.17.

The charge/discharge measurements were carried out in a three-electrode glass cell configuration, with in-house-prepared pasted electrodes used as the working electrode (WE), the commercial nickel electrode was used as a counter electrode (CE), a mercury/mercury oxide (M/MO) was used as reference electrode (RE), ($E_{\text{Hg}/\text{HgO}} = + 0.098\text{V}$ vs. NHE), a solution of potassium hydroxide (28.5 w/v% KOH, purity $\geq 85.0\%$) was used as the electrolyte. The cycling protocol consisted of a several steps procedure, where the cells cycled under galvanostatic mode up to 60 cycles to their rated capacity (0.35 Ah g^{-1}) at a C/5 rate from -0.8 to -1.4 V vs. MMO. All measurements were carried out at laboratory temperature.

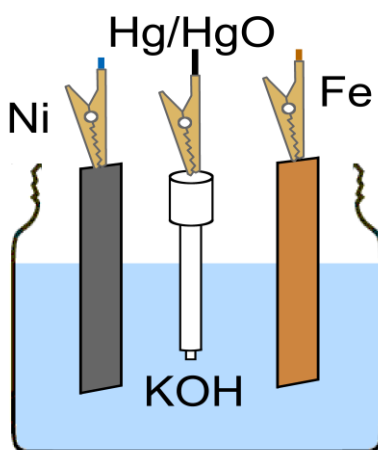


Figure 6.17 Schematic of the Cell configuration.

The battery efficiency was investigated using battery discharge capacity measurements, which definite as the total cell charge can be accumulated during a full discharge as the following Equation 6.12:

$$\text{Charge efficiency } (\eta_Q) = \frac{Q_{ch} - Q_H}{Q_{ch}} \times 100 \quad (6.12)$$

Where η_Q is the coulombic efficiency, Q_{ch} is the total charge, and Q_H is the charge wasted in electrolyte decomposition (Manohar *et al.* 2012). The charge used for hydrogen evolution was calculated with the current of hydrogen evolution, which in turn was calculated by using the Tafel relationship (Balasubramanian and Shukla, 1993). The increasing hydrogen overvoltage could, therefore, be explained by the total increase in the exchange current density.

6.7.4 Cycling voltammetry measurements

The cyclic voltammetry (CV) measurements were performed under potentiostatic control using an 8-channel Solartron Cell Test System (1470E/1455A potentiostat/galvanostat). The CV measurements were carried out in a three-electrode glass cells with prepared pasted electrode samples as the working electrode, Hg/HgO as the reference electrode, and the counter electrode (CE) was a platinum wire. The electrolyte was 5.1M solution of potassium hydroxide (KOH) at room temperature.

6.7.5 Characterization techniques

The electrode samples were removed from the cell, washed with distilled water and stored in the oven under vacuum. Then the electrodes sample either cut into 1 cm squares or carefully removed from the Ni foam manually by scraping with a spatula

and ground up with a mortar and pestle for XRD analyses. The phase structure of the samples was identified by X-ray diffraction (XRD) technique. Bruker D2 Phaser system X-ray powder diffraction model with (Cu-K α , $\lambda = 1.5406 \text{ \AA}$) radiation source was used. The Bragg angle range between 5° to 85° (θ) were used. The XRD data analysis was performed by ICDD PDF-4+ and Sieve+ software.

AFM has been implemented as a structural characterisation technique for examines the surface morphology at the iron electrodes before and after cycling formation, where the electrode samples electrodes after been subjected to charge/discharge cycling immediately rinsed with deionised water, followed by drying under stream nitrogen. The surface imaging was performed on (Bruker Dimension Icon), operating with the ScanAsyst system in soft tapping mode in air from, with the nominal force constant of 40 N m^{-1} , and a resonant frequency of 300 KHz.

Scanning electron microscopy was used (SEM) for morphological characterisations. The prepared and cycled iron electrode samples were characterised using Inspect F-SEM, to see the formation and effect of investigating the surface topography of the electrodes.

6.7.6 Results and discussion

6.7.6.1 Cycling performance

The charge/discharge cycling method was used to examine the electrochemical properties of the electrode samples (as prepared). Generally, the as prepared electrode samples were repeatedly cycled up to 60 cycles at room temperature until a stable state

is reached (usually 25-30 cycles)) (Posada *et al.* 2015), so meaningful comparisons could be drawn. Typical charge and discharge voltage profiles of a NiFe cell can be found in Figure 6.18a. The charge/discharge curves of the initial cycles from 17-35 are shown in Figure.6.18b. Figure. 6.18b clearly shows that cell performance increases with the cycle number.

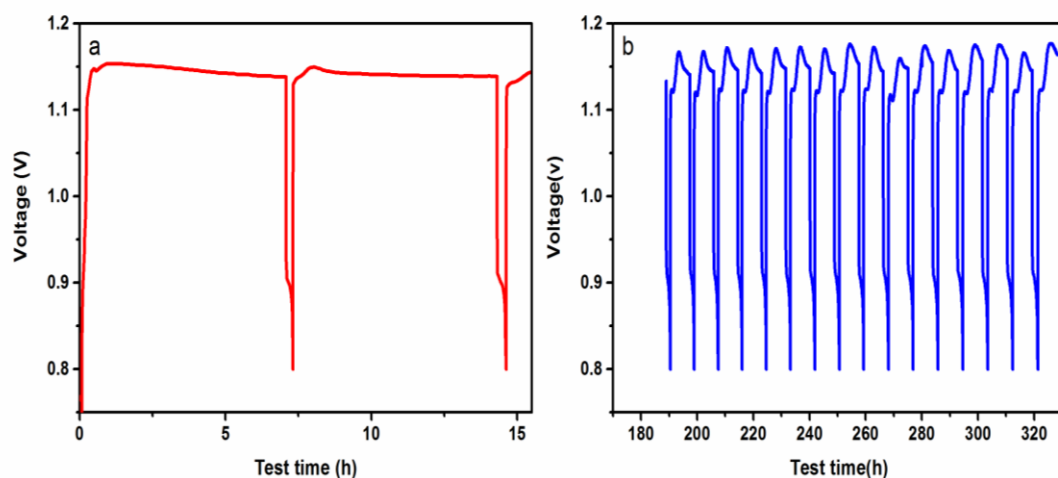


Figure 6.18. a) Charge-discharge curves of the first cycle of an iron electrode vs. Hg/HgO reference electrode at a C/5 rate, b) charge-discharge curves of the cycles from 17th-35th among 60 cycles.

Figure 6.18 confirms that the overall performance of the NiFe cell increases with the use of copper sulfate in the electrode samples. Formulations lacking copper tend to exhibit extremely low coulombic efficiencies (1-5%, results not shown). However, in the presence of copper sulfate, coulombic efficiencies increase by up to eight times.

Our experimental results demonstrate the benefit of copper sulfate as an electrode additive for improving the performance of iron electrode samples and clearly show that the use of CuSO_4 has a positive effect on increasing both the coulombic

efficiency and the capacity of the iron electrode as shown in Figure.6.19. Actually, under the experimental conditions explored here, it seems there is an optimal composition for copper sulfate at CuSO_4 3%_w, but more investigation is still required to optimise the formulation. It is also evident that the presence of FeS tends to increase the performance of the cells to a larger extent than copper sulfate. In fact, very high-performance FeS-based-batteries have already been reported (Posada and Hall, 2016b).

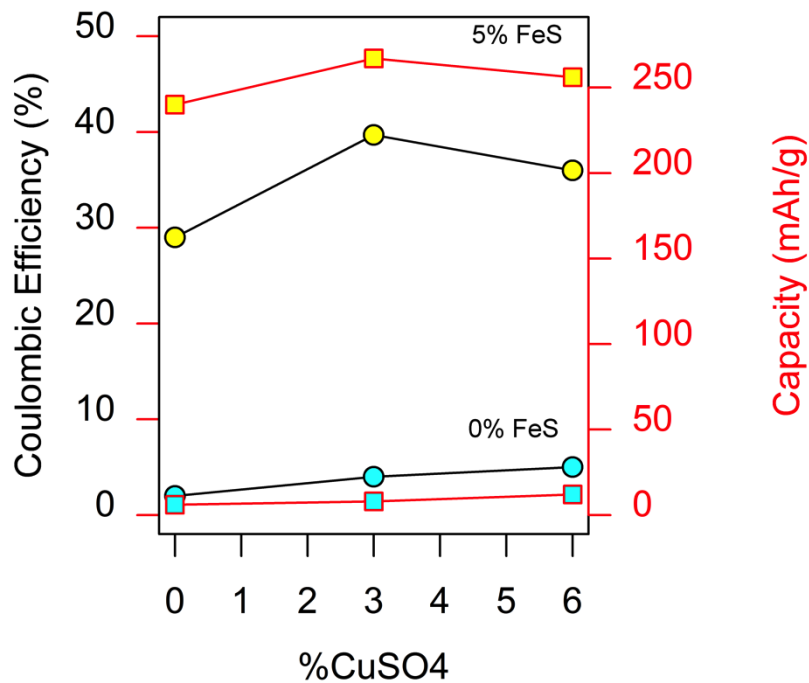


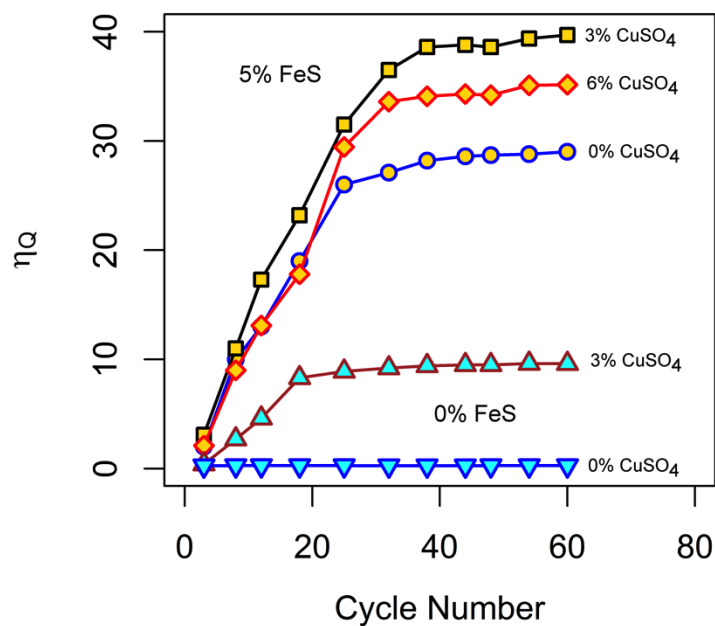
Figure 6-19 The cell performance as a function of composition. Squares and circles denote capacity and coulombic efficiency respectively. Likewise, cyan and yellow colours denote to compositions of 0% (curves on a lower part of the diagram) and 5% (curves on an upper part of the diagram) respectively of Fe

6.7.6.2 Coulombic efficiency (CE)

The coulombic efficiency of iron electrode samples with a number of different additives cycled up to 60 cycles at a C/5 rate. Figure 6.20 show the specific discharge capacities for our iron electrodes samples with and without additive as a function of the cycle number. As we can see from the Figure.6.20, the formulation base on FeS exhibits a relatively low coulombic efficiency of an average of $\eta_Q \approx 30\%$ (Table 6-8). However, the addition of copper sulfate to the same formulation renders nearly 10% increases in battery performance ($\eta_Q \approx 40\%$).

Table 6-8 Example of proposed composition for the Fe/FeS-CuSO4

Sample	Components weight fraction				η_Q (%)
	W [Fe g]	W [CuSO ₄ g]	W [FeS g]	W [PTFE]	
S1	0.900	0.015	0.005	0.080	≈ 20.4
S2	0.864	0.006	0.050	0.080	≈ 27.5
S3	0.832	0.038	0.050	0.080	≈ 37.6
S4	0.884	0.036	0.00	0.080	≈ 10.4
S5	0.864	0.006	0.055	0.080	≈ 26.5
S6	0.820	0.050	0.050	0.080	≈ 28.5
S7	0.861	0.029	0.03	0.080	≈ 18.6
S8	0.877	0.000	0.043	0.080	≈ 29.5
S9	0.863	0.050	0.007	0.080	≈ 25.4
S10	0.879	0.020	0.021	0.080	≈ 22.5
S11	0.841	0.029	0.050	0.080	≈ 39.7
S12	0.900	0.015	0.005	0.080	≈ 15.7
S13	0.899	0.000	0.021	0.080	≈ 19.5
S14	0.899	0.021	0.000	0.080	≈ 12.6
S15	0.863	0.050	0.007	0.080	≈ 15.9
S16	0.820	0.050	0.050	0.080	≈ 26.6



Figure

6.20 Coulombic efficiency versus cycle number for selected electrode formulations. The lower curves on the diagram (cyan colour) correspond to 0% FeS; likewise, the upper curves (gold) correspond to 5% FeS.

Our experimental results, it follows that the addition of copper sulfate increases the performance of the battery, by preventing electrolyte decomposition. This observation holds in the concentration range from between (0 - 6%) of copper sulfide. We believe that this might be due to the formation of a copper layer on different sectors of the iron electrode, that iron copper would increase the activation barrier for electrolyte decomposition, consequently increasing the overall performance of the iron electrode.

However, the electrode samples formulations based on CuSO₄ outperformed their plain-iron-based counterparts. However, at the confidence level $\alpha = 0.05$, we have found no meaningful differences across formulations based on 3 and 6% of CuSO₄. This would indicate that more research is still needed to determine the optimum concentration space where cell performance is being maximised.

Although we have developed formulations that decrease the evolution of hydrogen, our formulations exhibit a decrease in capacity after the 15th cycle, so we also propose to investigate the use of additives like bismuth sulfide, which increases the performance, and stability of NiFe cells. It has been proposed, however, that the reduction of electrode capacity can be counteracted by the addition of sodium sulfide to the electrolyte (Kessler *et al.* 2015), so it is worth exploring the incidence of this compound as a means to enhance cell performance. Finally, our experimental observations confirm that iron electrodes tend to fall apart with the cycle number; this observation has been reported many times before (Jorge Omar Gil Posada and Peter J. Hall 2014, Jorge Omar Gil Posada and Peter J. Hall 2014, Kessler *et al.* 2015). The authors believe the manufacturing process can still further be refined or even replaced by using different binders or manufacturing approaches.

6.7.6.3 Cyclic voltammetry of iron electrode

To evaluate the electrochemical performance of iron electrode samples with different additives are initially exposed to cyclic voltammetry measurement on the different iron electrode formulations as shown in Figure.6.21. Cyclic voltammograms of (CV) of the Fe composite with and without additives during initial 40 cycles at a scan rate of 10 mV s⁻¹ is illustrated in Figure 6.21a and 6.21b. The CV profile of iron electrode without additives are shown in Figure 6.21a, is shown the forward scan

(oxidation curve) for electrodes without additives reveals two oxidation/reduction, (O_{x1}/Red_1) which associated to $Fe/Fe(OH)_2$ and (O_{x2}/Red_2) for $Fe(OH)_2/Fe(III)$, respectively (Jayalakshmi and Balasubramanian, 2008, Černý and Micka, 1989, Kao *et al.*, 2011). The CV profile of the iron electrode samples with additives at different cycles is shown in Figure 6.21b. This profile clearly showed, that the electrode samples containing additives exhibit excellent cycling stability, and strongly affect the redox behaviour of Fe electrode. As confirmed in Figure 6.21b, there are three oxidation/reduction peaks, peak one (O_{x0}) at -0.38 V, (O_{x1}) -0.12, and (O_{x2}) at -0.6V. We have proposed, that formation of peak (O_{x0}) may be attributed to the oxidation of Cu/Cu_2O , peak 2 (O_{x2}) with Cu_2O/CuO , and the third anodic peak with $CuO/Cu(OH)_2$. The XRD result reveals that no definite evidence of reactions between iron and copper. The previous investigation by Hang *et al.*, indicated that the peak (O_{x0}) is might be associated with the formation of the α - $Fe(OH)_2$ layers or to the oxidation of adsorbed hydrogen atoms on the electrode surface or attributed to soluble species $HFeO_2$ (Hang *et al.*, 2006). It has been reported, that the reveals of both peak (O_{x0}) and peak (O_{x1}) involve the electro-oxidation of Fe to $Fe(OH)_2$ species, and the appears of the peak (O_{x0}) occurs only with the addition of S^{2-} ion. Moreover, the CV shows decreases to the peak Red_2 , which associated to the reduction of Fe_3O_4 , then reduced to Fe through $Fe(OH)_2$, contributing to increasing of the discharge capacity (XRD results confirm the present of Fe_3O_4). A similar phenomenon observed in the study of Fe_3C (Ujimine and Tsutsumi, 2006).

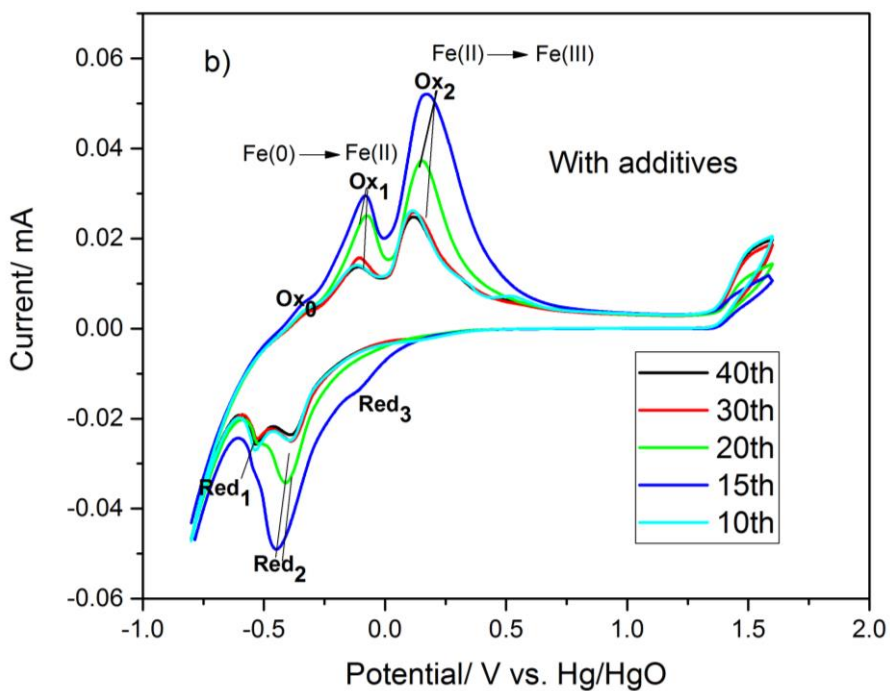
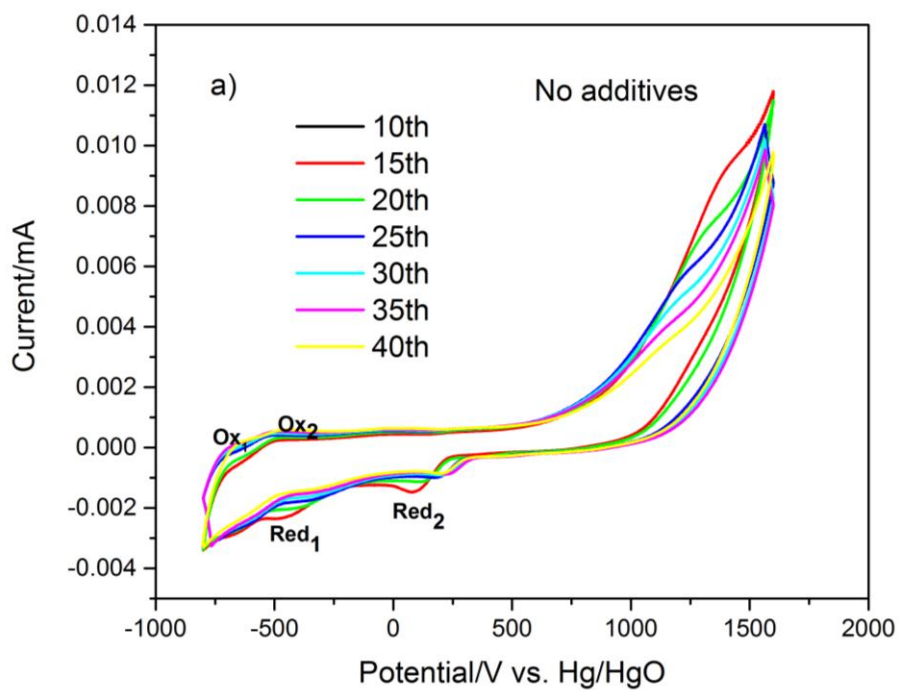


Figure 6.21 Cyclic voltammetry for the prepared iron electrode, (a) without additives (b) with additives, for the 10th, 15th, 20th, 30th, and 40th cycles, at a scan rate of 10 mV s⁻¹ in the voltage range of -0.8 -1.6 V.

6.7.6.4 Characterisation of the electrodes

XRD patterns of the Fe powder electrode samples before and after charge-discharge cycling are shown in Figure 6.22. As seen, the prepared Fe powder electrode (Figure 6.22a), the main XRD pattern reveals strong signals indicating well-crystallized peaks at 2θ values = 45.8° , 66.55° , and 83.8° corresponding to the main phases of Fe matched with the standard ICDD card no: 006-0696, the peaks at $2\theta = 26.19^\circ$, 40.6° correspond to FeS ICDD card no: 04-003-1443, and the peaks at $2\theta = 31.06^\circ$, and 38.07° correspond to CuSO_4 ICDD card no: 01-077-1900 respectively. No iron oxide impurities are detected.

Figure 6.22b and 6.22c shows the XRD patterns for the charge-discharged Fe powder electrode sample. In Figure 6.22b, the peaks at $2\theta = 45.8^\circ$, 52.7° , and 66.01° correspond to the main phases of Fe matched with the standard ICDD card no: 006-0696, the peaks at $2\theta = 15.5^\circ$, 39.56° , 49.1° , and 61.52° correspond to FeS ICDD card no: 04-003-1443, peaks at $2\theta = 57.7^\circ$ correspond to Cu_2O ICDD card no: 01-078-2076, and the peaks at $2\theta = 18.9^\circ$, 35.8° , 46.03° , and 56.17° correspond to Fe_3O_4 ICDD card no: 00-065-0731.

In Figure 6.22c, the peaks at $2\theta = 45.8^\circ$, 53.2° , 66.15° , and 82.7° correspond to the main phases of Fe matched with the standard ICDD card no: 006-0696, the peaks at $2\theta = 38.73^\circ$ correspond to Cu_2O ICDD card no: 01-078-2076, and the peaks at $2\theta = 19.17^\circ$, 35.8° , 46.03° , and 61.09° , 64.2° and 76.3° correspond to Fe_3O_4 ICDD card no: 00-065-0731.

It is worth nothing that after cycling, electrodes exhibited strong iron signals of higher intensity than their non-cycled counterparts.

As can be shown from Figure 6.22b to 6.22c, the formation of Fe_3O_4 is much stronger after the deep cycling. It is also worth noting that Fe_3O_4 was produced during the discharge reaction, as confirmed by the AFM image morphology. See Figure 6.23. The Cu_2O observed peaks are indicative that the copper was oxidised (as shown by Eq. 6) at the deep discharge state (Kao *et al.*, 2011).

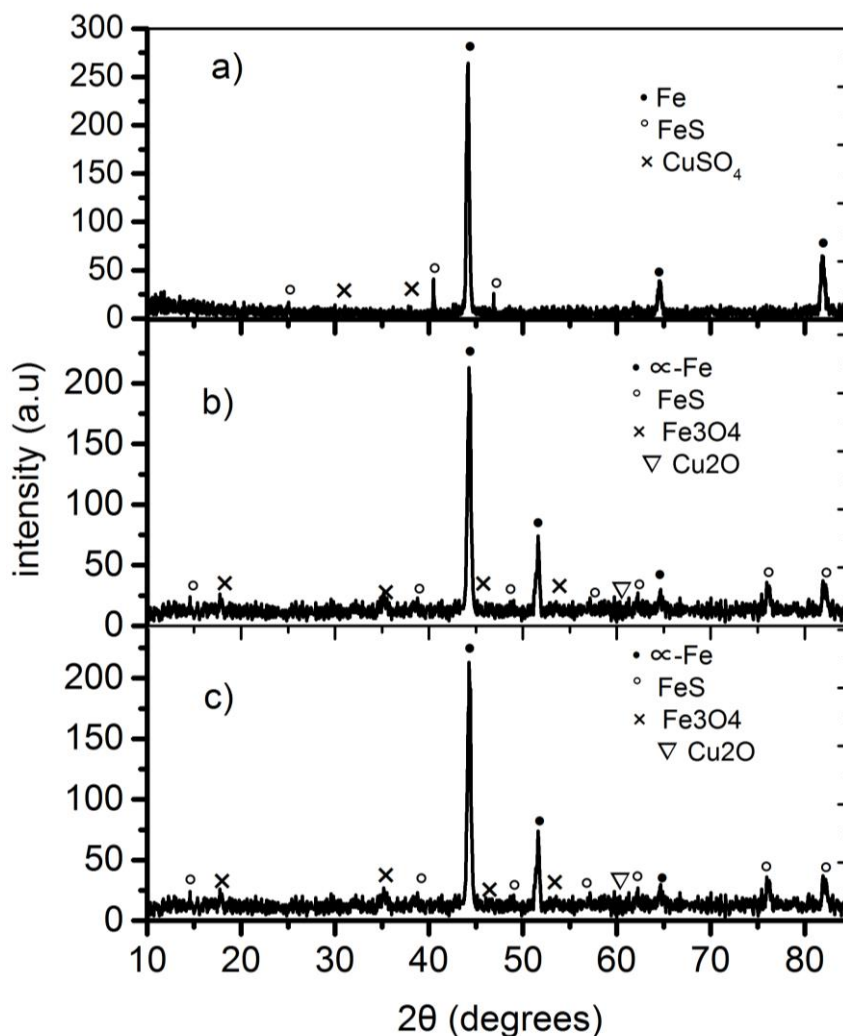


Figure 6.22 X-ray powder diffraction pattern for the iron electrode (a) before charging (b-c) after charging. Powder diffraction cards: Fe (00-006-0696), Fe_3O_4 (00-065-0731), FeS (04-003-01443), CuSO_4 (01-077-1900), Cu_2O (01-078-2076).

It is important to underscore that, broadly speaking our evidence is in line with our initial claim that copper (in the form of copper sulfate) would modify in some way the activation energy for electrolyte decomposition. Probably by rendering metallic copper centres on the surface of the electrolyte (as suggested by Equation 6.6); note that electrolyte decomposition of water is not favoured on copper as is of iron, so the overall performance of the battery is increased. The XRD analysis of our samples confirms the formation of Fe_3O_4 during the discharge reaction.

To investigate the surface morphology of the electrodes, AFM was used to study the structure of our samples. Figure 6. 23 show AFM 3D images of iron electrodes before and after cycling. The average surface roughness evaluated over the 3D surface before and after 60 cycles of charge and discharge was 2.69 nm and 21.0 nm, respectively. Finally, the AFM analysis would also suggest the surface of the electrode deteriorates with the cycle number; this observation is in line with the fact that electrodes tend to fall apart (to some extent) when cycled.

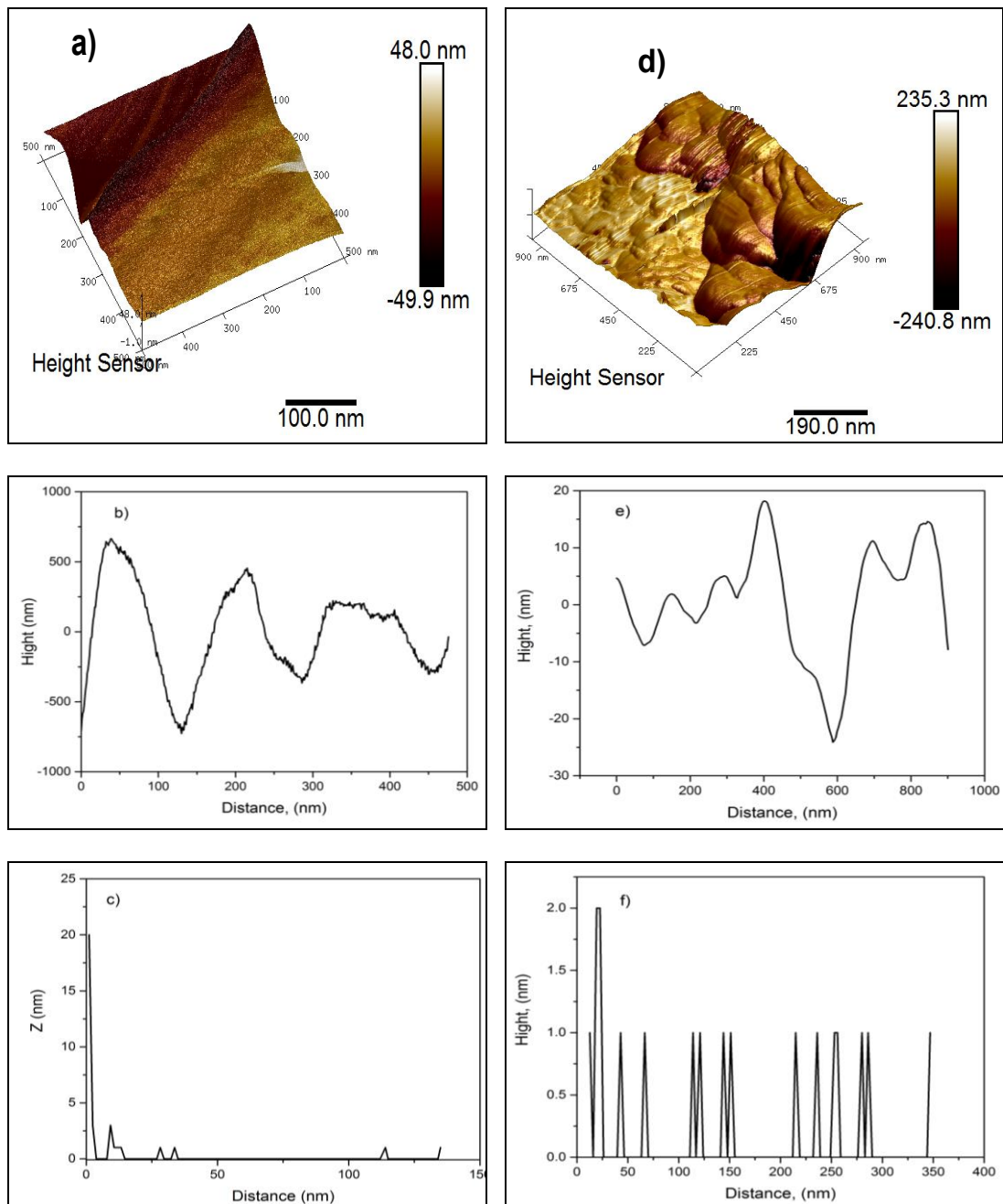


Figure 6.23. Soft tapping-mode AFM images: (a) Height sensor image of the iron powder electrode with additive before discharge/charge cycling;(b-e) cross section along the line in phase image;(c-f) the corresponding phase image, z-range; (d) Height sensor of the image iron powder electrode with additives after 60 cycles of charge and discharge.

In the plots shown in Figure 6.24 the surface morphology and cross-section of the prepared and after cycled composite electrode samples were investigated by SEM. Figure.6.24a is showed the cross section of the Ni foam without slurry coating. The Figure 6.24b-d, 6.25e-h showed SEM of the as prepared and formed cycled electrode samples, respectably. The images showed layered plates with irregularly shapes and smooth particle structures, compared to prepared electrode samples. Not that the particle size cannot be determined from the SEM image, due to the smooth structure and irregular shape. The SEM images of the iron electrode before cycling showed particles of mixed iron with additives surrounded by the PTFE binder.

SEM images (Figure.6.25h) shown the electrodes after cycling formation, the surface of the iron electrode was covered with acicular crystal iron particles with a rough surface (suggested to be iron(II) hydroxide, however, not confirmed by XRD).

However, higher magnification reveals clear differences in the surface morphology correlated with electrochemical performance and the addition of electrode additives. The EDX measurements for the electrode after formation contains iron, oxygen, carbon, sulfur and copper, suggesting the presence of electrode decomposition product like $\text{Fe}(\text{OH})_2$ (Figure.6.25i and j).

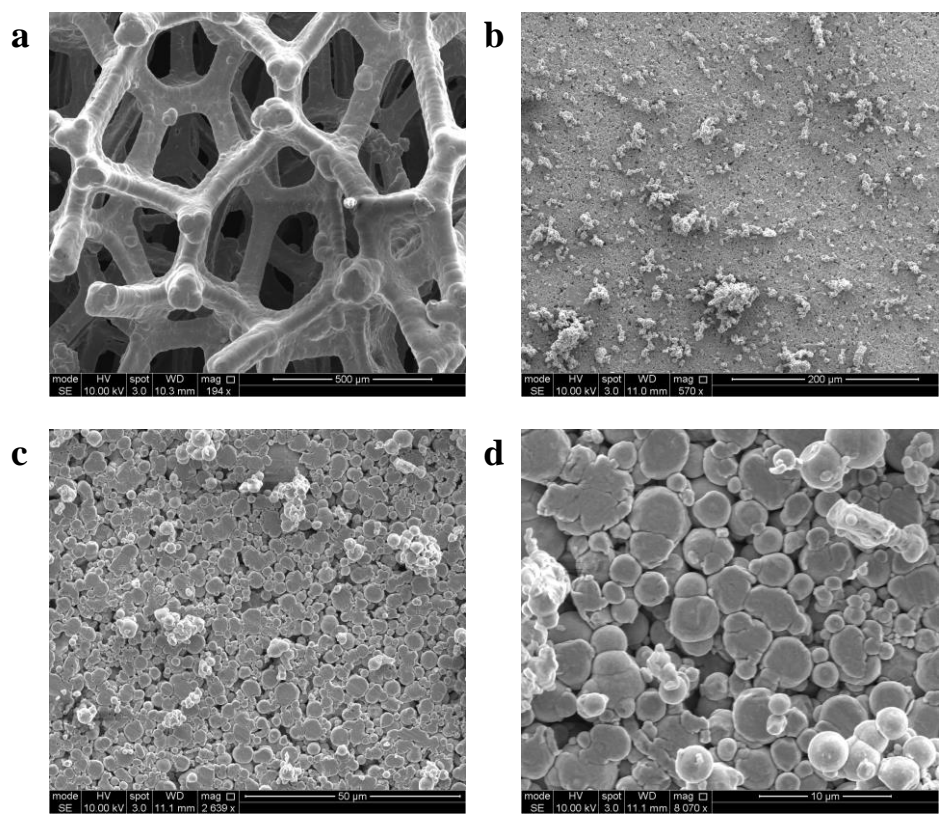


Figure 6.24 SEM images of (a) Ni foam free additives (b-d) Fe electrode as prepared.

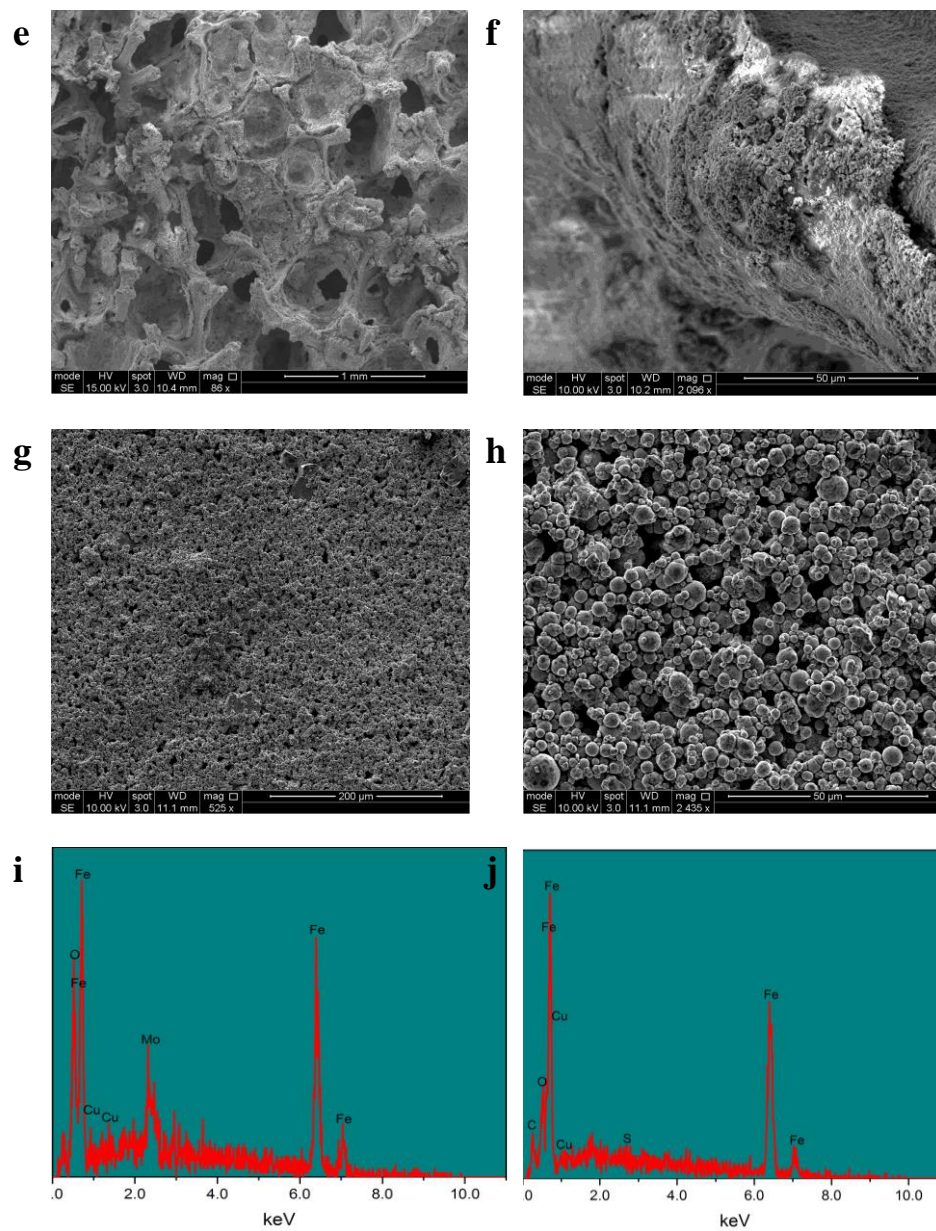


Figure 6.25 SEM images of (e-h) after formation cycling (i and j) EDX measurements of the cycled iron electrodes.

6.7.7 Summary

In the effort to develop highly efficient NiFe cells, iron electrodes based on iron sulfide and copper composites were investigated. The prepared iron electrode samples electrochemistry and physically was characterised by using galvanostatic charge/discharge, cyclic voltammetry and X-ray diffraction (XRD), atomic force microscopy (AFM) techniques and scanning electron microscopy (SEM). Our experimental results indicate that copper sulfate increases the performance of iron-based electrodes in the range from between 0 to 6 %. Similarly, we could confirm that the presence of iron sulfide in the electrode has a real incidence on its performance; basically, the addition of iron sulfide has a much greater influence than using copper alone. This study also involved investigating the behaviour of the iron-containing electrode in KOH electrode containing K₂S additives. AFM and visual inspection have confirmed that the cycling of electrodes under strongly alkaline conditions would most certainly compromise the structural integrity of the cells. Coulombic efficiencies on the order of 40% and enormous capacities exceeding 300 mA g⁻¹ were found. It is important to mention that we have used commercial grade reactants and materials only, so this technology has the potential to be a cost-effective energy storage solution for large-scale applications.

6.8 Effect of K₂S additives to the electrolyte

6.8.1 Introduction

Various investigation has reported that employed metal sulfide such as FeS, K₂S, as additives with iron electrodes and electrolyte, respectively would enhance the performance of the iron electrode batteries (Posada and Hall, 2016a, Hang *et al.*, 2006). In this study, the inhabitation performance, the effect of K₂S on the electrochemical performance of the iron electrode was investigated. The effect of K₂S additives concentration in the electrolyte on the redox behaviour of the iron electrode was also investigated.

6.8.2 Cyclic Voltammogram Study

The polarisation measurements were performed using an 8-channel Solartron cell test system (1470E/1455A potentiostat/galvanostat). Conventional three-electrode cell assembly was used in this study. The reference electrode (RE) was Hg/HgO ($E_{\text{Hg}/\text{HgO}} = +0.098\text{V}$ vs. the standard hydrogen electrode), pasted-glassy carbon electrode (GCE) used as working electrode, and the counter electrode (CE) was a platinum wire. The electrochemical equipment was supplied with CorrWare/Zview software to control the experiment via a PC. The KOH solution containing a different concentration of K₂S were prepared by dissolving KOH and K₂S salt at required concentrations.

6.8.3 Results and discussion

The electrochemical redox behaviour with 0.05 to 0.1M K₂S solution in 5.1M KOH at GCE within the potential window of -1.4 to 0.1 scan rate was investigated. Figure 6.26 illustrate the recorded voltammograms of 0.1 M K₂S in KOH solution at various scan rates of 2,5,10,20,50 mV/s.

The voltammograms showed that both anodic and cathodic peak current linearly increases with the increase of scan rates. With the increase in scan rate, the anodic peak position slightly shifts towards the positive direction, while the cathodic peak moves a little towards the negative potential. In Figure 6.27, peak current versus square root of scan rate of 2, 5, 10, 20, and 50 mV/s for K₂S in KOH solution showed the linear increase in the anodic and cathodic peak currents with the increase in the square root of the scan rate suggesting that the electrode process is reversible.

Table 6-9 The peak current and peak potentials for the 0.1 M K₂S in KOH solution at various scan rates of 2,5,10,20,50, and 100mV/s..

Sample	<i>i</i> _{pc} (μA)		<i>i</i> _{pa} (μA)		<i>E</i> _{pc} (V)		<i>E</i> _{pa} (V)	
	<i>i</i> _{pc1} (-)	<i>i</i> _{pc2} (-)	<i>i</i> _{pa1}	<i>i</i> _{pa2}	<i>E</i> _{pc1}	<i>E</i> _{pc2}	<i>E</i> _{pa1}	<i>E</i> _{pa2}
0.1M K S								
2mV S ⁻¹	0.0223	-0.1	0.0223	0.0463	-0.86	-	-0.59	-0.24
5mV S ⁻¹	0.0151	-0.15	0.0151	0.015	-0.886	-	-0.55	-0.129
10mV S ⁻¹	0.00556	-0.158	0.006	0.065	-0.87	-	-0.98	-0.48
20mV S ⁻¹	0.0375	-0.26	0.0375	0.1	-0.87	-	-0.996	-0.478
50mV S ⁻¹	0.123	-0.3	0.123	0.13	-0.67	-	-1.0336	-0.397
100mV S ⁻¹	-	-0.3	0.123	0.133	-0.89	-	-1.033	0.322

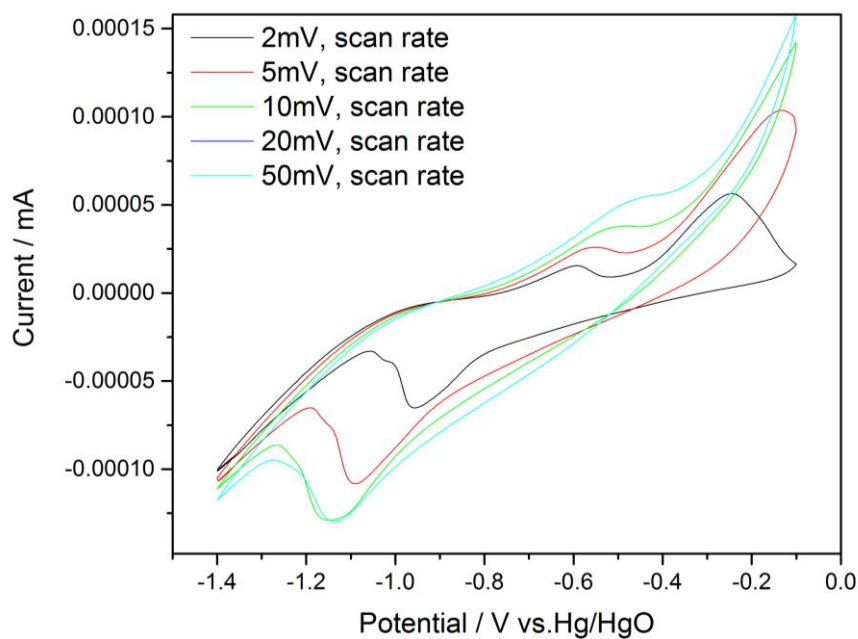


Figure 6.26 Cyclic voltammograms response of 0.1M K_2S in KOH solution with a scan rate of 2, 5, 10, 20, and 50 mVs^{-1} at GCE.

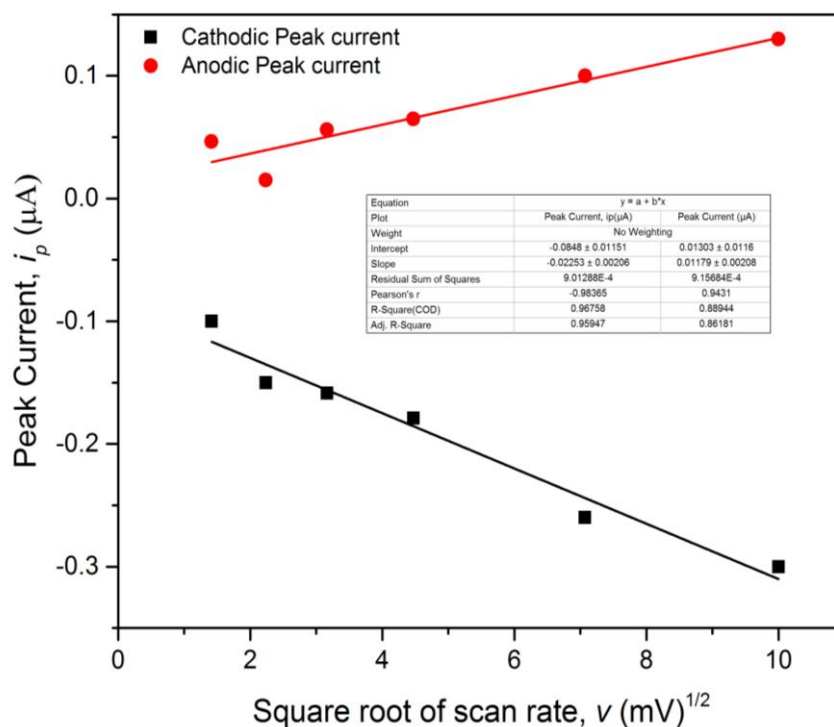


Figure 6.27 Anodic and cathodic peak current versus square root of scan rate of K_2S in KOH solution.

6.8.3.1 Polarisation measurements

The effect of electrolyte concentration on the redox behaviour of K_2S was also investigated. Two types of electrolyte solutions were used, 5.1M KOH free of K_2S , and mixtures of 5.1M KOH and different concentration of K_2S . The inhibition effect of K_2S on the hydrogen evolution reaction and corrosion behavior of iron in 5.1M potassium hydroxide solutions was investigated. Table 6.10 shows the experimental factors and level used during the experiments.

Table 6-10 Main factors and levels used in experiments

Factors	Level of concentration (M)	
	Low	High
KOH	0.5	5.1
K_2S	0	1

The polarisation studies were conducted using Corrware software supplied with the electrochemical testing system, which used for the polarisation studies. The studies carried out from a cathodic potential of -0.02 to a anodic potential of +0.02 with respect to the corrosion potential at a scan rate of 10mV/s. To obtain the corrosion current densities (i_{corr}), the anodic and cathodic Tafel linear segments curves in E versus $\log I$ were concluded to corrosion potential. The corrosion inhibition efficiency was calculated from i_{corr} values using the following relationship (Khaled and Hackerman 2003);

$$IE\% = \frac{i_{corr} - i_{corr}^-}{i_{corr}} \times 100 \quad (6.13)$$

Where i_{corr} is the corrosion current densities without additives, and i_{corr}^- is the corrosion current densities with additives. The inhibition efficiency has been calculated from the measured polarisation resistance (R_p) values that calculated from the slope of η versus i in the vicinity of corrosion potential using the following relationship;

$$IE\% = \frac{R_p^- - R_p}{R_p^-} \times 100 \quad (6.14)$$

Where, R_p is the polarization resistance values without additives, and R_p^- is polarization resistance values with additives.

The cathodic and anodic polarisation curves recorded for the iron electrode in 5.1M KOH solutions with and without various concentrations of K_2S electrolyte additives at a scan rate of 10mV s^{-1} are illustrated in Fig. 6.28. The corrosion kinetic parameter derived from polarization curves are presented in Table.6.11. The results indicate, that the addition of K_2S to the electrolyte, in the concentration range 0.05M – 0.1M clearly affects the electrochemical behaviour of the iron electrode, and significantly reduces the dissolution rate of iron in 5.1M KOH. From the Table 6.9, the corrosion current density, i_{corr} is decreased with the addition of 0.05M K_2S to the electrolyte, with the inhibition efficiency up to 86%. However, current density, i_{corr} obtained from polarisation curves showed a decrease with the increasing of the K_2S concentration. The Table also revealed that there are no marked changes with the addition of $CuSO_4$. Posada and Hall proposed that the electrolyte containing sulfur species such as (HS^- or

KS⁻) could control the corrosion rate, and improve the performance of the iron electrode (Posada and Hall, 2016a).

Table 6-11 Corrosion kinetics, corrosion current in inhabitation efficiencies, associated with Tafel polarization measurements recorded for iron electrodes in 5.1M KOH solution with and without different concentration of electrolyte additives.

Additives type	Concentration of additives (M)	E_{corr} (V) vs. M/MO	b_a (mV/dec)	b_c (mV/dec)	i_{corr} ($\mu\text{A}/\text{cm}^2$) (-)	IE (%)
Blank	5.1	-1.09	257	218	7.5×10^{-3}	---
K ₂ S	0.1	-0.85	491	641	4.1×10^{-2}	55
K ₂ S	0.05	-0.85	350	363	6.5×10^{-3}	86
K ₂ S+	0.1+0.1	-1.05	174	150	5.6×10^{-2}	75
CuSO ₄						

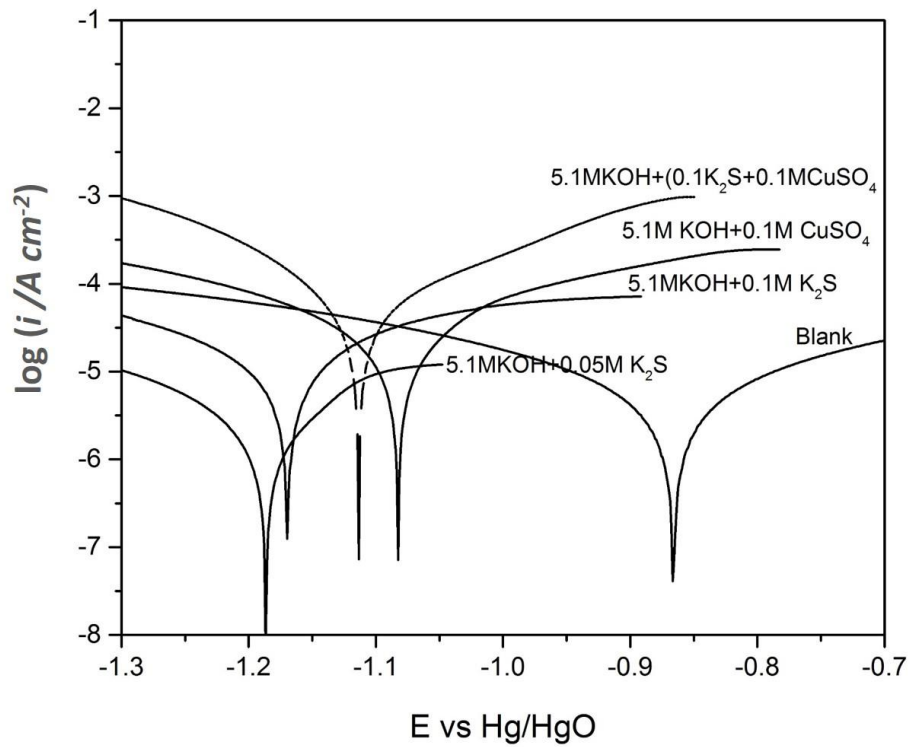


Figure 6.28 Polarisation curves of iron electrode samples at a scan rate of 10mV in 5.1M KOH with various concentrations of K_2S electrolyte additives.

6.8.4 Summary

The addition of metal sulfide such as K_2S in 5.1M KOH solution inhibits the dissolution of the iron was investigated. It is suggested that the addition of an optimal amount of sulfide additives such as K_2S (0.05-0.1M) is an effective inhibitor. However, further investigation is needed using different electrolyte additives.

Chapter 7 OVERALL SUMMARY AND CONCLUSIONS

As the results have been presented in Chapter 6, this chapter will evaluate some of the interesting point. A summary of what this thesis has presented, and results is discussed, and comments on the scope for further study are presented.

7.1 Conclusions

The work proposes the potential of NiFe batteries for large-scale energy storage. With the aim of developing a high-efficiency NiFe battery, iron electrodes containing additives were investigated. The challenges facing the commercial of NiFe have been addressed. The encouraging electrochemical performance of the cell-treated electrode and electrolyte additives was attributed to increased battery performance and a decrease of the hydrogen evolution. Traditionally, there have been several approaches to mitigating the effects of hydrogen evolution, including new anode additives (electrode and electrolyte materials), cells design, and nano-sized materials. Mitigating the hydrogen evolution through the use of additives is an effective way and popularly used.

In summary, the experimental study was mainly based on paste-type electrode additives and hot-pressed types for comparisons. Their impacts on NiFe rechargeable batteries have been investigated. The fabrication of paste-type modified electrode materials was the primary topic of focus. The findings gathered from this study should be taken into consideration for a range of electrode types and materials during production. The results gained are by no means limited to the originally investigated systems and can have a significant impact on device (cells) performance. The galvanostatic charge-discharge cycling and cyclic voltammetry techniques are mainly

used for the electrochemical evaluation of battery cycling performance and to investigate the electrochemical performance of the prepared electrodes. The reversibility of the electrode reaction was studied using cyclic voltammetry. The prepared electrode samples were thoroughly characterised by a variety of physical methods including X-ray powder diffraction (XRD), atomic force microscopy (AFM), scanning electron microscopy (SEM), and transmission electron microscopy (TEM).

The present study led to the following ;

- * The bismuth powder, copper powder, bismuth sulfide, iron sulfide, and copper sulfide additives, and the free process are discussed.
- * The results revealed that additives such as bismuth sulfide did improve the performance of the battery with coulombic efficiency on average of $\approx 30\%$.
- * Overall, the addition of both the iron sulfide and copper sulfate additives to iron electrodes resulted in an improvement in chargeability over cycling.
- * The best charge efficiency of the iron electrode of Fe-loaded with 5% FeS and the addition of copper sulfate (a certain amount of CuSO_4 additives) to the same formulation renders nearly 10% increases in battery performance ($\eta_Q \approx 40\%$), with enormous mA capacities exceeding 300 mA g^{-1} .
- * The addition of Cu powder does not have an effect on cell performance.
- * The results indicate that the combination of both iron copper sulfide, or iron sulfide and copper sulfide additives have a significant impact on improving the overall battery performance.
- * The addition of sulfide additives in the electrolyte such as potassium sulfide (K_2S) enhances the performance of the anode electrode by working as a de-passivation agent during the discharging process.

Table 7-1 Summary of some additives used and the results achieved.

Iron materials	Particle size [μm]	Support materials	Additives	Electrode design	Charging efficiency
Fe powder	≤ 10μm	None	FeS	Paste-type + PTFE	30% at C/5 rate
Fe powder	≤ 10μm	None	4.5% FeS + % CuSO ₄	Paste-type + PTFE	40% at C/5 rate
Fe powder	≤ 10μm	None	4.5% Bi ₂ O ₃ + CuSO ₄	Hot-pressed + PP + K ₂ CO ₃	≈ 25% at C/5 rate
Fe powder	≤ 10μm	None	Cu or CuSO ₄	Paste-type + PTFE	-----

7.2 Recommendation and future work

From our results, taking them into consideration, many innovative ideas could be applied to the NiFe system such as:

- * Synthesis strategies of the electrode anode materials based on mixed sulfide additives
- * Modification the iron electrode and cell design.
- * Also, it would be useful to explore the particle size effect on battery performance using different commercial forms of iron (wet and thermal routes).

7.3 References

- Allen, J. B. and Bard, A. J. (1980) *Electrochemical methods : fundamentals and applications*, New York ; Chichester: New York ; Chichester : Wiley, c1980.
- Bezerra, M. A., Santelli, R. E., Oliveira, E. P., Villar, L. S. and Escaleira, L. A. (2008) 'Response surface methodology (RSM) as a tool for optimization in analytical chemistry', *Talanta*, 76(5), 965-977.
- Chang, Z., Zhao, Y. and Ding, Y. (1999) 'Effects of different methods of cobalt addition on the performance of nickel electrodes', *Journal of Power Sources*, 77(1), 69-73.
- Gil Posada, J. O. and Hall, P. J. (2014) 'Multivariate investigation of parameters in the development and improvement of NiFe cells', *Journal of Power Sources*, 262(0), 263-269.
- Jean-François, F. and Patrice, S. (2009) 'Principles of Electrochemistry and Electrochemical Methods' in *Carbons for Electrochemical Energy Storage and Conversion Systems*, CRC Press, 1-36.
- Lundstedt, T., Seifert, E., Abramo, L., Thelin, B., Nyström, Å., Pettersen, J. and Bergman, R. (1998) 'Experimental design and optimization', *Chemometrics and Intelligent Laboratory Systems*, 42(1-2), 3-40.
- Oseghale, C. I., Abdalla, A. H., Posada, J. O. G. and Hall, P. J. (2015) 'A new synthesis route for sustainable gold copper utilization in direct formic acid fuel cells', *International Journal of Hydrogen Energy*, 41(37), 16394-16401.
- vander Heyden, Y. (2006) 'Experimental Design Approaches in Method Optimization', *LC-GC Europe*, 19(9), 469-475.
- Yang, Q. M., Ettl, V. A., Babjak, J., Charles, D. K. and Mosoiu, M. A. (2003) 'Pasted Ni(OH)₂ Electrodes Using Ni Powders for High-Drain-Rate, Ni-Based Batteries', *Journal of the Electrochemical Society*, 150(4), A543-A550.

- Abdalla, A. H., Oseghale, C. I., Posada, J. O. G. and Hall, P. J. (2016) 'Rechargeable nickel-iron batteries for large-scale energy storage', *IET Renewable Power Generation*, 10(10), 1529-1534.
- Ahmed, N. A., Miyatake, M. and Al-Othman, A. K. (2008) 'Power fluctuations suppression of stand-alone hybrid generation combining solar photovoltaic/wind turbine and fuel cell systems', *Energy Conversion and Management*, 49(10), 2711-2719.
- Akinyele, D. O. and Rayudu, R. K. (2014) 'Review of energy storage technologies for sustainable power networks', *Sustainable Energy Technologies and Assessments*, 8, 74-91.
- Allen, J. B. and Bard, A. J. (1980) *Electrochemical methods : fundamentals and applications*, New York ; Chichester: New York ; Chichester : Wiley, c1980.
- Alotto, P., Guarnieri, M. and Moro, F. (2014) 'Redox flow batteries for the storage of renewable energy: A review', *Renewable and Sustainable Energy Reviews*, 29, 325-335.
- Anani, A., Mao, Z., Srinivasan, S. and Appleby, A. J. (1991) 'Dispersion deposition of metal — Particle composites and the evaluation of dispersion deposited nickel — Lanthanum nickelate electrocatalyst for hydrogen evolution', *Journal of Applied Electrochemistry*, 21(8), 683-689.
- Andersson, B. and Öjefors, L. (1976) 'Slow Potentiodynamic Studies of Porous Alkaline Iron Electrodes', *Journal of The Electrochemical Society*, 123(6), 824-828.
- Aneke, M. and Wang, M. (2016) 'Energy storage technologies and real life applications – A state of the art review', *Applied Energy*, 179, 350-377.
- Baker, J. N. and Collinson, A. (1999) 'Electrical energy storage at the turn of the Millennium', *Power Engineering Journal*, 13(3), 107-112.
- Balasubramanian, T. S. and Shukla, A. K. (1993) 'Effect of metal-sulfide additives on charge/discharge reactions of the alkaline iron electrode', *Journal of Power Sources*, 41(1–2), 99-105.

- Balasubramanian, T. S., Vijayamohan, K. and Shukla, A. K. (1993) 'Mechanisms of the discharge of porous-iron electrodes in alkaline medium', *Journal of Applied Electrochemistry*, 23(9), 947-950.
- Balducci, P. J. (2008) *Plug-in hybrid electric Vehicle market penetration scenarios*.
- Beaudin, M., Zareipour, H., Schellenberg, A. and Rosehart, W. (2010) 'Energy storage for mitigating the variability of renewable electricity sources: An updated review', *Energy for Sustainable Development*, 14(4), 302-314.
- Bednarkiewicz, E. and Kublik, Z. (1980) 'Cyclic and stripping voltammetry of iron in alkaline hydroxide solutions at the HMDE', *Journal of Electroanalytical Chemistry and Interfacial Electrochemistry*, 106(0), 61-69.
- Benitez, L. E., Benitez, P. C. and van Kooten, G. C. (2008) 'The economics of wind power with energy storage', *Energy Economics*, 30(4), 1973-1989.
- Bezerra, M. A., Santelli, R. E., Oliveira, E. P., Villar, L. S. and Escaleira, L. A. (2008) 'Response surface methodology (RSM) as a tool for optimization in analytical chemistry', *Talanta*, 76(5), 965-977.
- Bhattacharyya, S. C. (2012) 'Energy access programmes and sustainable development: A critical review and analysis', *Energy for Sustainable Development*, 16(3), 260-271.
- BP (2015a) 'BP Energy Outlook 2035', [online], available: <http://www.bp.com/en/global/corporate/energy-economics/energy-outlook-2035.html> [accessed 2014].
- BP (2015c) *BP Statistical Review of World Energy*, BP.
- Bryant, W. A. (1979) 'The structure and performance of sintered iron electrodes', *Electrochimica Acta*, 24(10), 1057-1060.
- Caldas, C. A., Lopes, M. C. and Carlos, I. A. (1998) 'The role of FeS and (NH₄)₂CO₃ additives on the pressed type Fe electrode', *Journal of Power Sources*, 74(1), 108-112.
- Černý, J., Jindra, J. and Micka, K. (1993) 'Comparative study of porous iron electrodes', *Journal of Power Sources*, 45(3), 267-279.

- Černý, J. and Micka, K. (1989) 'Voltammetric study of an iron electrode in alkaline electrolytes', *Journal of Power Sources*, 25(2), 111-122.
- Chakkaravarthy, C., Periasamy, P., Jegannathan, S. and Vasu, K. I. (1991) 'The nickel/iron battery', *Journal of Power Sources*, 35(1), 21-35.
- Chang, Z., Zhao, Y. and Ding, Y. (1999) 'Effects of different methods of cobalt addition on the performance of nickel electrodes', *Journal of Power Sources*, 77(1), 69-73.
- Changhongbatteris (2013) 'Pocket plate type NiFe cell', [online], available: <http://http://www.Changhongbatteris.com> [accessed 2013].
- Changhongbatteris (2014) 'Changhong NF-S series Nickel-Iron batteries for solar PV appliances', [online], available: http://www.changhongbatteries.com/Ni-Fe_battery_for_Solar_&_wind_appliances_p53_m2.2.2.html [accessed 2014].
- Chanson, C., Blanchard, P., Wattiaux, A. and Grenier, J. C. (1989) 'A Ring- Disk Study of Electrochemical Behavior of Iron in Strong Alkaline Medium: Influence of Additive Sulfide Ions', *Journal of The Electrochemical Society*, 136(12), 3690-3695.
- Chen, H., Cong, T. N., Yang, W., Tan, C., Li, Y. and Ding, Y. (2009) 'Progress in electrical energy storage system: a critical review', *Progress in Natural Science*, 19(3), 291-312.
- Cho, J., Jeong, S. and Kim, Y. (2015) 'Commercial and research battery technologies for electrical energy storage applications', *Progress in Energy and Combustion Science*, 48, 84-101.
- Chou, K.-S. and Kao, C.-Y. (2009) 'Iron/copper composite nanoparticles as iron electrode material in rechargeable alkaline battery', *Meeting Abstracts*, MA2009-02(5), 269.
- Chun, S. (2006) 'Wind energy in libya: combining education, experience and a pilot project to develop a new market', *Refocus*, 7(3), 44-45.
- Conway, B. E. (1999) *Electrochemical supercapacitors : scientific fundamentals and technological applications*, New York ; London: New York ; London : Kluwer Academic/Plenum, c1999.

- Corbyn, D., Vianello, M., Welford, K., Morton, H., Stevens, L., Bourne, A. W., Perera, N. and Taheri, L. (2013) *Poor People's Energy Outlook 2013*, Rugby, UK: Practical Action Publishing: Rugby, UK: Practical Action Publishing.
- Dang, T. M. D., Le, T. T. T., Fribourg-Blanc, E. and Dang, M. C. (2011) 'The influence of solvents and surfactants on the preparation of copper nanoparticles by a chemical reduction method', *Advances in Natural Sciences: Nanoscience and Nanotechnology*, 2(2), 025004.
- Dell, R. M. (2000) 'Batteries: fifty years of materials development', *Solid State Ionics*, 134(1–2), 139-158.
- Demirbaş, A. (2006) 'Global Renewable Energy Resources', *Energy Sources, Part A: Recovery, Utilization, and Environmental Effects*, 28(8), 779-792.
- Divisek, J., Schmitz, H. and Balej, J. (1989) 'Ni and Mo coatings as hydrogen cathodes', *Journal of Applied Electrochemistry*, 19(4), 519-530.
- Dursun, B. and Alboyaci, B. (2010) 'The contribution of wind-hydro pumped storage systems in meeting Turkey's electric energy demand', *Renewable and Sustainable Energy Reviews*, 14(7), 1979-1988.
- Evans, A., Strezov, V. and Evans, T. J. (2012) 'Assessment of utility energy storage options for increased renewable energy penetration', *Renewable and Sustainable Energy Reviews*, 16(6), 4141-4147.
- Fernandes, D., Pitié, F., Cáceres, G. and Baeyens, J. (2012) 'Thermal energy storage: "How previous findings determine current research priorities"', *Energy*, 39(1), 246-257.
- Gil Posada, J. O. and Hall, P. J. (2014) 'Post-hoc comparisons among iron electrode formulations based on bismuth, bismuth sulphide, iron sulphide, and potassium sulphide under strong alkaline conditions', *Journal of Power Sources*, 268(0), 810-815.
- Giri, S. D. and Sarkar, A. (2016) 'Electrochemical study of bulk and monolayer copper in alkaline solution', *Journal of The Electrochemical Society*, 163(3), H252-H259.
- Gong, M., Wang, D.-Y., Chen, C.-C., Hwang, B.-J. and Dai, H. (2015) 'A mini review on nickel-based electrocatalysts for alkaline hydrogen evolution reaction', *Nano Research*, 9(1), 28-46.

- Greaves, C., Thomas, M. A. and Turner, M. (1984) 'Structural and electrochemical characteristics of plastic (PTFE) bonded nickel hydroxide electrodes', *Journal of Power Sources*, 12(3–4), 195-202.
- Guney, M. S. and Tepe, Y. 'Classification and assessment of energy storage systems', *Renewable and Sustainable Energy Reviews*.
- Gutiérrez-Martín, F., Da Silva-Álvarez, R. A. and Montoro-Pintado, P. (2013) 'Effects of wind intermittency on reduction of CO₂ emissions: The case of the Spanish power system', *Energy*, 61, 108-117.
- Haddad, F., Eddine Amara, S. and Kesri, R. (2008) 'Liquidus surface projection of the Fe–Co–C ternary system in the iron-rich corner', *International Journal of Materials Research*, 99(9), 942-946.
- Hadjipaschalis, I., Poulikkas, A. and Efthimiou, V. (2009) 'Overview of current and future energy storage technologies for electric power applications', *Renewable and Sustainable Energy Reviews*, 13(6-7), 1513-1522.
- Hall, P. J., Mirzaeian, M., Fletcher, S. I., Sillars, F. B., Rennie, A. J. R., Shitta-Bey, G. O., Wilson, G., Cruden, A. and Carter, R. (2010) 'Energy storage in electrochemical capacitors: designing functional materials to improve performance', *Energy & Environmental Science*, 3(9), 1238-1251.
- Halpert, G. (1984) 'Past developments and the future of nickel electrode cell technology', *Journal of Power Sources*, 12(3–4), 177-192.
- Hang, B. T., Thang, D. H. and Kobayashi, E. (2013) 'Fe/carbon nanofiber composite materials for Fe–air battery anodes', *Journal of Electroanalytical Chemistry*, 704(0), 145-152.
- Hang, B. T., Watanabe, T., Egashira, M., Watanabe, I., Okada, S. and Yamaki, J.-i. (2006) 'The effect of additives on the electrochemical properties of Fe/C composite for Fe/air battery anode', *Journal of Power Sources*, 155(2), 461-469.
- Hariprakash, B., Martha, S. K., Hegde, M. S. and Shukla, A. K. (2005) 'A sealed, starved-electrolyte nickel–iron battery', *Journal of Applied Electrochemistry*, 35(1), 27-32.

- Hasan, N. S., Hassan, M. Y., Majid, M. S. and Rahman, H. A. (2013) 'Review of storage schemes for wind energy systems', *Renewable and Sustainable Energy Reviews*, 21, 237-247.
- Hill, C. A., Such, M. C., Chen, D., Gonzalez, J. and Grady, W. M. (2012) 'Battery energy storage for enabling integration of distributed solar power generation', *IEEE Transactions on Smart Grid*, 3(2), 850-857.
- Hori, T., Nagata, K., Iwase, A. and Hori, F. (2014) 'Synthesis of Cu nanoparticles using gamma-ray irradiation reduction method', *Japanese Journal of Applied Physics*, 53(5S1), 05FC05.
- Howlader, A. M., Urasaki, N., Yona, A., Senjyu, T. and Saber, A. Y. (2013) 'A review of output power smoothing methods for wind energy conversion systems', *Renewable and Sustainable Energy Reviews*, 26, 135-146.
- Huang, K.-C. and Ehrman, S. H. (2006) 'Synthesis of iron nanoparticles via chemical reduction with palladium ion seeds', *Langmuir*, 23(3), 1419-1426.
- Huo, G., Lu, X., Huang, Y., Li, W. and Liang, G. (2014) 'Electrochemical performance of α -Fe₂O₃ particles as anode material for aqueous rechargeable batteries', *Journal of The Electrochemical Society*, 161(6), A1144-A1148.
- IEA (2011) *World Energy Outlook 2011*, OECD Publishing.
- IEA (2012) *World Energy Outlook 2012*, OECD Publishing.
- IEA (2013) *Annual Energy Outlook 2013*.
- IEA (2014) *World Energy Outlook 2014*, OECD Publishing.
- IEA (2015a) *World Energy Outlook 2015*, OECD Publishing.
- IEA (2015b) *World Energy Outlook 2015*, OECD Publishing.
- Jayalakshmi, M. and Balasubramanian, K. (2008) 'Cyclic voltammetric behavior of copper powder immobilized on paraffin impregnated graphite electrode in dilute alkali solution', *International Journal of Electrochemical Science*, 3(11), 1277-1287.

- Jayalakshmi, N. and Muralidharan, V. S. (1990) 'Developmental studies on porous iron electrodes for the nickel · iron cell', *Journal of Power Sources*, 32(4), 341-351.
- Jean-François, F. and Patrice, S. (2009) 'Principles of electrochemistry and electrochemical methods' in *Carbons for Electrochemical Energy Storage and Conversion Systems*, CRC Press, 1-36.
- Jiang, W., Liang, F., Wang, J. W., Su, L., Wu, Y. M. and Wang, L. M. (2014) 'Enhanced electrochemical performances of FeOx-graphene nanocomposites as anode materials for alkaline nickel-iron batteries', *RSC Advances*, 4(30), 15394-15399.
- Kalaigan, G. P., Muralidharan, V. S. and Vasu, K. I. (1987) 'Triangular potential sweep voltammetric study of porous iron electrodes in alkali solutions', *Journal of Applied Electrochemistry*, 17(5), 1083-1092.
- Kaldellis, J. K. and Zafirakis, D. (2007) 'Optimum energy storage techniques for the improvement of renewable energy sources-based electricity generation economic efficiency', *Energy*, 32(12), 2295-2305.
- Kaldellis, J. K., Zafirakis, D. and Kavadias, K. (2009) 'Techno-economic comparison of energy storage systems for island autonomous electrical networks', *Renewable and Sustainable Energy Reviews*, 13(2), 378-392.
- Kao, C.-Y., Tsai, Y.-R. and Chou, K.-S. (2011) 'Synthesis and characterization of the iron/copper composite as an electrode material for the rechargeable alkaline battery', *Journal of Power Sources*, 196(13), 5746-5750.
- Khatib, H. (2012) 'IEA World Energy Outlook 2011—A comment', *Energy Policy*, 48, 737-743.
- Kim, J.-K., Nishikata, A. and Tsuru, T. (2003) 'Influence of copper on iron corrosion in weakly alkaline environment containing chloride ions', *MATERIALS TRANSACTIONS*, 44(3), 396-400.
- Kitamura, H., Zhao, L., Hang, B. T., Okada, S. and Yamaki, J.-i. (2012) 'Effect of charge current density on electrochemical performance of Fe/C electrodes in alkaline solutions', *Journal of The Electrochemical Society*, 159(6), A720-A724.

- Köhler, U., Antonius, C. and Bäuerlein, P. (2004) 'Advances in alkaline batteries', *Journal of Power Sources*, 127(1–2), 45-52.
- Kousksou, T., Bruel, P., Jamil, A., El Rhafiki, T. and Zeraouli, Y. (2014) 'Energy storage: Applications and challenges', *Solar Energy Materials and Solar Cells*, 120, Part A(0), 59-80.
- Kurzweil, P. (2010) 'Gaston Planté and his invention of the lead–acid battery—The genesis of the first practical rechargeable battery', *Journal of Power Sources*, 195(14), 4424-4434.0
- Lei, D., Lee, D.-C., Magasinski, A., Zhao, E., Steingart, D. and Yushin, G. (2016) 'Performance enhancement and side reactions in rechargeable nickel–iron batteries with nanostructured electrodes', *ACS Applied Materials & Interfaces*, 8(3), 2088-2096.
- Leopold, A., Stevens, L. and Gallagher, M. (2014) *Poor People's Energy Outlook 2014, Perspectives énergétiques des populations pauvres 2014*.
- Liao, L., Zhu, J., Bian, X., Zhu, L., Scanlon, M. D., Girault, H. H. and Liu, B. (2013) 'MoS₂ Formed on Mesoporous Graphene as a Highly Active Catalyst for Hydrogen Evolution', *Advanced Functional Materials*, 23(42), 5326-5333.
- Linden, D. and Reddy, T. B. (2002) *Handbook Of Batteries*, McGraw,2002.
- Liu, J., Chen, M., Zhang, L., Jiang, J., Yan, J., Huang, Y., Lin, J., Fan, H. J. and Shen, Z. X. (2014) 'A flexible alkaline rechargeable Ni/Fe battery based on graphene foam/carbon nanotubes hybrid film', *Nano Letters*, 14(12), 7180-7187.
- Loisel, R. (2012) 'Power system flexibility with electricity storage technologies: A technical–economic assessment of a large-scale storage facility', *International Journal of Electrical Power & Energy Systems*, 42(1), 542-552.
- Lund, P. (2012) 'Large-scale urban renewable electricity schemes – Integration and interfacing aspects', *Energy Conversion and Management*, 63, 162-172.
- Luo, X., Wang, J., Dooner, M. and Clarke, J. (2015) 'Overview of current development in electrical energy storage technologies and the application potential in power system operation', *Applied Energy*, 137, 511-536.
- Lv, P., Wang, Z.-m., Peng, Y., Liu, W.-p., Balogun, M.-S. and Zhou, H.-y. (2014) 'Effect of Cu content on structure, hydrogen storage properties and electrode

performance of $\text{LaNi}_{4.1-x}\text{Co}_{0.6}\text{Mn}_{0.3}\text{Cu}_x$ alloys', *Journal of Solid State Electrochemistry*, 18(9), 2563-2572.

Mahela, O. P. and Shaik, A. G. (2016) 'Power quality improvement in distribution network using DSTATCOM with battery energy storage system', *International Journal of Electrical Power & Energy Systems*, 83, 229-240.

Mahlia, T. M. I., Saktisahdan, T. J., Jannifar, A., Hasan, M. H. and Matseelar, H. S. C. (2014) 'A review of available methods and development on energy storage; technology update', *Renewable and Sustainable Energy Reviews*, 33, 532-545.

Maja, M. and Penazzi, N. (1988) 'Effect of some elements on oxygen reduction and hydrogen evolution at lead-acid battery negative plates', *Journal of Power Sources*, 22(1), 1-9.

Malkhandi, S., Yang, B., Manohar, A. K., Prakash, G. K. S. and Narayanan, S. R. (2013) 'Self-assembled monolayers of n-alkanethiols suppress hydrogen evolution and increase the efficiency of rechargeable iron battery electrodes', *Journal of the American Chemical Society*, 135(1), 347-353.

Manohar, A. K., Malkhandi, S., Yang, B., Yang, C., Surya Prakash, G. K. and Narayanan, S. R. (2012) 'A high-performance rechargeable iron electrode for large-scale battery-based energy storage', *Journal of the Electrochemical Society*, 159(8), A1209-A1214.

Manohar, A. K., Yang, C., Malkhandi, S., Prakash, G. K. S. and Narayanan, S. R. (2013) 'Enhancing the performance of the rechargeable iron electrode in alkaline batteries with bismuth oxide and iron sulfide additives', *Journal of the Electrochemical Society*, 160(11), A2078-A2084.

Manohar, A. K., Yang, C., Malkhandi, S., Yang, B., Surya Prakash, G. K. and Narayanan, S. R. (2012) 'Understanding the factors affecting the formation of carbonyl iron electrodes in rechargeable alkaline iron batteries', *Journal of the Electrochemical Society*, 159(12), A2148-A2155.

Manohar, A. K., Yang, C. and Narayanan, S. R. (2015) 'The role of sulfide additives in achieving long cycle life rechargeable iron electrodes in alkaline batteries', *Journal of the Electrochemical Society*, 162(9), A1864-A1872.

Marini, S., Salvi, P., Nelli, P., Pesenti, R., Villa, M. and Kiros, Y. (2013) 'Oxygen evolution in alkali with gas diffusion electrodes', *International Journal of Hydrogen Energy*, 38(26), 11496-11506.

- McDowall, J. (2006) 'Integrating energy storage with wind power in weak electricity grids', *Journal of Power Sources*, 162(2), 959-964.
- McKerracher, R. D., Ponce de Leon, C., Wills, R. G. A., Shah, A. A. and Walsh, F. C. (2015) 'A review of the iron–air secondary battery for energy storage', *ChemPlusChem*, 80(2), 323-335.
- Mears, D., Gotschall, H., Kamath, H., Institute, E. P. R., Energy, U. S. D. o., Insights, T. and Corporation, E. P. (2003) *EPRI-DOE Handbook of Energy Storage for Transmission and Distribution Applications*, EPRI.
- Miller, N., Manz, D., Roedel, J., Marken, P. and Kronbeck, E. (2010) *Utility scale Battery Energy Storage Systems*, translated by 1-7.
- Morard, G., Siebert, J., Andraut, D., Guignot, N., Garbarino, G., Guyot, F. and Antonangeli, D. (2013) 'The earth's core composition from high pressure density measurements of liquid iron alloys', *Earth and Planetary Science Letters*, 373, 169-178.
- Moura, P., López, G., Moreno, J. and De Almeida, A. (2013) 'The role of Smart Grids to foster energy efficiency', *Energy efficiency*, 6(4), 621-639.
- Nguyen, T. H., Nguyen, D. V., Dinh, M. T., Hoang, T. K., Nguyen, T. B. and Le, Q. M. (2012) 'Fabrication of $\text{TbPO}_4 \cdot \text{H}_2\text{O}$ nanorods/nanowires by the microwave technique and their characterization', *Advances in Natural Sciences: Nanoscience and Nanotechnology*, 3(1), 015007.
- Öjefors, L. (1976) 'Self-discharge of the alkaline iron electrode', *Electrochimica Acta*, 21(4), 263-266.
- Öjefors, L. and Carlsson, L. (1978) 'An iron—air vehicle battery', *Journal of Power Sources*, 2(3), 287-296.
- Oseghale, C. I., Abdalla, A. H., Posada, J. O. G. and Hall, P. J. (2015) 'A new synthesis route for sustainable gold copper utilization in direct formic acid fuel cells', *International Journal of Hydrogen Energy*, 41(37), 16394–16401.
- Oxley, A. and Barcza, N. (2013) 'Hydro–pyro integration in the processing of nickel laterites', *Minerals Engineering*, 54, 2-13.

- Paixão, T. R. L. C., Ponzio, E. A., Torresi, R. M. and Bertotti, M. (2006) 'EQCM behavior of copper anodes in alkaline medium and characterization of the electrocatalysis of ethanol oxidation by Cu(III)', *Journal of the Brazilian Chemical Society*, 17, 374-381.
- Periasamy, P., Ramesh Babu, B. and Venkatakrishna Iyer, S. (1996) 'Performance characterization of sintered iron electrodes in nickel/iron alkaline batteries', *Journal of Power Sources*, 62(1), 9-14.
- Posada, J. O. G. and Hall, P. J. (2015) 'The effect of electrolyte additives on the performance of iron based anodes for NiFe cells', *Journal of The Electrochemical Society*, 162(10), A2036-A2043.
- Posada, J. O. G. and Hall, P. J. (2016a) 'Controlling hydrogen evolution on iron electrodes', *International Journal of Hydrogen Energy*, 41(45).
- Posada, J. O. G. and Hall, P. J. (2016b) 'Towards the development of safe and commercially viable nickel-iron batteries: improvements to Coulombic efficiency at high iron sulphide electrode formulations', *Journal of Applied Electrochemistry*, 46(4), 451-458.
- Posada, J. O. G., Rennie, A. J. R., Villar, S. P., Martins, V. L., Marinaccio, J., Barnes, A., Glover, C. F., Worsley, D. A. and Hall, P. J. (2017) 'Aqueous batteries as grid scale energy storage solutions', *Renewable and Sustainable Energy Reviews*, 68(Part 2), 1174-1182.
- Pumera, M. (2010) 'Graphene-based nanomaterials and their electrochemistry', *Chemical Society Reviews*, 39(11), 4146-4157.
- Qin, Y.-H., Li, Y., Lv, R.-L., Wang, T.-L., Wang, W.-G. and Wang, C.-W. (2014) 'Pd-Au/C catalysts with different alloying degrees for ethanol oxidation in alkaline media', *Electrochimica Acta*, 144, 50-55.
- Rahman, F., Rehman, S. and Abdul-Majeed, M. A. (2012) 'Overview of energy storage systems for storing electricity from renewable energy sources in Saudi Arabia', *Renewable and Sustainable Energy Reviews*, 16(1), 274-283.
- Rajan, A. S., Sampath, S. and Shukla, A. K. (2014) 'An in situ carbon-grafted alkaline iron electrode for iron-based accumulators', *Energy & Environmental Science*, 7(3), 1110-1116.

- Ravikumar, M. K., Balasubramanian, T. S. and Shukla, A. K. (1995) 'A nickel-iron battery with roll-compacted iron electrodes', *Journal of Power Sources*, 56(2), 209-212.
- Ravikumar, M. K., Balasubramanian, T. S., Shukla, A. K. and Venugopalan, S. (1996) 'A cyclic voltammetric study on the electrocatalysis of alkaline iron-electrode reactions', *Journal of Applied Electrochemistry*, 26(11), 1111-1115.
- Ravikumar, M. K., Rajan, A. S., Sampath, S., Priolkar, K. R. and Shukla, A. K. (2015) 'In situ crystallographic probing on ameliorating effect of sulfide additives and carbon grafting in iron electrodes', *Journal of The Electrochemical Society*, 162(12), A2339-A2350.
- REN21, T. g. r. e. p. n. (2015) *Renewables 2015 Global Status Report*.
- Rennie, A. J. R., Martins, V. L., Smith, R. M. and Hall, P. J. (2016) 'Influence of particle size distribution on the performance of ionic liquid-based electrochemical double layer capacitors', *Scientific Reports*, 6, 22062.
- Rice, D. M. (1989) 'Effects of bismuth on the electrochemical performance of lead/acid batteries', *Journal of Power Sources*, 28(1–2), 69-83.
- Rosalbino, F., Carlini, R., Soggia, F., Zanicchi, G. and Scavino, G. (2012) 'Influence of rare earth metals addition on the corrosion behaviour of copper in alkaline environment', *Corrosion science*, 58(0), 139-144.
- Sarkar, D., Shukla, A. and Sarma, D. D. (2016) 'Substrate Integrated Nickel–Iron Ultrabattery with Extraordinarily Enhanced Performances', *ACS Energy Letters*, 82-88.
- Sarrias-Mena, R., Fernández-Ramírez, L. M., García-Vázquez, C. A. and Jurado, F. (2014) 'Improving grid integration of wind turbines by using secondary batteries', *Renewable and Sustainable Energy Reviews*, 34, 194-207.
- Shan, J., Pulkkinen, P., Vainio, U., Maijala, J., Merta, J., Jiang, H., Serimaa, R., Kauppinen, E. and Tenhu, H. (2008) 'Synthesis and characterization of copper sulfide nanocrystallites with low sintering temperatures', *Journal of Materials Chemistry*, 18(27), 3200-3208.
- Shangguan, E., Li, F., Li, J., Chang, Z., Li, Q., Yuan, X.-Z. and Wang, H. (2015) 'FeS/C composite as high-performance anode material for alkaline nickel–iron rechargeable batteries', *Journal of Power Sources*, 291(0), 29-39.

- Shukla, A. K., Ravikumar, M. K. and Balasubramanian, T. S. (1994) 'Nickel/iron batteries', *Journal of Power Sources*, 51(1–2), 29-36.
- Shukla, A. K., Venugopalan, S. and Hariprakash, B. (2001) 'Nickel-based rechargeable batteries', *Journal of Power Sources*, 100(1–2), 125-148.
- Sundararagavan, S. and Baker, E. (2012) 'Evaluating energy storage technologies for wind power integration', *Solar Energy*, 86(9), 2707-2717.
- Swider, D. J. (2007) 'Compressed Air Energy Storage in an Electricity System With Significant Wind Power Generation', *Energy Conversion, IEEE Transactions on*, 22(1), 95-102.
- Tan, X., Li, Q. and Wang, H. (2013) 'Advances and trends of energy storage technology in Microgrid', *International Journal of Electrical Power & Energy Systems*, 44(1), 179-191.
- Thomas, P. J. C. (2000) *Battery reference Book*, Newnes.
- Ujimine, K. and Tsutsumi, A. (2006) 'Electrochemical characteristics of iron carbide as an active material in alkaline batteries', *Journal of Power Sources*, 160(2), 1431-1435.
- UN (2012) 'Sustainable Energy for All', [online], available: <http://www.se4all.org> [accessed 2012].
- vander Heyden, Y. (2006) 'Experimental design approaches in method optimization', *LC-GC Europe*, 19(9), 469-475.
- Vassie, P. R. and Tseung, A. C. C. (1976) 'High performance, rechargeable sintered iron electrodes—I: The effect of preparative methods and additives on the structure and performance of sintered iron electrodes', *Electrochimica Acta*, 21(4), 299-302.
- Vela, N. and Aguilera, J. (2006) 'Characterisation of charge voltage of lead-acid batteries: application to the charge control strategy in photovoltaic systems', *Progress in Photovoltaics: Research and Applications*, 14(8), 721-732.
- Vijayamohanan, K., Balasubramanian, T. S. and Shukla, A. K. (1991) 'Rechargeable alkaline iron electrodes', *Journal of Power Sources*, 34(3), 269-285.

- Vijayamohanan, K., Shukla, A. K. and Sathyanarayana, S. (1990) 'Formation mechanism of porous alkaline iron electrodes', *Journal of Power Sources*, 32(4), 329-339.
- Wang, H., Liang, Y., Gong, M., Li, Y., Chang, W., Mefford, T., Zhou, J., Wang, J., Regier, T., Wei, F. and Dai, H. (2012) 'An ultrafast nickel–iron battery from strongly coupled inorganic nanoparticle/nanocarbon hybrid materials', *Nat Commun*, 3, 917.
- Warren, P. (2014) 'A review of demand-side management policy in the UK', *Renewable and Sustainable Energy Reviews*, 29(0), 941-951.
- Wen, J., Li, J., Liu, S. and Chen, Q.-y. (2011) 'Preparation of copper nanoparticles in a water/oleic acid mixed solvent via two-step reduction method', *Colloids and Surfaces A: Physicochemical and Engineering Aspects*, 373(1–3), 29-35.
- Winter, M. and Brodd, R. J. (2004) 'What Are Batteries, Fuel Cells, and Supercapacitors?', *Chemical Reviews*, 104(10), 4245-4270.
- Yang, B., Makarov, Y., Desteese, J., Viswanathan, V., Nyeng, P., McManus, B. and Pease, J. (2008) *On the use of energy storage technologies for regulation services in electric power systems with significant penetration of wind energy*, translated by IEEE, 1-6.
- Yang, B., Malkhandi, S., Manohar, A. K., Surya Prakash, G. K. and Narayanan, S. R. (2014) 'Organo-sulfur molecules enable iron-based battery electrodes to meet the challenges of large-scale electrical energy storage', *Energy & Environmental Science*, 7(8), 2753-2763.
- Yang, Q. M., Ettl, V. A., Babjak, J., Charles, D. K. and Mosoiu, M. A. (2003) 'Pasted Ni(OH)₂ electrodes using Ni powders for high-drain-rate, Ni-based batteries', *Journal of The Electrochemical Society*, 150(4), A543-A550.
- Yano, M., Fujitani, S., Nishio, K., Akai, Y. and Kurimura, M. (1998) 'Effect of additives in zinc alloy powder on suppressing hydrogen evolution', *Journal of Power Sources*, 74(1), 129-134.
- Yekini Suberu, M., Wazir Mustafa, M. and Bashir, N. (2014) 'Energy storage systems for renewable energy power sector integration and mitigation of intermittency', *Renewable and Sustainable Energy Reviews*, 35, 499-514.

Zakeri, B. and Syri, S. (2015) 'Electrical energy storage systems: A comparative life cycle cost analysis', *Renewable and Sustainable Energy Reviews*, 42, 569-596.

Zhao, Q., Wang, J., Huang, X., Yao, Y., Zhang, W. and Shao, L. (2016) 'Copper-enriched palladium-copper alloy nanoparticles for effective electrochemical formic acid oxidation', *Electrochemistry Communications*, 69, 55-58.

7.4 Appendix A

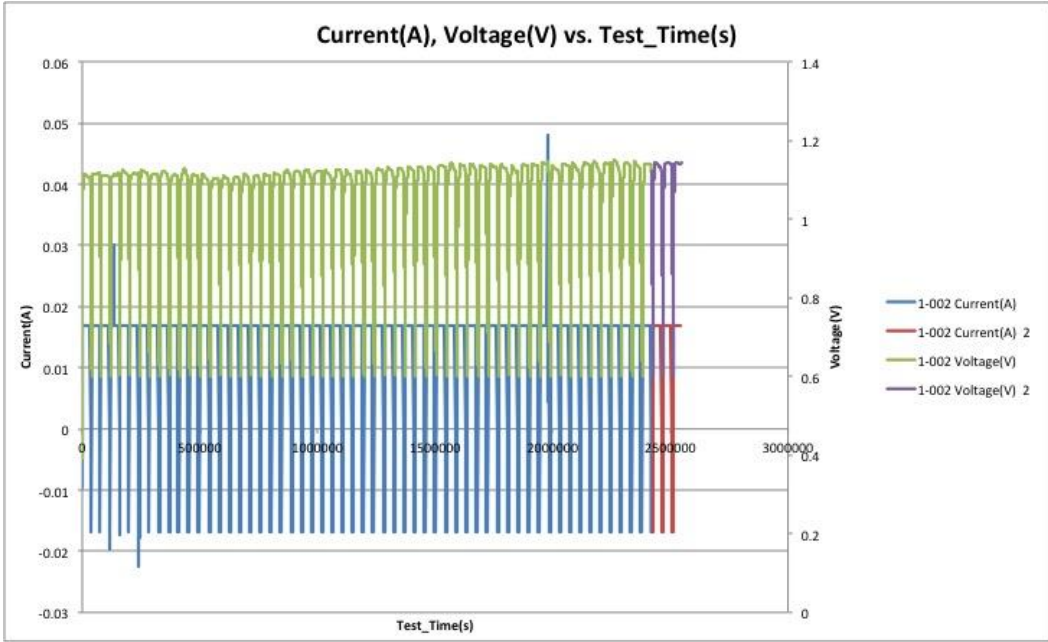
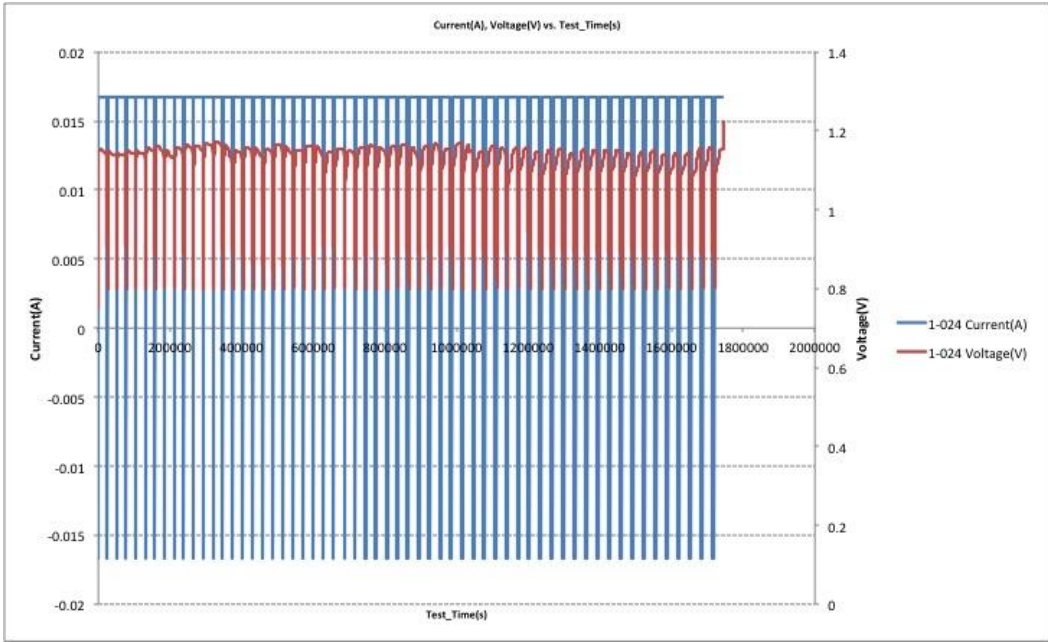


Figure 7-1 Charge/discharge constant current cycling (up to 60 cycles) of the selected mixed iron electrodes vs. Hg/HgO reference electrode of (a) Fe/Bi₂S₃ (b) Fe/FeS-CuSO₄.

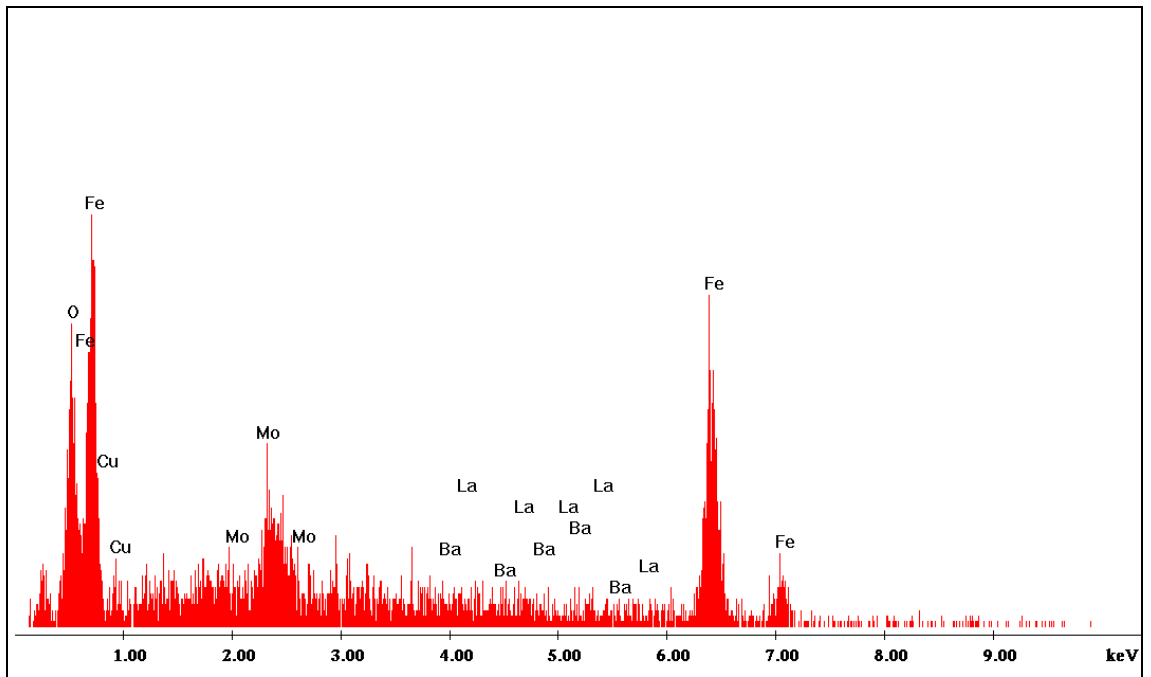


Figure 7-2i EDX measurement of the mixed iron electrode after been subjected to charge-discharge cycling

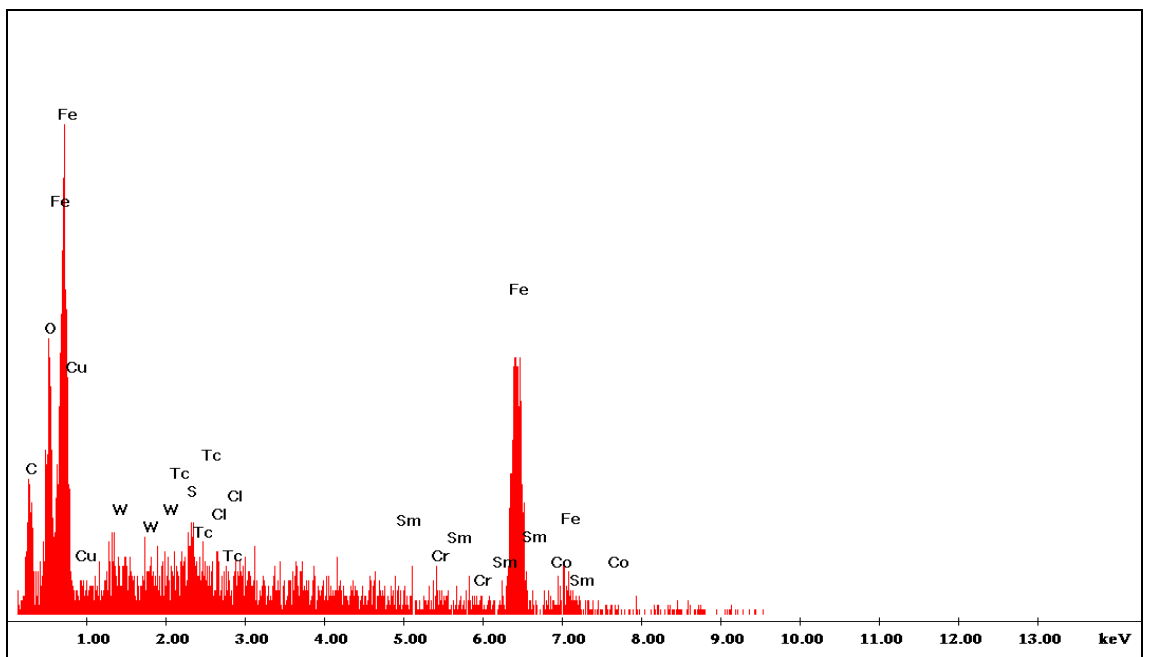


Figure 7-3j EDX measurement of the mixed iron electrode after been subjected to charge-discharge cycling.

7.5 Appendix B

Included Publication

Abdalla, A. H., Oseghale, C. I., Posada, J. O. G. and Hall, P. J. (2016) 'Rechargeable nickel-iron batteries for large-scale energy storage', *IET Renewable Power Generation*, Volume 10 , Issue (10), p 1529-1534.

Conferences

- 1- Investigation of the effect of some additives on the electrochemical performance of Nickel Iron (NiFe) batteries, The International Renewable Energy and Environment Conference (IREEC), June 2015, Czech Republic.
- 2- Rechargeable Nickel-Iron Battery for large-scale energy storage, the offshore Energy & Storage (OSSES) Symposium, July 2015, University of Edinburgh.
- 3- Nickel-Iron (Ni/Fe) Batteries for Large-Scale Energy Storage, 8th International Conference on Sustainable Energy & Environmental Protection (SEEP), August 2015, University of the West of Scotland.
- 4- Study of Mixed Metal Sulfide as Potential Electrode For Rechargeable Nickel-Iron Battery, Electrochem 2016, August 2016, University of Leicester.

7.6 Appendix C

Rechargeable nickel–iron batteries for large-scale energy storage

ISSN 1752-1416
Received on 20th January 2016
Revised 9th September 2016
Accepted on 18th September 2016
E-First on 14th November 2016
doi: 10.1049/iet-rpg.2016.0051
www.ietdl.org

Abdallah H. Abdalla¹, Charles I. Oseghale¹, Jorge O. Gil Posada¹, Peter J. Hall¹ 

¹Department of Chemical and Biological Engineering, Faculty of Engineering, University of Sheffield, Mappin Street, Sheffield S1 3JD, UK

 E-mail: peter.hall@sheffield.ac.uk

Abstract: This study reports the effect of iron sulphide and copper composites on the electrochemical performance of nickel–iron batteries. Nickel stripes were coated with an iron-rich electroactive paste and were cycled against commercial nickel electrodes. The electrodes electrochemical and physical characterisation were carried out by using galvanostatic charge/discharge, cyclic voltammetry, X-ray diffraction, and atomic force microscopy techniques. The authors' experimental results would indicate that the addition of iron sulphide and copper (II) sulphate significantly enhances the performance of the battery. Their in-house made iron-based electrodes exhibit good performance, with great potential for grid energy storage applications.

1 Introduction

The increasing demand for energy, depletion of supply of fossil fuels, and rising concerns over environmental pollution have encouraged the development and use of alternative, sustainable, and renewable energy resources [1–3]. Due to its natural environmental friendliness, abundance, renewable sources have the potential to reduce greenhouse gas emissions while offering a practical way of reducing our dependence on fossil fuels, it not surprising that most countries are taking serious steps to implement effective policies that will accelerate our use of such technologies [4, 5]. Moreover, it has been reported that the use of renewable energy continues to grow as global energy consumption increases. A staggering 19.1% of the global energy consumption during 2011–2012 was met by using renewable sources [6].

In recent years, renewable energy sources, such as the wind and solar power have emerged as a suitable solution to increase energy security, the supply of electricity, and mitigating environmental issues. Wind is a clean and non-polluting renewable source of energy that has received much attention for its potential to convert wind energy into more useful forms of energy such as electricity. Moreover, among all of the types of power production, renewable energy is considered as one of the fastest growing resources [6]. It is not surprising that in 2014, global wind energy production reached 370 GW, corresponding to an increase of almost 30% compared with the previous decade [6]. However, energy generation from renewable sources is not always possible when most needed (temporary wind profiles, seasonal availability of resources such as water, sunlight, etc.). Storing the energy during low load demand and then releasing it during the peak demand can overcome these problems. Combining renewable energy with energy storage, therefore, provides the natural solution to the asynchronous problem between energy generation from

intermittent power sources and demand [5]. Fig. 1 illustrates how energy storage could be used to help balance the electric grid.

Among various energy storage technologies, electrochemical energy storage has been identified as a practical solution that would help balance the electric grid by mitigating the asynchronous problem between energy generation and demand [5]. Moreover, electrochemical energy storage has been widely accepted as one of the most promising alternatives to store energy from intermittent power sources such as wind and solar for its high round-trip efficiency [5, 7, 8], long cycle life, low cost, high efficiency, and scalability [9, 10]. In the last century, several battery systems have been developed, but only a few have been demonstrated in large-scale applications. Among them, aqueous batteries have the potential to help balance the future electric grid at a lower cost than any of their non-aqueous counterparts (such as Li-ion, Na-ion, etc.) owing to its abundant raw materials and low-cost electrolyte (water based). Finally, non-aqueous batteries require costly safety systems to reduce the risk of arson; such expensive systems are not required with aqueous batteries [11–14].

Lead acid batteries are the earliest and well recognised as the leading technology for renewable applications, hence, their low energy density (about 30 Wh/kg), the toxicity of raw materials, and low cycle life [15, 16]. In contrast, invented and commercialised in the early 20th century, nickel–iron (NiFe) cells could provide 1.5–2 times the specific energy of lead/acid batteries, with their increased ruggedness and longer cycle life at deep discharge state (2000 cycles at 80% Depth of Discharge) [8, 11, 13, 16, 17]. In addition, NiFe batteries are well known for their long cycle life, typically exceeding 2000 cycles of charge and discharge [11, 18], vastly exceeding most of their competing technologies, this is lead/acid (300 cycles), nickel/cadmium (1500 cycles), and nickel metal hydride (500–800) [18].

Renewed interest in the iron-based batteries (such as NiFe) has been driven by the incentive to develop cost-effective, highly efficient energy storage technologies. NiFe cells are secondary batteries that are well known for robustness, non-toxicity, and eco-friendliness [19–22]. Besides, the relative abundance of chemicals and raw materials required to build these cells indicate that this technology could provide a cost-effective solution to store energy for grid system applications. However, the commercial deployment of these batteries has been limited by their poor charging efficiency (50–60%) and low discharge capability. These two problems are a direct consequence of the parasitic evolution of hydrogen that takes place during the charging of the battery. Considerable efforts have been devoted to overcoming the issues mentioned above.

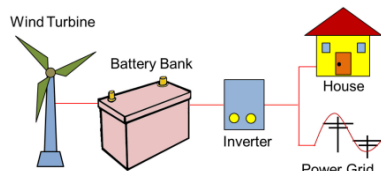


Fig. 1 Schematic diagram of the battery-based interactive wind/solar power system